Part I. Scandium Hydride and Alkyl Complexes with A Linked Monocyclopentadienyl-Amido Ligand-Framework: Single Component Catalysts for the Polymerization of α-Olefins

Part II. Hydrazido(1-) and 2,2-Dimethylhydrazido(1-) Derivatives of Permethylscandocene. Preparation and Structural Characterization of Their Products from Reactions with Acetonitrile

Thesis by

Pamela J. Shapiro

In Partial Fulfillment of the Requirements

for the Degree of

Doctor of Philosophy

California Institute of Technology

Pasadena, California

1991

(submitted June 19, 1990)

To My Grandmother

ACKNOWLEDGEMENTS

Believe it or not, I've learned several lessons about life over these past five years at Caltech in addition to my learning about chemistry. The people mentioned below have contributed to my growth in one or both of these areas:

General thanks go to the Bercaw group for providing a stimulating and entertaining environment in which to learn.

Special thanks go to John Bercaw for his patient teachings and his infectious enthusiasm for science.

I am grateful to Emilio Bunel for teaching me the tricks of the trade and for making me feel guilty about not working hard enough.

Trim initiated me to vacuum line techniques and was a patient line-mate.

Barb introduced me to "swivel-frit" technology.

I don't know how I would have gotten anything done without the services of people such as John Pirolo, Gabor Faludi, Tom Dunn, Larry Henling and Fenton Harvey.

Scott Ross, Dave Wheeler and Dom McGrath are gratefully acknowledged for assistance with use of the high field NMR instruments.

Bill Schaefer is gratefully acknowledged for performing most of the crystal structure determinations in this thesis.

Thanks go to Pat Anderson for fashion and diet tips, rice cakes and pleasant conversation.

Thanks go to Andrew H. for being my aerobics buddy, for his cheerful "hello" and for instruction on the 500 MHz NMR.

Thank you, Leroy, for letting me graduate 25th and for bringing in a Hanuka bush every December.

John P., Donnie, Janet, Bryan, Eric, Warren, Helmut and Kaspar are acknowledged for their encouragement, support and teachings about chemistry.

I am grateful to Harry Gray for always making me feel important.

Many thanks go to Jay Labinger for his receptiveness to questions and for extensive help with the polymerization kinetics discussed in Chapter 2.

Mark Olson is the Gauss expert who helped me with the non linear least-squares analyses discussed in Chapter 2.

I will be eternally grateful to Roger for his generosity, reliability and willingness to accompany me on frozen yogurt and Winchell's-muffin breaks.

Thanks go to David Montgomery for being a very special friend over this past year. He may think that he came to Caltech for his benefit, but I am convinced he was sent here for mine.

Most importantly, I am grateful to my grandmother for her constant love, support and encouragement.

ABSTRACT

Various monocyclopentadienyl scandium amido derivatives with the general formulas $\{(\eta^5\text{-}C_5Me_4)SiMe_2(\eta^1\text{-}NCMe_3\}ScR$, $(Cp^*SiNR)ScR$, and $\{(\eta^5\text{-}C_5H_3CMe_3)SiMe_2(\eta^1\text{-}NCMe_3\}ScR$, $(^{tBu}CpSiNR)ScR$, have been prepared. $[(Cp^*SiNR)(PMe_3)ScH]_2$ is prepared from the hydrogenation of $(Cp^*SiNR)ScCH(SiMe_3)_2$ in the presence of PMe_3. The scandium hydride effects the multiple insertion of α-olefins in a controlled fashion to form low molecular weight polymers. β-H elimination appears to be a principal chain-transfer pathway in this catalyst system. The stoichiometric reaction between $[(Cp^*SiNR)(PMe_3)ScH]_2$ and two equivalents of ethylene produces the ethylene bridged dimer $[(Cp^*SiNR)(PMe_3)Sc]_2(\mu, \eta^2, \eta^2\text{-}C_2H_4)$ and an equivalent of ethane. The stoichiometric reaction between the scandium hydride and either propene or butene affords the PMe_3-free, alkyl-bridged scandium dimers $[(Cp^*SiNR)Sc]_2(\mu\text{-}CH_2CH_2CH_3)_2$ and $[(Cp^*SiNR)Sc]_2(\mu\text{-}CH_2CH_2CH_2CH_3)_2$. The absence of coordinating phosphine makes these complexes more active olefin polymerization catalysts. The complexes $(Cp^*SiNR)(PMe_3)ScCH_2CH(CH)_3CH_2CH_3$ and $(Cp^*SiNR)(PMe_3)ScCH(C_6H_5)CH_2CH_2CH_2(C_6H_5)$ have also been prepared and spectroscopically characterized.

Kinetic analysis of the rate dependence of 1-pentene polymerization by $[(Cp^*SiNR)(PMe_3)ScH]_2$ on added PMe_3 reveals a phosphine dissociation pre-equilibrium to form a PMe_3-free active intermediate. The monomeric nature of this intermediate is revealed by the kinetic analysis of 1-pentene polymerization by $[(Cp^*SiNR)Sc]_2(\mu\text{-}CH_2CH_2CH_3)_2$ as a function of scandium concentration.

$(Cp^*SiNR)ScR$ was found to be >99% head-to-tail regioselective in the polymerization of propene. Preliminary ^{13}C NMR data indicate lower regioselectivity in propene polymerization by $(^{tBu}CpSiNR)ScR$. A slight syndiotactic preference is observed in

the stereochemistry of the polypropene produced with $[(Cp^*SiNR)Sc]_2(\mu\text{-}CH_2CH_2CH_3)_2$. By contrast, $[(^{tBu}CpSiNR)ScMe]_x$ displays no stereocontrol, producing an atactic polymer.

A rare example of an unsubstituted hydrazido(1-) complex, $Cp^*_2ScNHNH_2$ ($Cp^* = (\eta^5\text{-}C_5Me_5)$), prepared by reaction of one equivalent of anhydrous hydrazine with $Cp^*_2ScCH_3$, reacts with acetonitrile to form $Cp^*_2Sc\overline{N(H)C(CH_3)NNH_2}$. The crystal structure of $Cp^*_2Sc\overline{N(H)C(CH_3)NNH_2}$ reveals a five-membered, nearly planar [$Sc\overline{\text{-NH-C(CH}_3\text{)-N-NH}_2}$] ring. The results of a labeling study using $^{15}N{\equiv}CCH_3$ are consistent with a mechanism involving insertion of acetonitrile into the Sc-N bond of $Cp^*_2ScNHNH_2$, followed by tautomerization to form $Cp^*_2Sc\overline{N(H)C(CH_3)NNH_2}$. The closely related compounds $Cp^*_2ScNHNMe_2$ and $Cp^*_2Sc\overline{N(H)C(CH_3)NNMe_2}$ have also been prepared, and the structure of the latter compound has been determined.

TABLE OF CONTENTS

Part I

Scandium Hydride and Alkyl Complexes with A Linked Monocyclopentadienyl-Amido Ligand-Framework: Single Component Catalysts for the Polymerization of α-Olefins.

INTRODUCTION

In 1953 Ziegler *et al.* made the serendipitous discovery that the binary system of a transition metal salt with an alkyl-aluminum species catalyzes the polymerization of ethylene to linear, high molecular weight, high density polyethylene.[1] Shortly thereafter, Natta and coworkers applied these catalysts to the polymerization of propene and other α-olefins and demonstrated the ability of these systems to produce stereoregular (isotactic) macromolecules.[2] These discoveries coupled with the independent discovery of ethylene polymerization catalysis by metal oxides supported on silica or alumina, most notably the Phillips Petroleum CrO_3/SiO_2 catalyst,[3] virtually revolutionized the polymer industry.

Although new generations of Ziegler-Natta catalyst systems which are more active and more stereospecific have developed at a rapid pace, the structures of the active catalysts have remained elusive.[4] As with many catalysts, direct characterization of these systems has been complicated by their heterogeneous, multicomponent composition and the low concentration of active centers in the bulk material. Models for the active centers have relied on indirect studies of polymerization kinetics, polymer microstructure and molecular weight distribution and active-site concentration. As a result the structures for the active catalysts have been highly speculative.[5]

The most favored mechanistic model is that developed by Cossee and Arlman.[6] The primary feature of this model is the insertion of the olefin into the M-C bond of a transition metal alkyl species (Scheme 1).

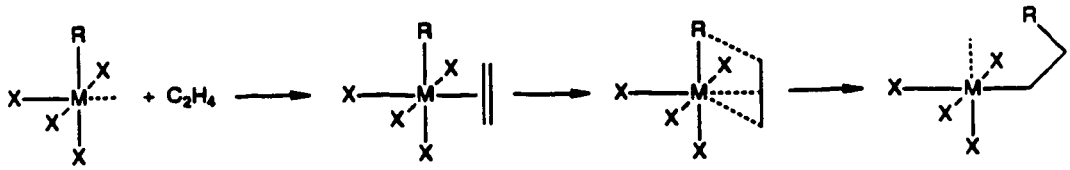

Scheme 1. Cossee-Arlman Mechanism for Olefin Polymerization

Although this mechanism was proposed for an octahedral titanium site in a heterogenous $TiCl_3$-based catalyst system, compelling evidence in support of it has recently been derived from soluble, well-defined organometallic model systems.[7]

An alternative mechanism put forth by Green and coworkers also involves propagation at the transition metal but requires the formation of a metal carbene intermediate, which adds olefin in a 2+2 fashion, as in the olefin metathesis reaction (Scheme 2).[8]

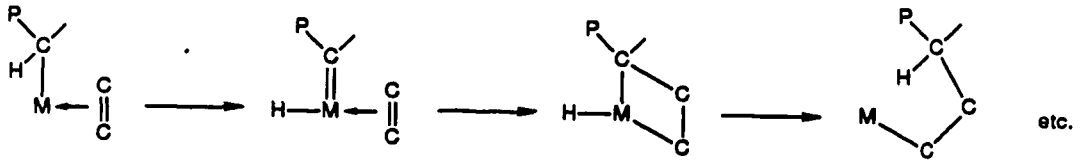

Scheme 2. Green-Rooney Mechanism for Olefin Polymerization

So far, only one well-defined, ethylene-polymerizing organometallic species, a tantalum alkylidene complex reported by Turner and Schrock, has appeared to operate by the Green-Rooney mechanism.[9] Most other organometallic Ziegler-Natta model systems are d^0 and therefore cannot undergo the two electron oxidation state change associated with α-H abstraction. A more subtle form of C-H activation involving an agostic interaction for assisting olefin insertion has been proposed for these d^0 systems (Scheme 3).[10] The involvement of an α-agostic interaction in the olefin-insertion mechanism is currently being explored by our group as well as by others.[11]

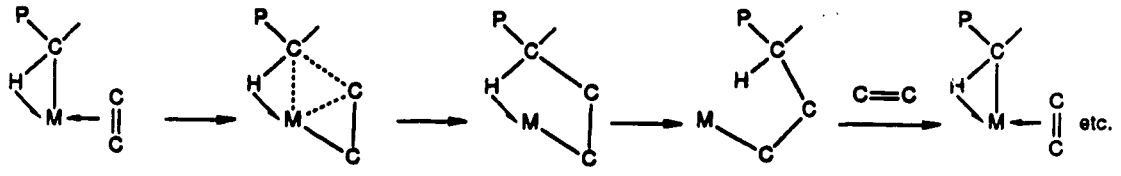

Scheme 3. Agostic α-C-H Assisted Mechanism for Olefin Polymerization

It is through these well-defined, single-component organometallic systems that much of our understanding of elementary processes pertinent to Ziegler-Natta polymerization, such as olefin insertion and the microscopic reverse reactions of β-H and β-alkyl elimination, has evolved. In fact, many of these systems, based mainly on early transition metals or lanthanide metals (Figure 1), are quite active catalysts for the polymerization of ethylene. Their utility in unravelling the mechanism of Ziegler-Natta catalysis, especially with respect to the remarkable regio- and stereospecificity of most Ziegler-Natta systems, has been limited, however, by their inability to polymerize α-olefins. At best, a few of these systems have been reported to oligomerize propene to chain lengths of $C_{\leq 24}$.[7b,e]

Reported herein are well-defined organoscandium systems that are rare examples of single-component, homogeneous catalysts for the polymerization of α-olefins. The systems, (Cp*SiNR)ScR and (^{tBu}CpSiNR)ScR (see below), which will be described may be considered the third generation of organoscandium compounds that have emerged from our research group. These complexes differ from their predecessors, $(\eta^5\text{-}C_5Me_5)_2ScR$,[12] $\{(\eta^5\text{-}C_5Me_4)_2SiMe_2\}ScR$ and $\{(\eta^5\text{-}C_5H_3CMe_3)_2SiMe_2\}ScR$,[13] in that one of the cyclopentadienyl ligands on the scandium is replaced by a bulky amido group.

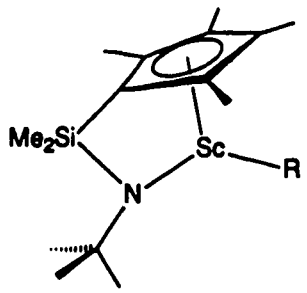

"(Cp*SiNR)ScR"

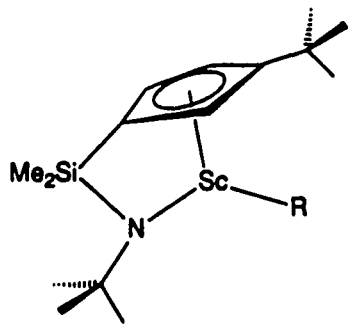

"(^{tBu}CpSiNR)ScR"

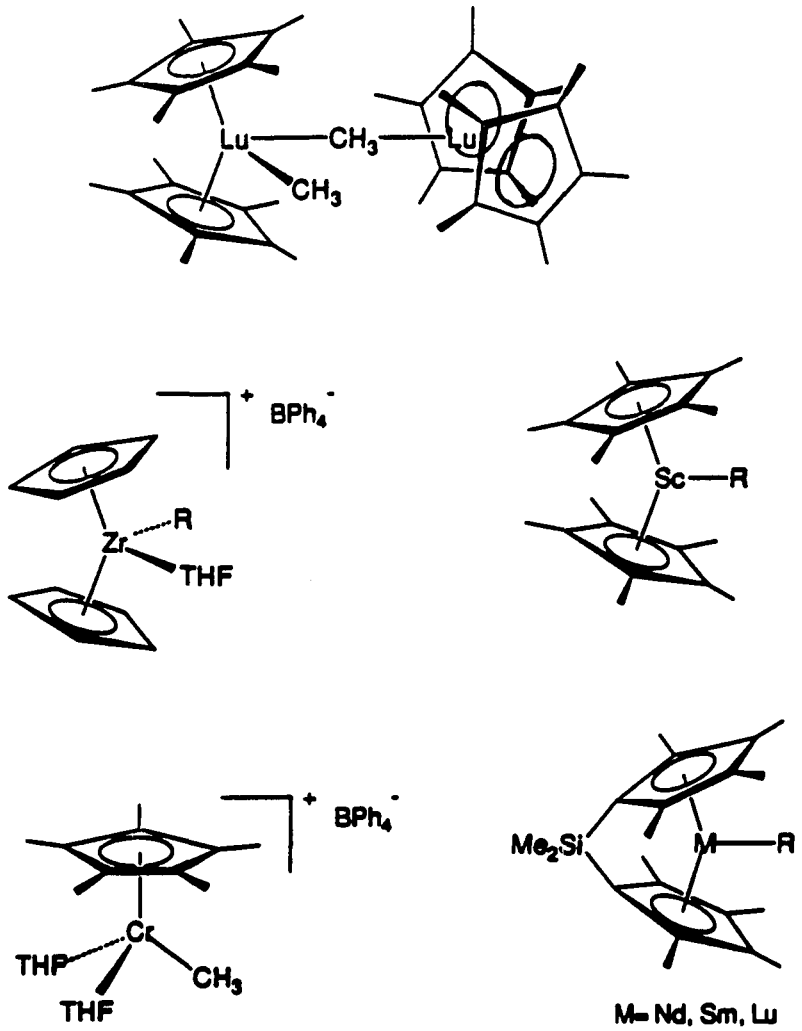

Figure 1. Some Organometallic Systems that Polymerize Ethylene

The reactivity of the scandium has been found to be highly sensitive to changes in the sterics of its supporting ligand system. Thus, we were guided by the reactivity profiles of the earlier organoscandium systems in choosing this ligand modification as a logical next step in our efforts to design a catalyst system for the multiple insertion of α-olefins.[14]

The syntheses of various derivatives of these monocyclopentadienyl scandium amido complexes, along with their spectroscopic and x-ray crystallographic characterization, is discussed in the first chapter of this thesis. Characterization of the polymerization activity of these systems and experiments to elucidate the nature of the active catalyst are covered in Chapter 2.

References

1. Ziegler, K.; Holzkamp, E.; Breil, H; Martin, H. *Angew.Chem.* 1955, *67*, 541.

2. Natta, G.; Pino, P.; Corradini, P.; Danusso, F.; Mantica, E.; Mazzanti, G.; Moraglio, G. *J. Am. Chem. Soc.* 1955, *77*, 1708.

3. Clark, A.; Hogan, J. P.; Banks, R. L.; Lanning, W.C. *Ind. Eng. Chem.*, 1956, *48*, 1152.

4. For reviews on Ziegler-Natta polymerization, see: (a) Sinn, H.; Kaminsky, W. *Adv. Organomet. Chem.* 1980, *99*. (b) Pino, P.; Mulhaupt, R. *Angew. Chem., Int. Ed. Engl.* 1980, *19*, 857. (c) Boor, J. *Ziegler-Natta Catalysts and Polymerizations*; Academic Press: New York, 1979. (d) Tait, P. J. T. In *Comprehensive Polymer Science*; Allen, G.; Bevington, J. C., Eds.; Pergamon Press: Oxford, 1989; Chapter 1.

5. Tait, P. J. T. In *Comprehensive Polymer Science*; Allen, G.; Bevington, J. C., Eds.; Pergamon Press: Oxford, 1989; Chapter 2.

6. a) Cossee, P. *J. Catal.* 1964, *3*, 80. b) Arlman, E. J.; Cossee, P. *J. Catal.* 1964, *3*, 99.

7. (a) Watson, P. L.; Parshall, G. W. Acc. Chem. Res. 1985, 18, 51 and references therein. (b) Watson, P. L.; Herskovitz, T. ACS Symp. Ser. 1983, No. 212, 459. (c) Jordon, R. F. *J. Chem. Educ.* 1988, *65*(4), 285 and references therein. (d) Jeske, G.; Lauke, H.; Mauermann, H.; Swepston, P. N.; Schumann, H.; Marks, T. J. *J. Am. Chem. Soc.* 1985, *107*, 8091. (e) Jeske, G.; Schock, L. E.; Swepston, P. N.; Schumann, H.; Marks, T. J. *J. Am. Chem. Soc.* 1985, *107*, 8103. (f) Ballard, D. G. H.; Courtis, A.; Holton, J.; McMeeking, J.; Pearce, R. *J. Chem. Soc., Chem. Commun.* 1978, 994. (g) Schmidt, G. F.; Brookhart, M. *J. Am. Chem. Soc.* 1985, *107*, 1443. (h) Thomas, B. J.; Theopold, K. H. *J. Am. Chem. Soc.* 1988, *110*, 5902. (i) Taube, R.; Krakowa, L. *J. Organomet. Chem.* 1988, *347*, C9. (j) Hlatky, G. G.; Turner, H. W.; Eckman, R. R. *J. Am. Chem. Soc.* 1989, *111*, 2728.

8. Ivin, K. J.; Rooney, J. J.; Stewart, C. D.; Green, M. L. H.; Mahtab, R. *J. Chem. Soc. Chem. Commun.* 1978, 604.

9. Turner, H. W.; Schrock, R. R. *J. Am. Chem. Soc.* 1982, *104*, 2331.

10. Brookhart, M.; Green, M. L. H. *J. Organometal. Chem.* 1983, *250*, 395.

11. a) An interaction of the hydrogen on the α-carbon with either the transition metal or the aluminum in a Ziegler-Natta catalyst system has been probed by examinination of the deuterium isotope effect on the stereochemistry of intramolecular olefin insertion by titanocene alkenyl chloride complexes catalyzed by ethylaluminum dichloride (Clawson, L.; Soto, J.; Buchwald, S. L.; Steigerwald, M. L.; Grubbs, R. H. *J. Am. Chem. Soc.* 1985, *107*, 3377). Similar experiments involving the cyclization of deuterium labeled α,ω-diolefins by $Cp(PMe_3)ScH$ are currently being performed in our labs (Piers, W. E., unpublished results). b) Brintzinger and coworkers have calculated that an α-C-H agostic interaction stabilizes the transition state for olefin insertion by ca 20 kcal mol^{-1} (personal communication).

12. Thompson, M. E.; Baxter, S. M.; Bulls, A. R.; Burger, B. J.; Nolan, M. C.; Santarsiero, B. D.; Schaefer, W. P.; Bercaw, J. E. *J. Am. Chem. Soc.* **1987**, *109*, 203.

13. Bunel, E.; Burger, B. J.; Bercaw, J. E. *J. Am. Chem. Soc.* **1988**, *110*, 976.

14. For a review of our work with organoscandium compounds see: Piers, W. E.; Shapiro, P. J.; Bunel, E. E.; Bercaw, J. E. *Synlett*, **1990**, *2*, 74.

Chapter 1

The Synthesis and Structural Characterization of (Cp*SiNR)ScR and (^{tBu}CpSiNR)ScR Complexes

Introduction

Work in our group with organoscandium complexes has revealed the reactivity of these compounds to be excellent models for Ziegler-Natta catalysis. Our entry into this chemistry began with the permethylscandocene hydrides and alkyls of general formula Cp^*_2ScR.[1] The use of the bulky Cp* ligand ($Cp^* = \eta^5$-C_5Me_5) has been a general strategy in our group for the steric stabilization of monomeric, electronically unsaturated, early transition metal compounds.[2] The 14 electron Cp^*_2ScR complexes are monomeric, in contrast to the normal-ring scandocene analogs, which tend to form dimers.[3] Permethylscandocene alkyl derivatives were found to be active ethylene polymerization catalysts and were amenable to kinetic studies of chain propagation (olefin insertion) and chain transfer by β-H elimination.[4] As predicted by these experiments and later demonstrated in oligomerization studies, $Cp^*_2ScCH_2CH_2CH_3$ was found to initiate true "living" ethylene polymerization at -80°C (Equation 1).

(1)

The insertion of α-olefins by permethylscandocene alkyls does not occur, however. Instead, the scandium activates a vinylic C-H bond of the olefin in a σ-bond metathesis reaction to form a scandium alkenyl species and free alkane (Equation 2).[1]

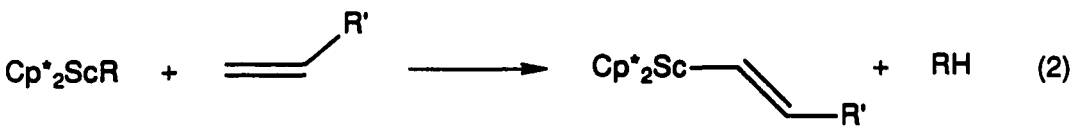

(2)

We attribute this behavior to unfavorable steric interactions between the substituent on the olefin and the (η^5-C_5Me_5) ligand when the olefin π orbital approaches the metal-carbon bond for insertion (A). An orthogonal approach of the olefin to the metal (B) minimizes steric repulsions, favoring the σ bond metathesis reaction.

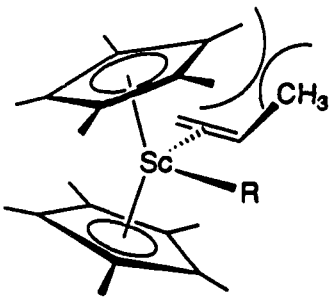

A

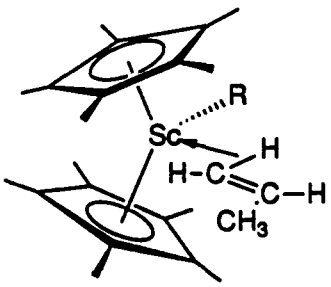

B

Efforts to relieve steric crowding at the scandium led to the synthesis of the scandocene complexes {(η^5-$C_5Me_4)_2SiMe_2$}(PMe$_3$)ScH, Op(PMe$_3$)ScH, and [{(η^5-$C_5H_3CMe_3)_2SiMe_2$}ScH]$_2$, [DpScH]$_2$. By tying the cyclopentadienyl rings back with a dimethylsilylene bridge, we hoped to increase access of the olefin to the scandium center and in this way promote α-olefin insertion. As expected, these scandium hydride complexes are more reactive than the parent permethylscandocene hydride derivative, catalytically *dimerizing* α-olefins by the mechanism shown below (Scheme I).[5] Following the second olefin insertion, β-H elimination from the tertiary β-carbon to liberate the olefin dimer and regenerate Sc-H is rapid relative to a sterically disfavored, third α-olefin insertion.

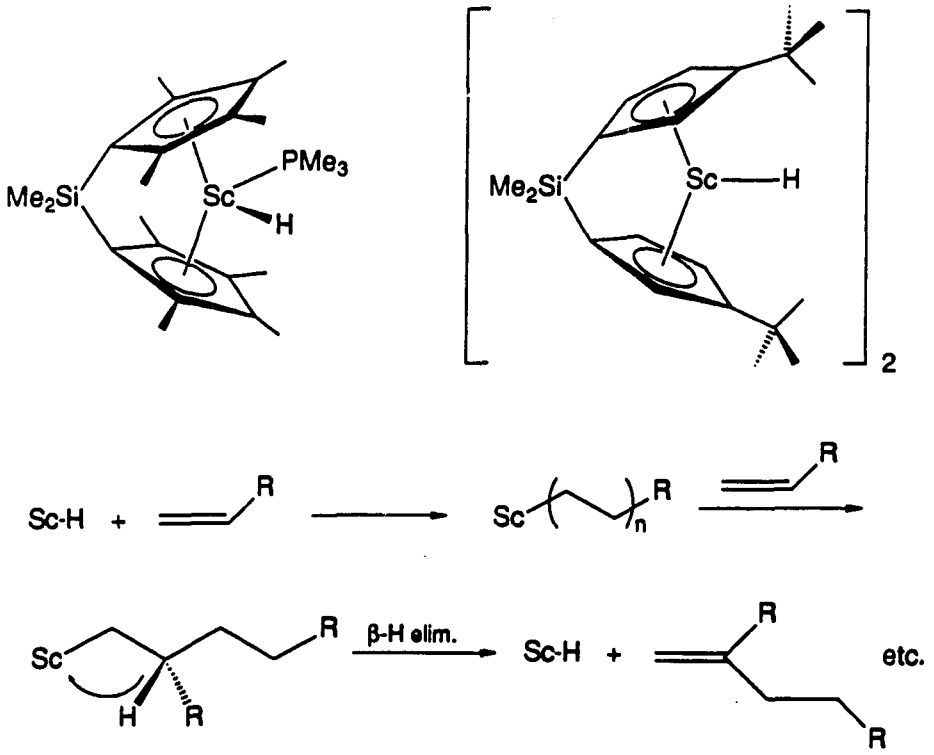

Scheme I. Catalytic α-Olefin Dimerization by (Op)(PMe_3)ScH and [DpScH]$_2$

Thus, we were approaching our goal of developing an organoscandium system capable of inserting α-olefins in a multiple fashion. It was clear from our experience with the linked metallocene systems that varying the sterics of the supporting ligand system has a striking effect on the reactivity of the scandium center. This prompted us to examine further variations of the ligand framework. We anticipated that scandium derivatives of the type {(η^5-C_5Me_4)Me_2Si(η^1-NCMe_3)}ScR ("(Cp*SiNR)ScR") would differ significantly from the scandocene derivatives, since the amido group should render the metal more Lewis-acidic and even more electron deficient, two properties that we felt would encourage olefin insertion. Also, to the extent that the steric bulk of the cyclopentadienyl rings promote chain transfer by β-H elimination, this less sterically crowded scandium system would be more likely to effect the multiple insertion of α-olefins.

Results and Discussion

The Synthesis and Characterization of $[(Cp^*SiNR)(PMe_3)Sc(\mu\text{-}H)]_2$

The Cp*SiNR ligand [Cp*SiNR = $(\eta^5\text{-}C_5Me_4)SiMe_2(\eta^1\text{-}NCMe_3)$] is prepared straightforwardly by reacting $(C_5Me_4)SiMe_2Cl$ with lithium t-butyl amide (Equation 2).

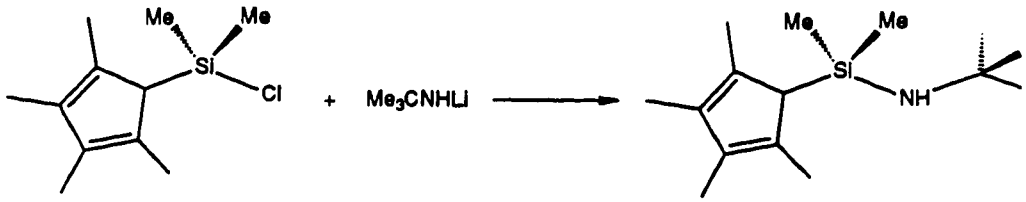

(3)

Double deprotonation of the ligand with n-BuLi followed by reaction of the dilithium salt of the ligand with $ScCl_3(THF)_3$ affords (Cp*SiNR)ScCl complexed by variable, non-stoichiometric amounts of THF and LiCl. The presence of THF in all of our scandium complexes is undesirable since it blocks the reactivity of the metal by binding tightly to the active site. In this compound, THF is removed by heating the solid $(Cp^*SiNR)ScCl\cdot(THF)_x\cdot(LiCl)_n$ at 100°C *in vacuo* for one day. The lithium halide may be removed by sohxlet extraction of $[(Cp^*SiNR)ScCl]_x$ with hot toluene, although it does not interfere with the subsequent alkylation step.

The bulky bis(trimethylsilyl)methyl derivative (3) is the only alkyl derivative that could be successfully prepared from (Cp*SiNR)ScCl. The reaction of other alkyllithium reagents such as MeLi, PhLi and Me_3SiCH_2Li with the scandium chloride complex did not afford clean products. Despite several attempts, single crystals of 3 suitable for x-ray analysis could not be obtained and ebulliometric molecular weight analyses were inconclusive in determining its molecularity in solution.[6] Compound 3 is hydrogenated cleanly in the presence of PMe_3 to form the hydride complex $[(Cp^*SiNR)Sc(PMe_3)]_2(\mu\text{-}H)_2$(4) in 20% overall yield starting from $ScCl_3(THF)_3$ (Scheme II). Hydrogenation of 3 in the absence of PMe_3 affords a mixture of products. The usefulness of PMe_3 as a soft, weakly binding Lewis base for stabilizing

these highly electronically and coordinatively unsaturated organoscandium complexes was discovered in earlier work with $\{(\eta^5\text{-}C_5Me_4)_2SiMe_2\}ScR$ and some mixed-ring complexes, $(Cp^*)(Cp')ScR$ ($Cp' = \eta^5\text{-}C_5H_5$, $\eta^5\text{-}1,3,4\text{-}C_5H_2Me_3$).[7]

Single crystals of 4 (as toluene-d_8 solvate) grew in an NMR tube when a concentrated solution of 3 in toluene-d_8 was hydrogenated. An x-ray structure determination revealed a double hydrogen-bridged dimer of C_2 symmetry. As can be seen from the ORTEP drawing in Figure 1.1, the ligand framework of the molecule is reminiscent of that of the bent metallocene systems, although the bite angle of 104.8(3)° is closer to a tetrahedral geometry than the 133.9° ring centroid-Sc-ring centroid angle found in $\{(\eta^5\text{-}C_5Me_4)_2SiMe_2\}(PMe_3)ScH$. An extremely long Sc-P bond length of almost 3Å is a notable feature of the structure. This distance is half an angstrom larger than the sum of the covalent radii for Sc and P.[8] It is also longer than the Sc-P bond in $\{(\eta^5\text{-}C_5Me_4)_2SiMe_2\}(PMe_3)ScH$ (2.75Å).[6] Consistent with the long Sc-P distance, variable temperature ^{31}P NMR studies reveal that PMe_3 dissociation is rapid. The atoms connected to nitrogen are coplanar to within ±0.02Å, indicating sp^2 hybridization of the nitrogen atom. The Sc-N bond distance of 2.058(3)Å is comparable to the 2.049Å Sc-N bond length found in tris-(hexamethyldisilylamido)scandium.[9] The Si-N bond length of 1.663(3)Å is a bit short in comparison to typical values of 1.70-1.76Å for related ligand systems,[10] indicating that a significant amount of N-Si($p\pi \longrightarrow d\pi$) interaction is competing with nitrogen lone pair donation to the scandium.[11]

The poor solubility of 4 has prevented determination of its solution molecular weight; however, a monomer/dimer equilibrium in solution is indicated by the presence of two peaks (ca. 4:1 ratio) in the ^{31}P spectrum of 4 measured at -66°C. The variable temperature ^1H NMR study was less informative, revealing only a single, detectable species over the range -80°C to 25°C.

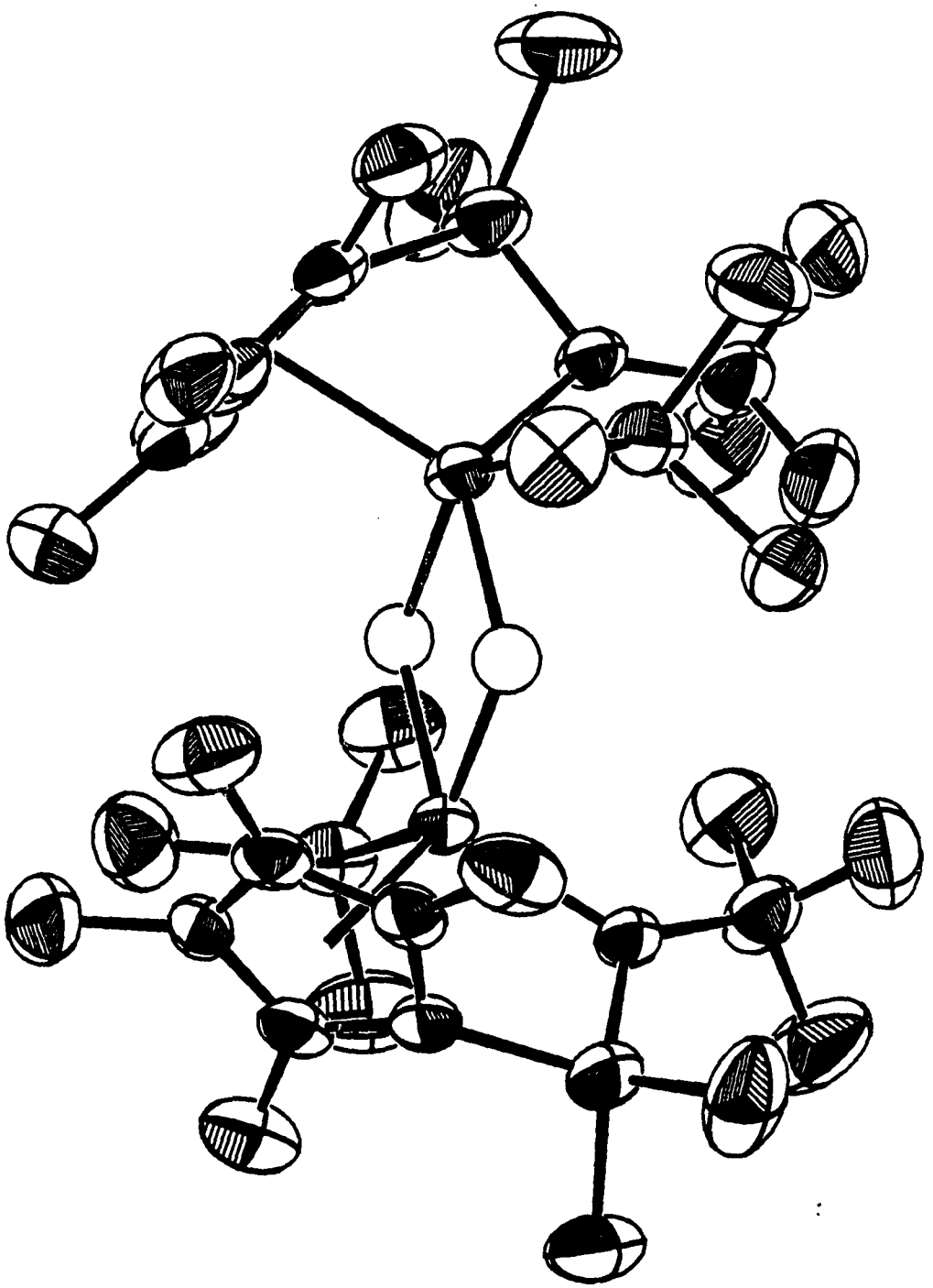

Figure 1.1. ORTEP drawing of [(Cp*SiNR)(PMe_3)ScH]$_2$ (4) with 50% probability ellipsoids.

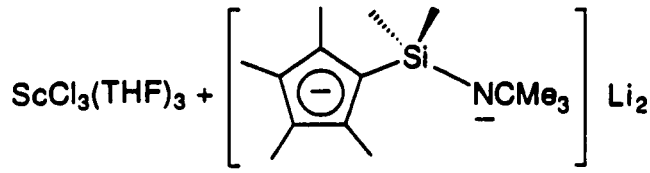

25°C, toluene

$(Cp^*SiNR)ScCl\bullet(LiCl)_n\bullet(THF)_x$ (1)

1. vacuum, 100°C
2. $LiCH(SiMe_3)_2$

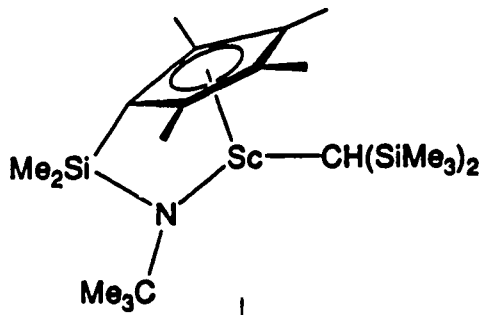

(2)

H_2, PMe_3

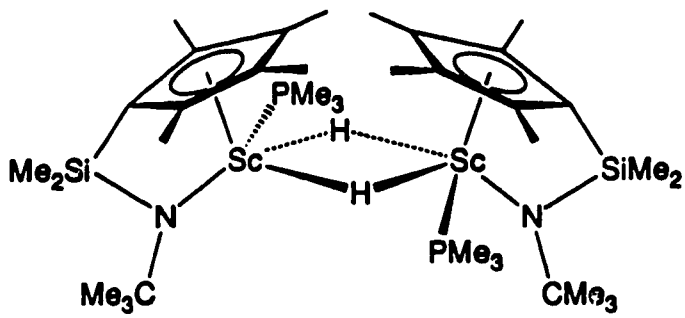

(3)

Scheme III. Synthesis of $[(Cp^*SiNR)(PMe_3)ScH]_2$

The hydride resonance occurs at δ 4.45 in the ^{1}H NMR spectrum and is considerably broadened because of its proximity to the quadrupolar scandium nucleus (I = 7/2, 100% abundance, -0.22x10^{28} Q/m^2).[12] An attempt was made to locate the Sc-H stretch by IR analysis. The Nujol spectrum of 4 includes a broad band of medium intensity at 1152.4 cm^{-1} that is absent in the spectrum of the corresponding deuteride, 4-d_1. If this band corresponds to ν Sc-H, the corresponding Sc-D band should be shifted to *ca* 817 cm^{-1}. This region of the spectrum is already obscured by other absorption bands, although there does appear to be a broadening and increase in intensity in the group of bands in this region for 4-d_1, perhaps from the presence of an overlapping Sc-D band. A vibrational energy of 1152.4 cm^{-1} is rather low, even for a bridging metal hydride.[13] To determine if this could be due to some polymeric composition of the scandium hydride complex resulting from its manner of isolation (precipitation from hexane), a Nujol mull of 4 that had been recrystallized from toluene was examined by IR. No spectral changes were observed.

As mentioned, the trimethylphosphine in 4 is quite labile, dissociating reversibly from the metal on the NMR time scale. By contrast, the PMe_3 ligands of Jordan's $[Cp_2Zr(H)(PMe_3)_2][BPh_4]$[14] do not exchange with free PMe_3 on the NMR time scale. To determine if a bis-phosphine adduct, $(Cp^*SiNR)(PMe_3)_2ScH$, analogous to Jordan's compound might be formed, a tenfold excess of PMe_3 was added to 4 in an NMR tube. No new resonances were detected in this sample by either ^{1}H or ^{31}P NMR from 25°C to -80°C, indicating that coordination of a second phosphine by the scandium does not occur to a significant extent.

$[(Cp^*SiNR)Sc(PMe_3)]_2(\mu\text{-}H)_2$ does indeed cleanly catalyze the polymerization of α-olefins, albeit rather slowly. For example, with 0.1 mole percent $[(Cp^*SiNR)Sc(PMe_3)]_2(\mu\text{-}H)_2$ in neat pentene at 25°C, polymerization rates of *ca* 50 turnovers/Sc/hr are found, and after 19 hrs polypentene with M_n = 3,000 ($X_n \approx 43$) and PDI = 2.1 (gpc relative to polystyrene) is obtained. Propene, 1-butene, hexadiene and butadiene have also been polymerized with

this catalyst system. The polymerization activity appears to be fairly general to monosubstituted olefins (some exceptions will be discussed later in this chapter and in Chapter 2). In order to gain insight into the nature of the active propagating species, we set out to isolate and characterize products resulting from olefin insertion into the Sc-H bond of this compound. These species are discussed in the sections that follow.

[(Cp*SiNR)(PMe$_3$)Sc]$_2$(μ,η^2,η^2-C$_2$H$_4$): An Unusual Ethylene Bridged Dimer from the Stoichiometric Reaction of [(Cp*SiNR)(PMe$_3$)Sc(μ-H)]$_2$ with Ethylene

The seemingly simplest place to start in preparing an olefin insertion product from [(Cp*SiNR)(PMe$_3$)ScH] was with ethylene. Addition of one equivalent of ethylene to 4 afforded an unexpected product, however. Instead of the familiar triplet, quartet pattern of an ethyl group, a singlet at δ -0.17ppm was observed in the ^{1}H NMR spectrum. When the reaction was performed with $^{13}C_2H_4$, the proton-coupled ^{13}C NMR spectrum of the product revealed a triplet pattern, with a principal J_{CH} coupling of 142Hz. Fine structure from second order coupling effects is also apparent (Figure 1.2).

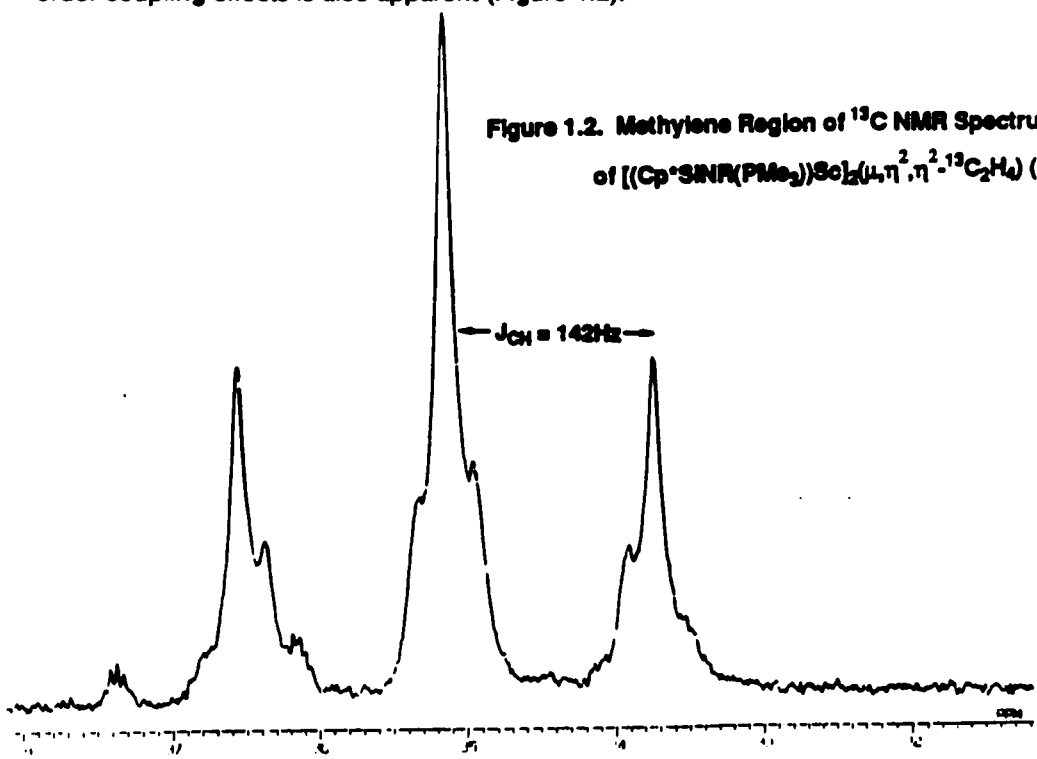

Figure 1.2. Methylene Region of ^{13}C NMR Spectrum of [(Cp*SiNR(PMe$_3$))Sc]$_2$(μ,η^2,η^2-^{13}C$_2$H$_4$) (5).

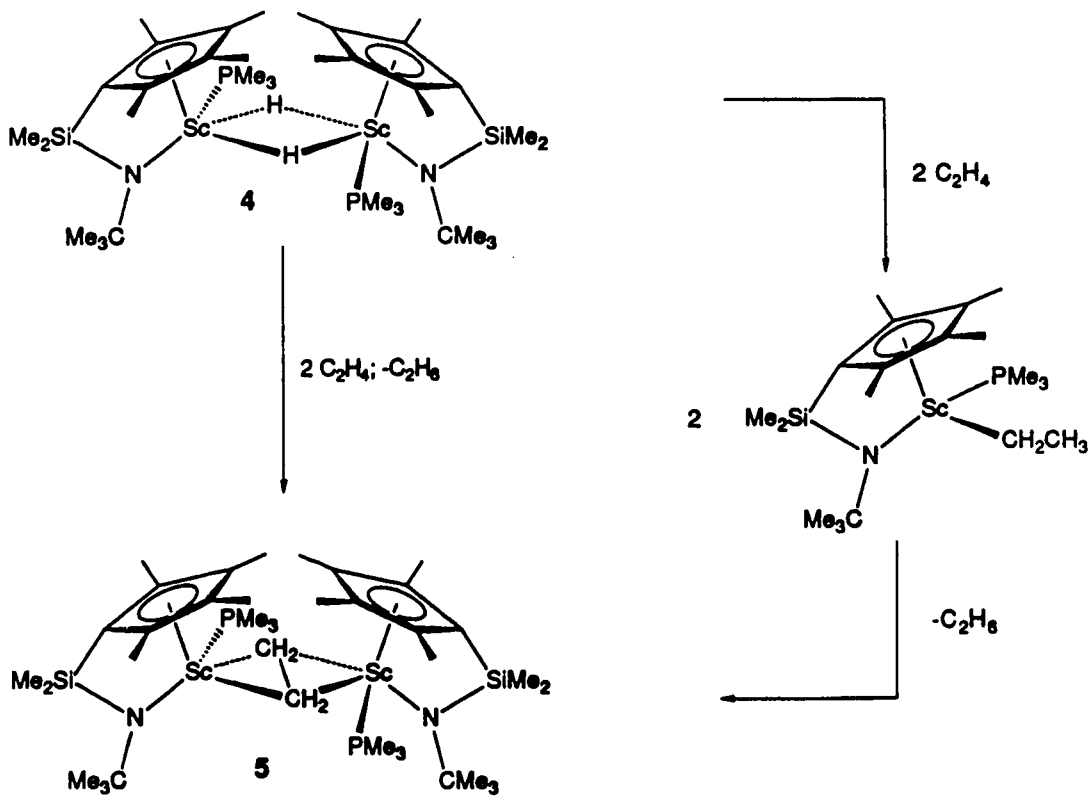

Scheme III. Reaction Pathway for the Formation of $[(Cp^*SiNR)(PMe_3)Sc]_2(\mu, \eta^2,\eta^2\text{-}C_2H_4)$

Upon closer inspection of the ^1H NMR spectrum, a resonance consistent with free ethane was located at *ca* 0.75 ppm. The NMR evidence indicated that the reaction shown in Scheme III had occurred to produce the ethylene-bridged scandium dimer $[(Cp^*SiNR)Sc]_2(\mu\text{-}C_2H_4)$ (5). This assignment was somewhat puzzling since the C-H activation of benzene solvent by **4** does not occur readily until the system is heated to 80°C, whereas this intermolecular activation of a normally less reactive sp^3-hybridized C-H bond occurs readily at ambient temperature.

To confirm our assignment, an x-ray crystal structure determination was undertaken. As can be seen in the ORTEP drawing in Figure 1.3, an ethylene-bridged scandium dimer is indeed formed. The η^2, η^2 coordination of the ethylene bridge is quite unusual and has been observed in only a few other metal systems.[15] The C-C bond length of the ethylene bridge (1.433(12)Å) is intermediate between that of a single and a double C-C bond[7] and is comparable to the bond lengths observed in transition metal olefin complexes.[16] The sp^2 hybridization of the ethylene carbons of the C_2H_4 bridge is reflected in the H-C-H angle of 120(6)° as well as in the large J_{CH} of 142Hz. As in the structure for the Sc-H dimer, the cyclopentadienyl rings are more or less cis. The Sc-P bond length of 2.825(3)Å is significantly shorter than in **4**, although phosphine dissociation is still rapid. The amide group is again planar to within ±0.016Å. Both the Sc-N bond distance (2.071(6)Å) and the Si-N bond distance (1.722(6)Å) are longer than in compound **4**. This species has been found to polymerize ethylene as well as propene.

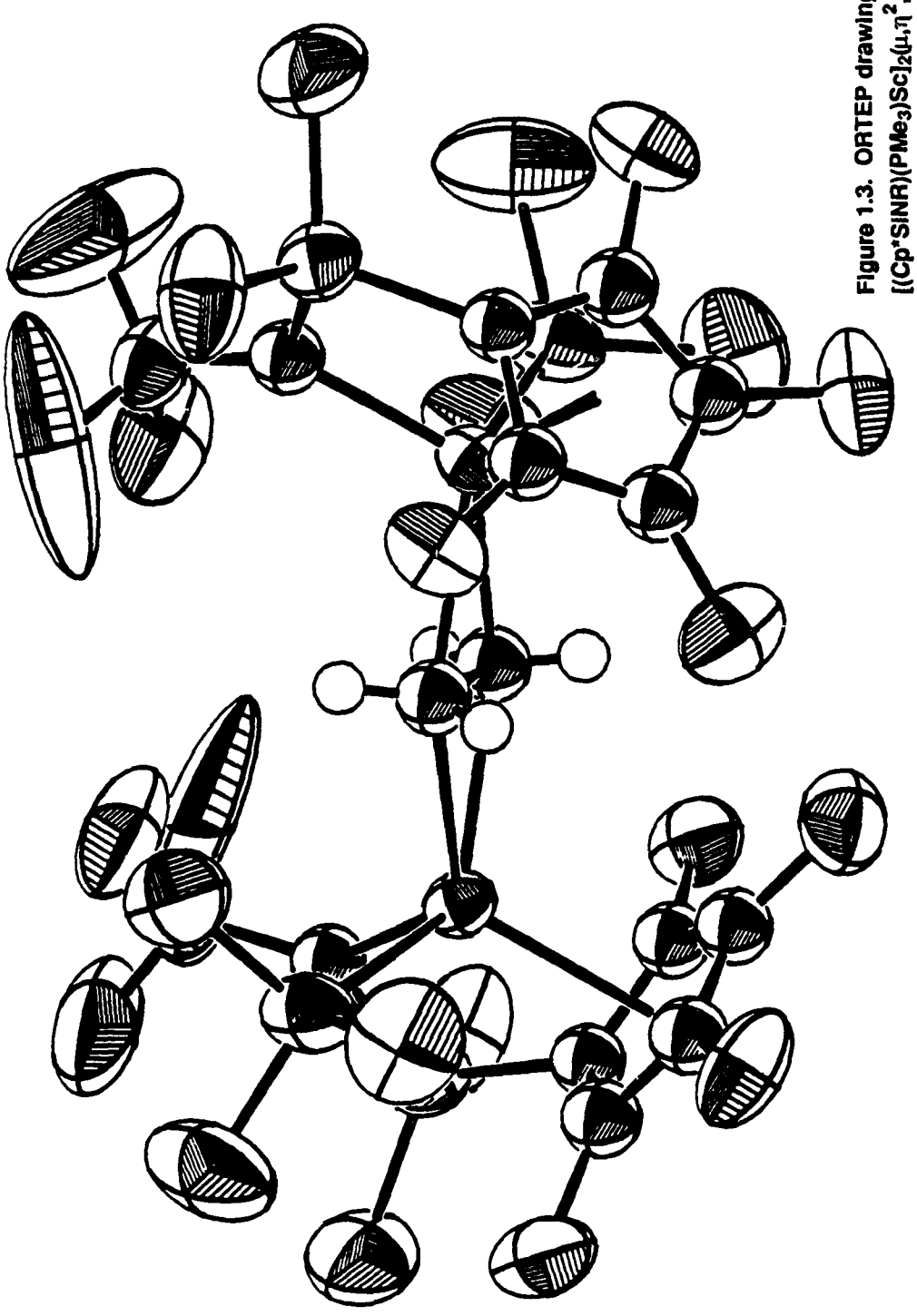

Figure 1.3. ORTEP drawing of $[(Cp^*SiNR)(PMe_3)Sc]_2(\mu,\eta^2,\eta^2\text{-}C_2H_4)$ (5) with 50% probability ellipsoids.

Although the formation of 5 was a surprising result, there is precedent for this type of reactivity in homogeneous Ziegler-Natta catalyst systems based on $Cp_2Ti^{IV}X_2$ and $Cp_2Zr^{IV}X_2$.[17] β-C-H activation to form a dimetalloalkane is believed to be involved in the reduction of $Cp_2Ti(IV)$ to catalytically inactive $Cp_2Ti(III)$ and is perhaps responsible for the aging process of titanium based heterogeneous Ziegler-Natta catalyst systems as well. Since Zr(IV) is more resistant to reduction than Ti(IV), ethylene-bridged products analogous to 5 could be isolated from Cp_2ZrX_2/Al_2Et_6 mixtures and were structurally characterized (Figure 1.4).[18]

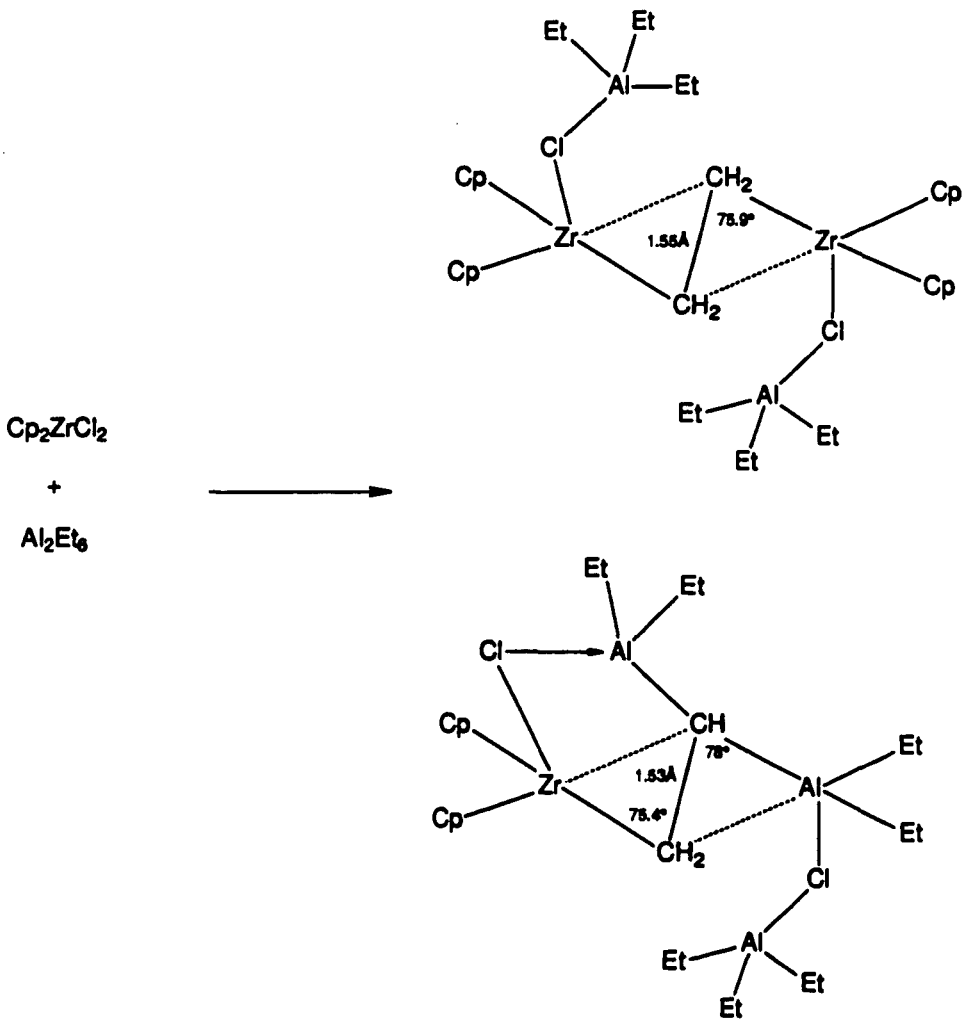

Figure 1.4. Ethylene-Bridged Dimers Isolated from Cp_2ZrCl_2 / Al_2Me_3 Mixture

To elucidate the mechanism of formation of 5, the reaction was followed by low-temperature ^{1}H NMR spectroscopy. We found that at *ca* 0 °C all the ethylene (one equivalent per scandium) was consumed to form a new species, presumably the ethylene insertion product. Because of the fluxionality of this intermediate, a clear spectrum was obtained only by cooling the NMR sample to -90 °C. In addition to the signals for the Cp*SiNR ligand and PMe_3, a broad multiplet at *ca* δ 0.0 corresponding to the α-methylene and a multiplet at *ca* δ 0.96 for the β-methyl group were observed. When the sample was allowed to warm to 25 °C, the insertion intermediate converted to the ethylene-bridged product, 5. The production of half an equivalent of ethane per equivalent of ethylene in this reaction was confirmed by a Toepler experiment, in which 95.5% percent of the theoretical amount of ethane was collected.

The ^{1}H NMR spectrum of compound 5 displays interesting variable temperature behavior. As in the hydride dimer, PMe_3 dissociation is sufficiently rapid that the diastereotopic methyl substituents on the cyclopentadienyl ring and on the silylene bridge of 4 are equivalent in the room temperature ^{1}H NMR spectrum. A slower process resulting in an averaging of the signals of the inequivalent methylene protons of the $-CH_2CH_2-$ bridge is also observed (Figure 1.5).

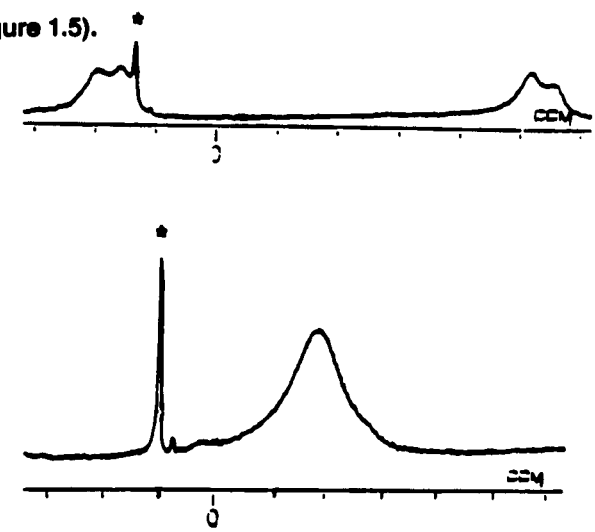

Figure 1.5. a) 400 MHz 1H NMR spectrum of ethylene bridge hydrogens in compound 5 ("frozen out" at ca. -90°C. b) Spectrum after coalescence. (ca. -40°C). Asterisked peak is an impurity.

The exchange of environments of these protons requires the ethylene bridge to, in effect, undergo a 180° flip about the carbon-carbon axis. The mechanism by which this rearrangement occurs is currently unknown. A diastereotopic site exchange rate constant ($k_{exchange}$) at 274°K of 1.6×10^3 sec^{-1} was determined by using coalescence methods. This value is unchanged by the addition of excess phosphine to the solution of the complex. The rate constant corresponds to a $\Delta G^{\ddagger}$ of 12 kcal/mole for the exchange at this temperature.

The Isolation and Structural Characterization of PMe_3-free Scandium Alkyl Dimers, $[(Cp^*SiNR)Sc]_2(\mu\text{-alkyl})_2$.

When 4 is reacted with an equivalent of propene per scandium, a PMe_3-free scandium propyl derivative (6) is formed (Equation 4). An x-ray structure determination of 6 revealed it to be a dimer in the solid state with two three-center, two electron alkyl bridges. A similar PMe_3-free scandium n-butyl derivative (7) is obtained when 1-butene is used instead of propene. Loss of PMe_3 in this case is less facile, so that a few cycles of redissolving the product in toluene and then stripping off the volatiles is necessary to completely remove the PMe_3. A double alkyl-bridged dimer is presumably formed in this case as well.

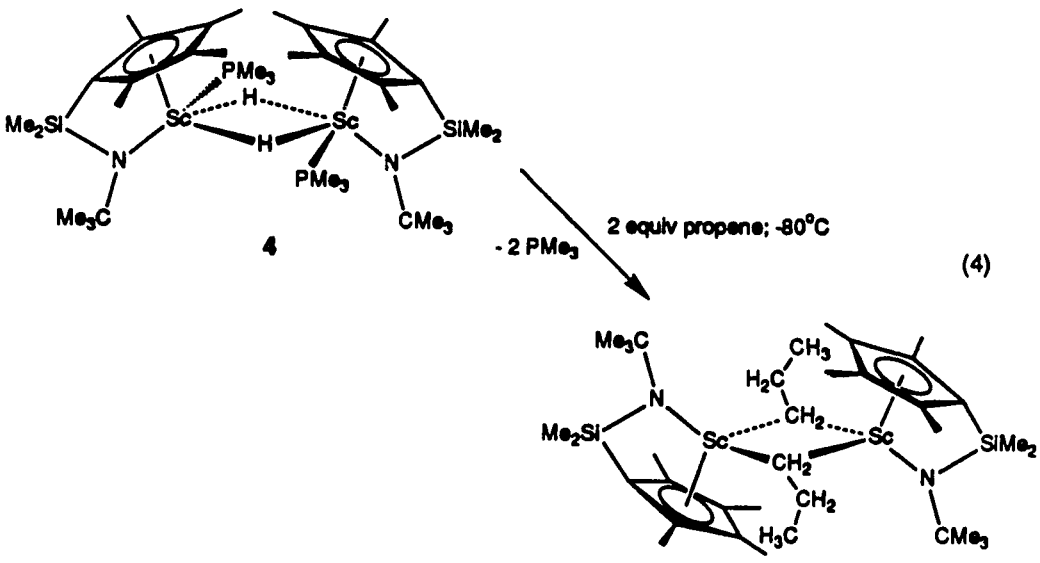

(4)

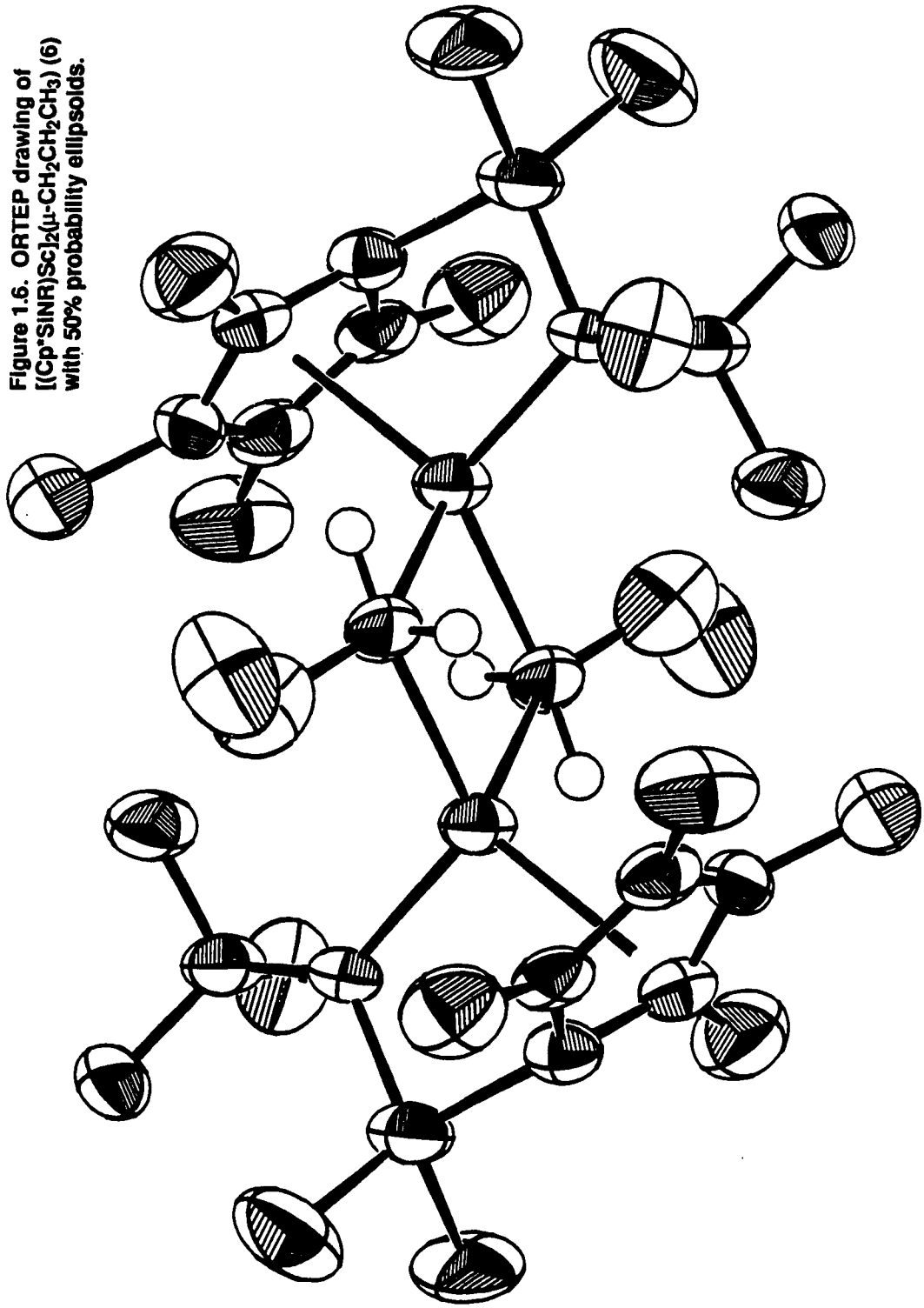

Figure 1.6. ORTEP drawing of [(Cp*SiNR)Sc]$_2$(μ-$CH_2CH_2CH_3$) (6) with 50% probability ellipsoids.

As can be seen from the ORTEP drawing of **6** (Figure 1.6), and in contrast to **4** and **5**, the two halves of the dimer are related by a center of inversion. The Sc-C-Sc bridge angle of 89.4(2)° is considerably more acute than the corresponding Sc-H-Sc bridge angle in **4** (114.1°). This reflects the higher directionality of the carbon sp^3 orbital as compared with the s orbital of the hydride, such that a narrowing of the bridge angle is necessary to maximize orbital overlap. Similar structural trends are evident in other μ-H and μ-alkyl systems. For example, the 114(3)° Y-H-Y' bridge angle in $[(CH_3C_5H_4)_2YH(THF)]_2$[12] contracts to 87.7(3)° in $[Cp_2YMe]_2$,[19] angles surprisingly similar to those found in the scandium systems described here, considering yttrium's larger size. Likewise, the μ-H bridge angle of 103(2)° in the dimethylaluminum hydride dimer[20] contracts to 74.7(4)° when the hydrides are replaced by methyl groups in the trimethylaluminum dimer.[21]

As expected, the atoms connected to the amide nitrogen are coplanar to within ±0.01Å. The bite angle of the chelating Cp*SiNR ligand (102.5°) is slightly smaller than in the Sc-H dimer, and the Sc-N bond distance (2.083(5)Å) is even longer than in the ethylene-bridged complex **5**, although the Si-N bond distance (1.722(6)Å) is about the same.

^1H and ^{13}C NMR data for **6** are consistent with its solid state structure. In the ^1H NMR spectrum, a broad pseudotriplet ($^3J_{HH}$ = 8.6 Hz) is observed upfield at -0.11 ppm for the methylene group next to scandium along with a triplet at δ 1.06 ($^3J_{CH}$ = 6.6 Hz) for the end methyl group. The β-methylene protons form a complex pattern that is partly obscured by the the t-butyl amide resonance. This complexity may be attributed to the diastereotopic nature of the two hydrogens as well as to their coupling to both the α-methylene and γ-methyl hydrogens of the propyl ligand. An almost identical ^1H NMR spectrum is observed for the n-butyl derivative, with the exception of an extra multiplet at 1.38 ppm for the γ-methylene hydrogens.

The ^1H NMR spectrum of the propyl derivative does not change from 25°C to -80°C in toluene-d_8. Upon addition of an equivalent of PMe_3 to the NMR tube, however, an entirely

new set of resonances is observed, probably as a result of PMe_3 coordination to form $(Cp^*SiNR)(PMe_3)ScCH_2CH_2CH_3$. Site exchange of the PMe_3 in the propyl derivative is rapid, so that at -80°C the methyl resonances of the Cp*SiNR ligand are broadened but not resolved into their diastereotopic components. Interestingly, excess PMe_3 appears to enhance the rate of PMe_3 dissociation, such that the ligand resonances are sharp (i.e., in the fast exchange limit) even at -80°C in the presence of five equivalents of PMe_3.

As is common to all our scandium alkyl complexes, the ^{13}C resonance for the α-carbon in both the n-propyl and the n-butyl derivatives is broad and shifted considerably downfield (δ 50.52). This signal appears as a triplet in the proton-coupled spectrum. The five-coordinate bridging geometry of the α-carbon is reflected in the low $^1J_{CH}$ of 103Hz since in non-bridging Sc-alkyl systems sp^3 couplings of *ca* 118-125 Hz are typically observed.[22] There is no evidence for an agostic C-H interaction in these complexes in either the crystal structure of **6** or the IR spectra of **6** and **7**.

Unfortunately, the low solubilities of both the Sc-n-propyl complex and the Sc-n-butyl complex in benzene prevent their solution molecular weight determination. As discussed in Chapter 2, the absence of PMe_3 makes these systems more active olefin polymerization catalysts than the Sc-H dimer.

Reaction of $[(Cp^*SiNR)(PMe_3)Sc(\mu\text{-}H)]_2$ with the Gem-Disubstituted Olefin 2-Methyl-1-Pentene

While dimerization serves as a driving force for PMe_3 loss in the Sc-n-alkyl derivatives mentioned above, bulkier derivatives such as the 2-methylpentyl derivative do not form μ-alkyl bridges as readily and therefore retain PMe_3 in their coordination sphere. $(Cp^*SiNR)(PMe_3)ScCH_2CH(CH_3)CH_2CH_2CH_3$ (**8**) was prepared by treating **4** with an excess of 2-methyl-1-pentene (Equation 5). Our interest in this derivative arose from the question of whether branching can occur in α-olefin polymerization by reinsertion of the olefinic polymer

chain ends (formed in chain transfer by β-H elimination) into the propagating metal alkyl. Since **8** does not react further with 2-methyl-1-pentene, the formation of branched polyolefin in the polymerizations is unlikely.

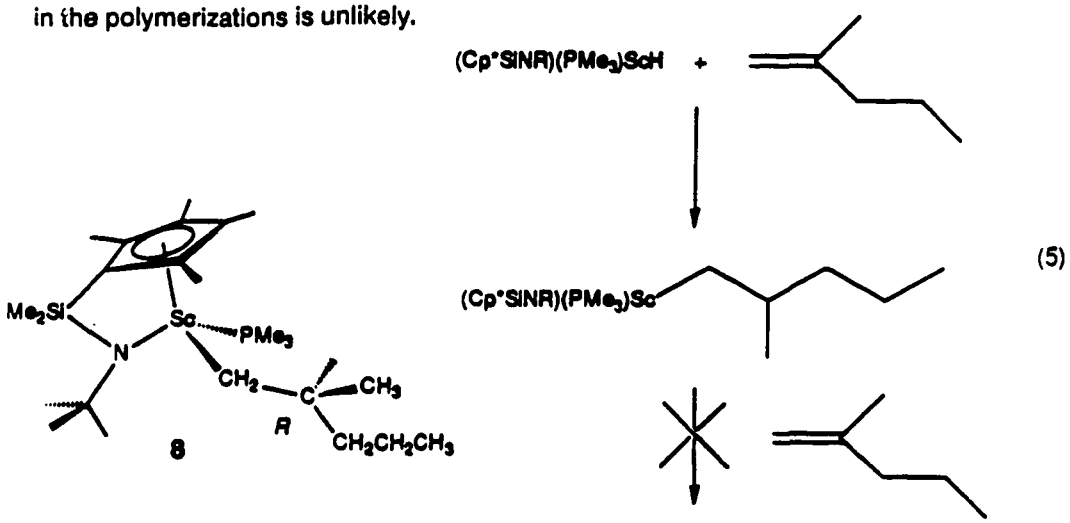

(5)

Although a solution of **8** yields a gold-brown oil upon removal of solvent, cooling a concentrated solution of the compound in pentane affords white microcrystalline material in reasonable yield (50%). Because of the fluctionality of **8**, presumably involving phosphine site exchange, its room-temperature ^{1}H NMR spectrum is quite broad and uninterpretable. Upon cooling the sample to -80°C, the spectrum becomes clearer, revealing the presence of two species in roughly equal amounts. It is likely that the two sets of resonances belong to two diastereomers since there are two stereocenters in the system (the Sc center and the β-carbon of the alkyl substituent). The signals of the alkyl substituent are difficult to sort out; however, hydrogenation of **8** affords 1.1 equivalents of 2-methylpentane relative to Sc, as measured by ^{1}H NMR (using hexamethyldisiloxane as a standard). The formulation of **8** is also confirmed by elemental analysis. Ebulliometric molecular weight analysis of the species in solution was unsuccessful, presumably because of the dissociable PMe_3, and after standing for a week in benzene solution, the complex had decomposed. As expected, although **8** does not further insert 2-methyl-1-pentene, it does polymerize propene.

The Reaction of Styrene with $[(Cp^*SiNR)Sc(PMe_3)]_2(\mu\text{-}H)_2$

When an excess of styrene is added to the scandium hydride complex **3**, instead of the formation of polymer, the reaction stops after two insertions. The product is isolated as a bright orange-yellow solid (**9**) in 80% yield. Cryogenic MW analysis of the product indicated that it was a monomer and that two styrenes had been incorporated by 4 (Exptl MW: 596 ±36; Calcd MW: 580). Efforts to grow crystals of this material for an x-ray structure were unsuccessful; however, the coupled ^{13}C NMR spectrum of material is consistent with the structure shown in Equation 6.

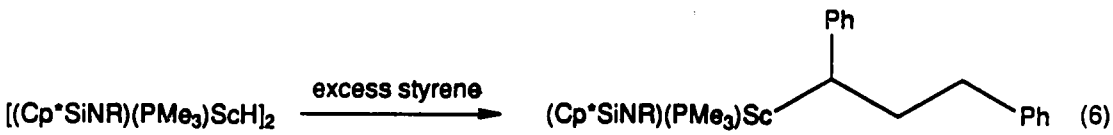

(6)

Deuterium-labeling studies were also performed but were difficult to interpret. The orientation of the second inserted monomer was probed by cleaving **9** with D_2 and locating the deuterium in the organic product by ^2H NMR. Likewise, the orientation of the first inserted monomer was probed by examining the ^2H NMR of the double-insertion product starting from the scandium deuteride, **9**-d_1. In both cases the major deuterium resonances appeared to be benzylic, appearing at *ca* δ 2.4 in the first case and *ca* δ 2.6 in the second; there were also broad resonances upfield of these signals, which might be assigned to non-benzylic positions. Thus, while the primary scandium product contains head-to-head coupled styrenes, some minor regioisomers may be formed as well. This is also indicated by the ^{13}C NMR of a second crop of isolated product, which contains a few small peaks besides those of the major isomer **9**. The head-to-head coupling of the two styrene molecules contrasts with the highly regioregular head-to-tail coupling observed with propene and may be attributed to the ability of the phenyl substitutuent to stabilize the partial

negative charge at the incipient α-carbon in the transition state for olefin insertion.[4,23,24] Steric interference from the "2-1" orientation of the second inserted styrene unit may be the cause for reaction stopping after two insertions. Reaction of **4** with a single equivalent of styrene was not clean and appeared to produce a mixture that contained some of the double insertion product **9**.

Synthesis of the Chiral System (^{tBu}CpSiNR)ScR

Among our goals in studying these Ziegler-Natta model systems is to understand the detailed interactions responsible for stereospecific olefin insertion to form either isotactic or syndiotactic polymer. We have therefore embarked on further modifications of the basic silylene-bridged, monocyclopentadienyl-amido ligand-framework in order to study the stereodirecting effect of the ligand on the polymerization.

As demonstrated with Brintzinger's *ansa*-metallocene complexes,[25] homogeneous Ziegler-Natta catalysts with chiral ligand frameworks can be effective at producing highly isotactic polymers. There are a number of ways to modify the Cp*SiNR ligand to make the scandium complex chiral. Asymmetry may be introduced at the amide group, at the silylene bridge or at the cyclopentadienyl ring. We thought that an asymmetrically substituted cyclopentadienyl ring would have the greatest influence on the active site of the metal. Our first effort in this direction has been the synthesis of the chiral system (^{tBu}CpSiNR)ScR [^{tBu}CpSiNR = {(η^5-$C_5H_4CMe_3$)Me_2Si(η^1-$NCMe_3$)}]. Preliminary results of our synthetic efforts with this new ligand system are discussed below.

The ligand ($C_5H_4CMe_3$)$SiMe_2$($NCMe_3$) is prepared in the same manner as its tetramethylcyclopentadienyl analog. ($C_5H_4CMe_3$)$SiMe_2Cl$ is prepared by a single ring substitution on $SiMe_2Cl_2$ and the remaining chloride is metathesized by Li($NHCMe_3$) (Equation 7).

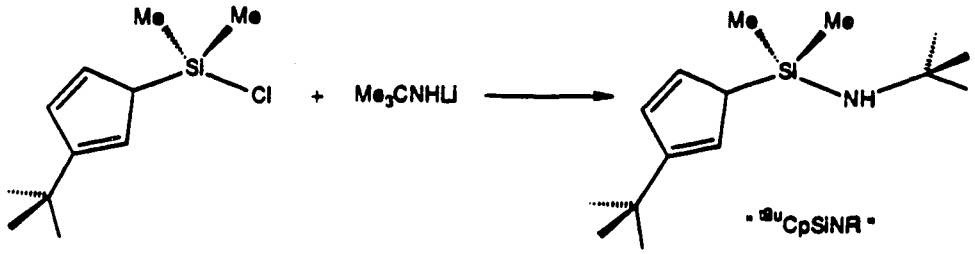

(7)

Deprotonation of the ligand with two equivalents of n-butyllithium in petroleum ether affords the dimetallated ligand, not as a powder, but as a polymeric material, which is isolated as a glassy solid upon complete removal of solvent. Although the ^{1}H NMR spectrum of $Li_2(^{tBu}CpSiNR)$ in benzene-d_6 is quite broad, a clear spectrum is produced upon reaction of the ligand with $ScCl_3(THF)_3$ to form $(^{tBu}CpSiNR)(THF)ScCl$ (12). Removal of THF from this compound is not accomplished as easily as for $(Cp^*SiNR)ScCl \cdot (THF)_x \cdot (LiCl)_n$. Heating the compound *in vacuo* to temperatures above 180°C is necessary before THF is liberated and complete removal of THF by this method is difficult. Replacement of the chloride with bulky ligands (e.g., -$CH(TMS)_2$) and chelating ligands (e.g., acetylacetonate) does not displace the coordinated THF. Reaction of 12 with $LiCH_2PMe_2$ in toluene, however, affords a precipitate that analyzes reasonably well for THF-free $[(Cp^*SiNR)ScCH_2PMe_2]_x$ (13) coprecipitated with LiCl. The ^{1}H NMR spectrum of 13 in THF-d_8 is complicated and indicates the presence of a mixture of species. Although 13 cannot be hydrogenolyzed, it does react with an equivalent of HCl gas to afford $(^{tBu}CpSiNR)(PMe_3)ScCl$ (14). The chloride derivative 14 is isolated in 53% overall yield based on $ScCl_3(THF)_3$ starting material (Scheme V). Ebulliometric analysis indicates that 14 is a monomer (Calcd MW: 406.1; Exptl MW: 476). Heating 14 to 120°C *in vacuo* for a few hours liberates PMe_3 to afford $[(^{tBu}CpSiNR)ScCl]_x$ (15).

A series of NMR tube reactions revealed that 14 reacts with a variety of alkyllithium reagents to cleanly form the phophine-coordinated scandium alkyl derivatives. We were able to isolate crystals of $(^{tBu}CpSiNR)(PMe_3)ScCH_2SiMe_3$ (16) for an x-ray structure analysis.

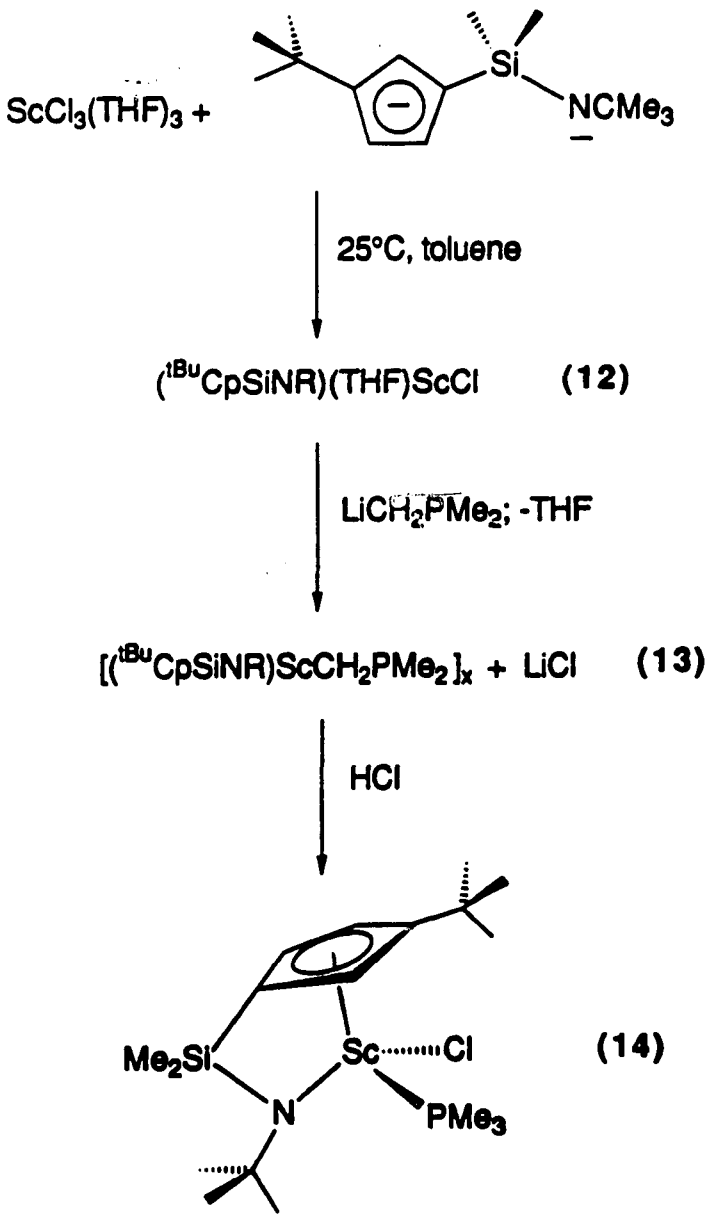

Scheme V. Synthesis of (^{tBu}CpSiNR)(PMe_3)ScCl

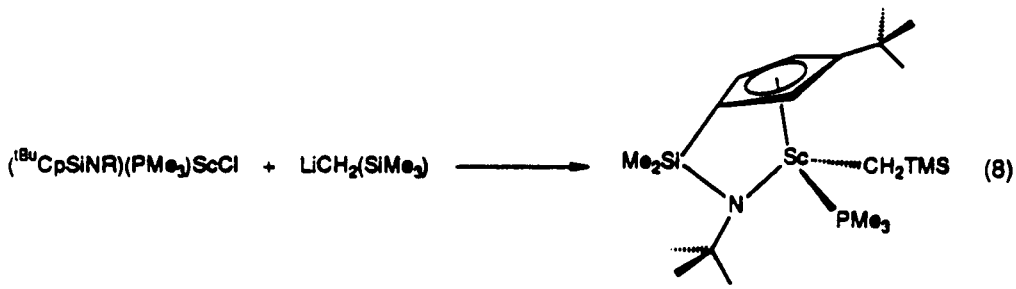

(8)

The ORTEP drawing of the complex is shown in Figure 1.7. The complex is a monomer with a distorted, three-legged piano stool structure. Only one of the two possible diastereomers, with the PMe_3 ligand positioned away from the t-butyl substituent on the Cp ring, is present in the structure. The bite angle (104.1°) of the ^{tBu}CpSiNR ligand is comparable to that of the Cp*SiNR system. The Sc-P bond length of 2.767(1) is shorter than that found in the two structurally characterized phosphine-coordinated (Cp*SiNR)Sc complexes (4 and 5). Once again, the amide nitrogen is planar, and the Sc-N (2.044(3)Å) and Si-N (1.731(3)Å) bond lengths are comparable to those found in (Cp*SiNR)Sc complexes. Preliminary observations indicate that the PMe_3 in 16 is non-labile and that the single diastereomer of 16 found in the crystal structure is formed directly from a single diastereomer of the chloride derivative 14. For instance, reaction of 14 with phenyllithium produces only a single diastereomer of (^{tBu}CpSiNR)(PMe_3)ScC_6H_5 (^{1}H NMR). When a benzene-d_6 solution of this "kinetic" isomer is heated to 80°C, it forms *ca* a 13:1 mixture of diasteriomers, in which the second, thermodynamically preferred isomer predominates. Heating a solution of either 14 or 16 in C_6D_6 at 80°C does not lead to any new resonances that might be attributed to the second diastereomer. A strong thermodynamic preference for the one isomer is likely in these cases. Addition of PMe_3 to the phosphine-free chloride derivative, 15, regenerates the ^{1}H spectrum for 14; again only the single diastereomer is observed.

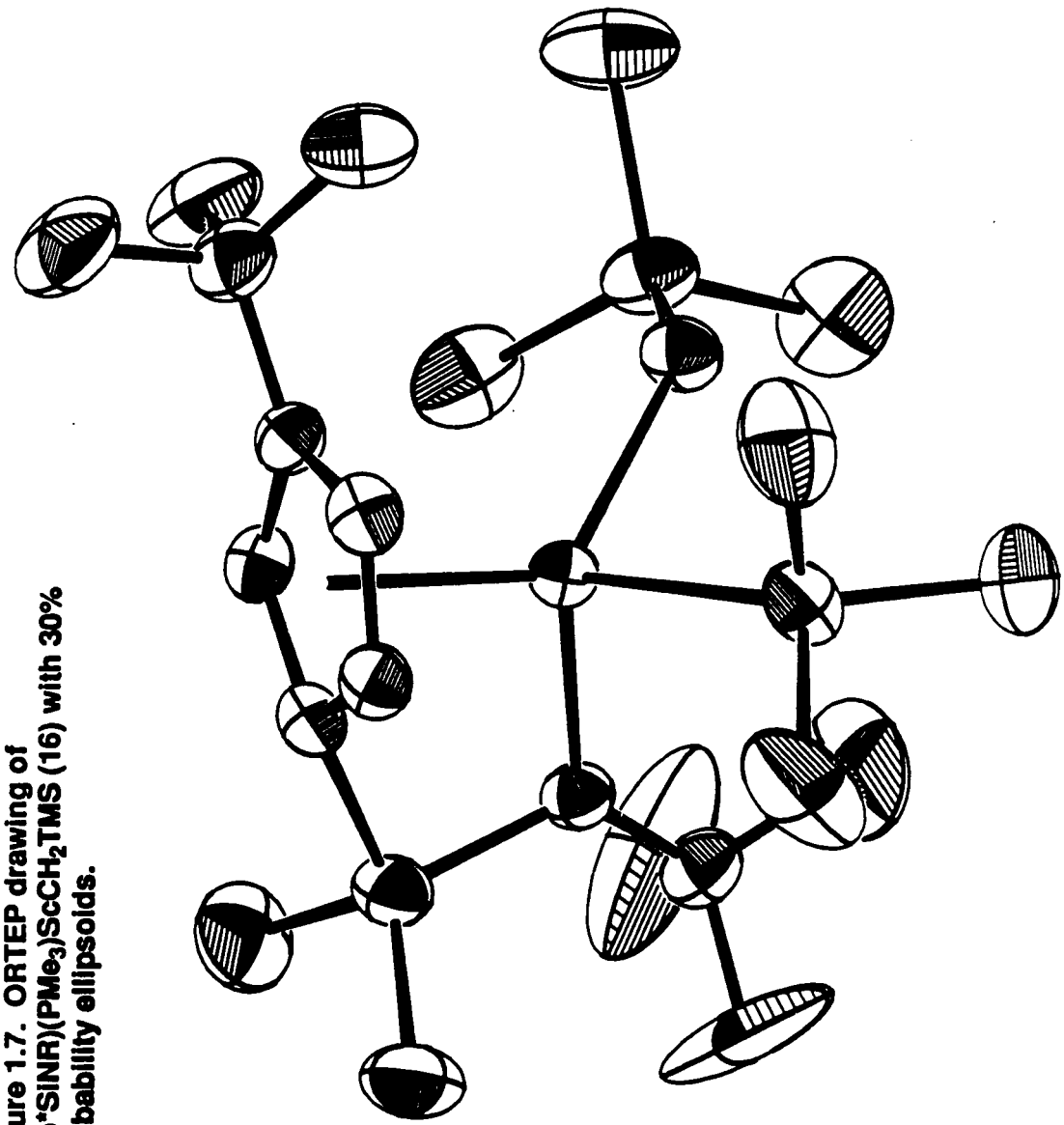

Figure 1.7. ORTEP drawing of $(Cp^*SiNR)(PMe_3)ScCH_2TMS$ (16) with 30% probability ellipsoids.

The inability of compound **16** to polymerize propene is attributed to the tight binding of PMe_3 by the complex. Polyethylene is formed with this system; however, only a small percentage of the material initiates the polymerization.

When either (^{tBu}CpSiNR)(PMe_3)ScCl (**14**) or [(^{tBu}CpSiNR)ScCl]$_x$ (**15**) is reacted with MeLi, a material analyzing correctly for [(^{tBu}CpSiNR)ScMe]$_x$ (**17**) is formed (Equation 9). The tendency of this material to precipitate from a benzene solution has prevented the measurement of its solution molecular weight. The compound exhibits a broad, ill-defined ^{1}H NMR spectrum; however, upon addition of PMe_3 to the solution, a sharp ^{1}H spectrum consistent with the species (^{tBu}CpSiNR)(PMe_3)ScMe is observed. Apparently, [(^{tBu}CpSiNR)ScMe]$_x$ is an oligomer that can be dissociated by the coordination of PMe_3. While [(^{tBu}CpSiNR)ScMe]$_x$ polymerizes α-olefins (albeit slowly), addition of an equivalent of PMe_3 to the complex shuts down polymerization completely.

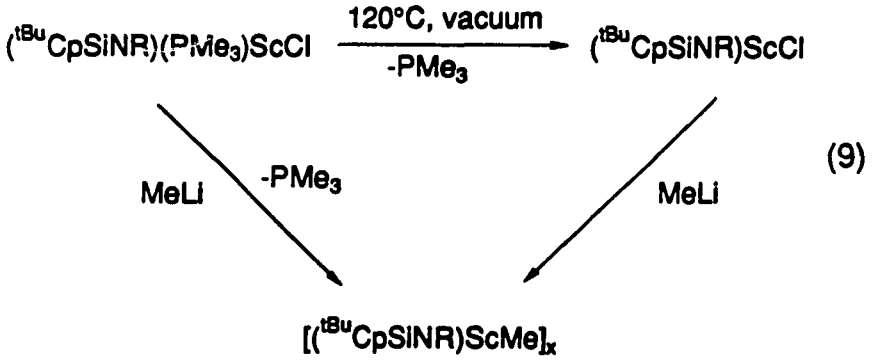

(9)

Most of the phosphine-free alkyl derivatives of this scandium system appear to form oligomers, since intractable oils with complicated ^{1}H NMR spectra are generally obtained. As with [(^{tBu}CpSiNR)ScMe]$_x$, addition of PMe_3 to these products results in a clear ^{1}H NMR spectra. Thus, while a number of phosphine-free alkyl derivatives of the type [(^{tBu}CpSiNR)ScR]$_x$ may be prepared, they are ill-defined; hence, their utility as model systems is limited. Although the synthetic possibilities using this ligand system have not

a bis(t-butyl)cyclopentadienyl amido complex, would be a more suitable target.

Summary

Synthetic entry into the monocyclopentadienyl amido complexes (Cp*SiNR)ScR and (^{tBu}CpSiNR)ScR has been described. Because of the reduced steric bulk of the ligand framework in these compounds, the scandium is more open to external substrates. The increased "exposure" of the scandium center serves to enhance its reactivity, hence the ability of these complexes to polymerize α-olefins. It also necessitates the development of special synthetic routes and "back-door" approaches for removing tightly coordinating Lewis bases that satisfy the demand of the coordinatively and electronically unsaturated scandium for electrons. Thus, there is a tradeoff between reactivity and ease of synthesis in working with these highly Lewis acidic organoscandium complexes. Historically we have used the bulky Cp* ligand in our labs to sterically stabilize highly unsaturated transition metal centers against the formation of unreactive oligomers. We have found, however, that despite the tendency of the less bulky monocyclopentadienyl amido scandium complexes to oligomerize, these complexes display greater olefin-insertion activity than our original monomeric Cp^*_2ScR complexes Therefore, our present strategy with scandium is to fine tune the sterics of the ligand environment to allow as much access of substrate to the metal as possible while preventing the formation of unreactive polynuclear compounds.

Table I. ^1H NMR Data for (Cp*SiNR)Sc Complexes.[a]

Compound	Assignment	δ (ppm)	Coupling (Hz)
$(Me_4CpH)SiMe_2(NCMe_3)$ (90 MHz, C_6D_6)	$(CH_3)_4CpH$	2.0 s, 1.8 s	
	$(CH_3)_4CpH$	2.7	
	$(CH_3)_3CN$	1.1 s	
	$(CH_3)_2Si$	0.1 s	
$[(Cp^*SiNR)ScCl]_x$ (2) (90 MHz, C_6D_6)	$[C_5(CH_3)_4Si]$	2.0 s, 1.9 s	
	$(CH_3)_3CN$	1.3 s	
	$(CH_3)_2Si$	0.7 s	
$(Cp^*SiNR)ScCH\{Si(CH_3)_3\}_2$ (3) (400MHz, C_6D_6)	$[C_5(CH_3)_4Si]$	2.05 s, 1.91s	
	$(CH_3)_3CN$	1.3 s	
	$(CH_3)_2Si$	0.66 s	
	$CH\{Si(CH_3)_3\}_2$	0.14 s	
	$CH\{Si(CH_3)_3\}_2$	-0.57 s	
$[(Cp^*SiNR)(PMe_3)Sc]_2(\mu\text{-}H)_2$ (4) (400 MHz, toluene-d_8)	$[C_5(CH_3)_4Si]$	2.21 s, 2.06 s	
	$(CH_3)_3CN$	1.28 s	
	$(CH_3)_2Si$	0.68 s	
	$(CH_3)_3P$	0.89 s	
	Sc-H	4.45 s, br	
$[(Cp^*SiNR)(PMe_3)Sc]_2(\mu\text{-}H)_2$ (4) (400 MHz, toluene-d_8, -80°C)	$[C_5(CH_3)_4Si]$	2.36 s, 2.16 s 1.99 s, 1.90 s	
	$(CH_3)_3CN$	1.31 s	
	$(CH_3)_2Si$	0.84 s, 0.74 s	
	$(CH_3)_3P$	0.89 d	$^2J_{PH} = 4$
	Sc-H	4.15 s, br	
$[(Cp^*SiNR)(PMe_3)Sc]_2(\mu\text{-}C_2H_4)_2$ (5) (400 MHz, toluene-d_8)	$[C_5(CH_3)_4Si]$	2.33 s, 1.89 s	
	$(CH_3)_3CN$	1.24 s	
	$(CH_3)_2Si$	0.79 s	
	$(CH_3)_3P$	0.88 d	$^2J_{PH} = 3.9$
	C_2H_4	-0.17 s	
$[(Cp^*SiNR)(PMe_3)Sc]_2(\mu\text{-}C_2H_4)_2$ (5) (400 MHz, toluene-d_8, -90°C)	$[C_5(CH_3)_4Si]$	2.46 s, 2.35 s, 1.89 s,1.86 s	
	$(CH_3)_3CN$	1.3 s	
	$(CH_3)_2Si$	0.98 s, 0.90 s	
	$(CH_3)_3P$	0.88 d	$^2J_{PH} = 3.9$
	C_2H_4	0.18 d, br, -0.54 d, br	

[(Cp*SiNR)Sc]$_2$(μ-$CH_2CH_2CH_3$)$_2$ (6) (400 MHz, C_6D_6)	[$C_5(CH_3)_4Si$]	2.17 s, 1.91 s
	(CH_3)$_3$CN	1.25 s
	(CH_3)$_2$Si	0.72 s
	$CH_2CH_2CH_3$	-0.11 t $^3J_{HH}$ = 8.6
	$CH_2CH_2CH_3$	*ca.* 1.5 m[b], *ca.* 1.2 m[b]
	$CH_2CH_2CH_3$	1.06 t $^3J_{HH}$ = 6.6
[(Cp*SiNR)(PMe$_3$)Sc$CH_2CH_2CH_3$ (400 MHz, toluene-d_8)	[$C_5(CH_3)_4Si$]	2.10 s, 2.05 s
	(CH_3)$_3$CN	1.4 s
	(CH_3)$_2$Si	0.66 s
	P(CH_3)$_3$	0.74 br
	$CH_2CH_2CH_3$	-0.094 m
	$CH_2CH_2CH_3$	*ca.* 1.67 m
	$CH_2CH_2CH_3$	1.15 ≈t
[(Cp*SiNR)Sc]$_2$(μ-$CH_2CH_2CH_2CH_3$)$_2$ (7) (400 MHz, C_6D_6)	[$C_5(CH_3)_4Si$]	2.18 s, 1.92 s
	(CH_3)$_3$CN	1.28 s
	(CH_3)$_2$Si 0.74 s	
	$CH_2CH_2CH_2CH_3$	-0.11 t $^3J_{HH}$ ≈ 9
	$CH_2CH_2CH_2CH_3$	*ca.* 1.4 m[b], *ca.* 1.2 m[b]
	$CH_2CH_2CH_2CH_3$	1.38 m[c]
	$CH_2CH_2CH_2CH_3$	0.96 t $^3J_{HH}$ = 7.2
(Cp*SiNR)(PMe$_3$)ScR (8)[d] R = $CH_2CH(CH_3)CH_2CH_2CH_3$ (500MHz, toluene-d_8, -80 °C)	[$C_5(CH_3)_4Si$]	(a: 2.43 s, 1.90 s) (b: 2.33 s, 2.34 s, 1.85, 1.84)
	(CH_3)$_3$CN	1.47
	(CH_3)$_2$Si	(a: 0.88 s) (b: 0.704 s, 0.698 s)
	(CH_3)$_3$P	0.5 d $^2J_{PH}$ = 4.4
	ScCH_2-	a&b: (0.14 m, -0.17 m; -0.08 m)
(Cp*SiNR)(PMe$_3$)ScR' (9) R' = $CH(C_6H_5)CH_2CH_2CH_2(C_6H_5)$ (400MHz, C_6D_6)	[$C_5(CH_3)_4Si$]	2.25 s, 2.10 s, 2.06 s, 1.93 s
	(CH_3)$_3$CN	1.27 s
	(CH_3)$_2$Si	0.77 s, 0.64 s
	(β, γ, δ)CH_2	(1.85 m, 1.65 m) 2.69 m, 2.02 m[e]
	α-CH_2	not assigned
	aryl region	6.53 d, 5.59 t, 7.3 t, 7.0-7.2 multiplets

[a]^{1}H (90Hz, 400 MHz and 500MHz)NMR spectra were obtained at ambient temperature unless otherwise stated. Chemical shifts (δ) are reported in ppm using either tetramethylsilane or residual protons in the solvent as an internal reference.

[b]Overlap with resonance for (CH_3)$_3$CN precludes accurate assignment of these signals.

[c]Signal appears as a quartet overlapping the β-CH_2 resonance.

[d]Two diastereomers (a and b) are present in roughly equal amounts. The chemical shifts of the alkyl substituent could not be assigned with confidence.

[e]Absolute assignments have been based on chemical shift and coupling behavior and have not been confirmed by a homonuclear decoupling experiment.

Table II. ^{13}C and ^{31}P data for (Cp*SiNR)Sc Complexes.[a]

Compound	Assignment	δ ^{13}C (ppm)	δ ^{31}P (ppm)	Coupling (Hz)
[(Cp*SiNR)(PMe$_3$)Sc(μ-H)]$_2$ (3) (toluene-d_8)	*P*Me$_3$		-54.1 (20°C) -43.7; -55.6 (4:1; -66°C)	
[(Cp*SiNR)(PMe$_3$)Sc(μ-$^{13}C_2H_4$)]$_2$ (4) (toluene-d_8)	*C*H$_2$*C*H$_2$	35.15		J_{CH} =142
	*P*Me$_3$		-42.2 (16°C) -39.37(-50°C)	
[(Cp*SiNR)Sc(μ-CH$_2$CH$_2$CH$_3$)]$_2$ (5) (toluene-d_8)	α-*C*H$_2$	50.5		J_{CH} =102
	β-*C*H$_2$	20.8		J_{CH} =124
	γ-*C*H$_3$	21.2		J_{CH} =126
	C$_5$(*C*H$_3$)$_5$Si	14.8; 12.6		J_{CH} =125; 126
	C$_5$(CH$_3$)$_5$Si	111.8; 110.7		
	(*C*H$_3$)$_3$CN	36.7		J_{CH} =125
	(CH$_3$)$_3$*C*N	55.2		
	(*C*H$_3$)$_2$Si	8.0		J_{CH} =118

Compound	Assignment	δ ^{13}C (ppm)	δ ^{31}P (ppm)	Coupling (Hz)
[(Cp*SiNR)Sc(μ-$CH_2CH_2CH_2CH_3$)]$_2$ (6) (toluene-d_8)	α-CH_2	46.7		J_{CH} =100.6
	β, γ-CH_2	29.6; 30.5		J_{CH} =122; 125
	δ-CH_3	14.0		J_{CH} =124
	$C_5(CH_3)_5Si$	14.8; 12.5		J_{CH} =125; 125
	$C_5(CH_3)_5Si$	113.9; 111.6		
	$(CH_3)_3CN$	36.6		J_{CH} =124
	$(CH_3)_3CN$	55.2		
	$(CH_3)_2Si$	8.0		J_{CH} =118
(Cp*SiNR)(PMe_3)ScR (7) R = -$CH_2CH(CH_3)CH_2CH_2CH_3$ (toluene-d_8)	PMe_3		-51.5 (-66°C)	
(Cp*SiNR)(PMe_3)ScR (8) R = -$CH(C_6H_5)CH_2CH_2CH_2(C_6H_5)$ (C_6D_6)	PMe_3		-45.9 (-50°C)	
	α-CH	60.6		J_{CH} =120
	β, γ, δ-CH_2	36.8; 33.5; 30.7		J_{CH} =125; 125; 120
	$C_5(CH_3)_5Si$	14.9; 14.6; 12.6; 11.8		J_{CH} =125; 125; 125
	$C_5(CH_3)_5Si$	108.1		

Compound	Assignment	δ ^{13}C (ppm)	δ ^{31}P (ppm)	Coupling (Hz)
(Cp*SiNR)(PMe_3)ScR **(8) (cont'd)** R = -$CH(C_6H_5)CH_2CH_2CH_2(C_6H_5)$	$(CH_3)_3CN$	35.5		J_{CH} =123
	$(CH_3)_3CN$	55.9		
	$(CH_3)_2Si$	7.4; 8.1		J_{CH} =118; 118
	$P(CH_3)_3$	14.2		J_{CH} =129
	$2(C_6H_5)$[b]	151.5		
		143.6		
		117.8		J_{CH} = 158
		121.5		J_{CH} = 158
		125.7		J_{CH} = 158
		126		J_{CH} = 158
		130.3		J_{CH} = 158

[a] ^{13}C NMR spectra were obtained at ambient temperature at an observation frequency of 100.38MHz. Chemical shifts are reported in ppm relative to tetramethylsilane and were referenced to signals from the solvent. ^{31}P spectra were obtained at the temperatures indicated and are reported in ppm relative to an external H_3PO_4 reference.

[b] Some peaks are obscured by solvent signals.

Table III. ^{1}H and ^{31}P NMR Data for (^{tBu}CpSiNR)Sc Complexes.[a]

Compound	Assignment	δ(ppm)	Coupling(Hz)
(tBu-CpH)$SiMe_2Cl$	(tBu-C_5H_3)H	6.62 d, 6.4 d, 6.05 s	
(^{1}H: C_6D_6, 400MHz)	(tBu-C_5H_3)*H*	3.6 s	
	$(CH_3)_3C$	1.12 s	
	$(CH_3)_2Si$	0.06 s, 0.07 s	
(tBu-CpH)$SiMe_2NCMe_3$	(tBu-C_5H_3)H	6.5 d, 6. d, 6.0 s	
(^{1}H: C_6D_6, 500MHz)	(tBu-C_5H_3)*H*	3.1 s	
	$(CH_3)_3C$	1.1 s	
	$(CH_3)_3CN$	0.9 s	
	$(CH_3)_2Si$	-0.2 s	
(^{tBu}CpSiNR)(THF)ScCl (11)	$[C_5H_3(C(CH_3)_3)Si]$	6.42 m, 6.36 m, 6.20 m	
(^{1}H: C_6D_6, 500MHz)	$[C_5H_3(C(CH_3)_3)Si]$	1.46 s	
	$(CH_3)_3CN$	1.32 s	
	$(CH_3)_2Si$	0.69 s, 0.65 s	
	C_4H_8O(THF)	3.46 m, 1.03 m	
(^{tBu}CpSiNR)(PMe_3)ScCl (13)	$[C_5H_3(C(CH_3)_3)Si]$	6.52 m, 6.37 m, 6.03 m	
(^{1}H: C_6D_6, 500MHz)	$[C_5H_3(C(CH_3)_3)Si]$	1.44 s	
	$(CH_3)_3CN$	1.32 s	
	$(CH_3)_2Si$	0.54[b] s	
	$(CH_3)_3P$	0.68 d	$^2J_{PH}$ = 5.7
(^{31}P: C_6D_6, 36.2MHz)	$(CH_3)_3P$	-44	
[(^{tBu}CpSiNR)ScCl]$_x$ (14)	$[C_5H_3(C(CH_3)_3)Si]$	6.67 m, 6.60 m, 6.22 m	
(^{1}H: C_6D_6, 90MHz)	$[C_5H_3(C(CH_3)_3)Si]$	1.35	
	$(CH_3)_3CN$	1.31	
	$(CH_3)_2Si$	0.70, 0.57	
(^{tBu}CpSiNR)(PMe_3)ScCH_2TMS (15)	$[C_5H_3(C(CH_3)_3)Si]$	6.47 m, 6.26 m, 5.8 m	
(^{1}H: C_6D_6, 400MHz)	$[C_5H_3(C(CH_3)_3)Si]$	1.46 s	
	$(CH_3)_3CN$	1.40 s	
	$(CH_3)_2Si$	0.72 s, 0.55 s	
	$(CH_3)_3P$	0.59 d	$^2J_{PH}$ = 5.4
	CH_2SiMe_3	0.16 d, 0.60 d	J_{CH} = 11
(^{31}P: toluene-d_8, 36.2MHz)	$(CH_3)_3P$	-48	

[(^{tBu}CpSiNR)ScCH$_3$]$_x$ (16)	[C_5H_3(C(CH$_3$)$_3$)Si]	6.4 br	
(^{1}H: C_6D_6, 400MHz)	[C_5H_3(C(CH_3)$_3$)Si]	1.42 br	
	& (CH_3)$_3$CN		
	(CH_3)$_2$Si	0.75 br	
	ScCH_3	-0.27	
(^{tBu}CpSiNR)(PMe$_3$)ScCH$_3$	[C_5H_3(C(CH$_3$)$_3$)Si]	6.42 m, 6.29 m, 5.74 m	
(^{1}H: C_6D_6, 400MHz)	[C_5H_3(C(CH_3)$_3$)Si]	1.36 s	
	(CH_3)$_3$CN	1.43 s	
	(CH_3)$_2$Si	0.68 s, 0.49 s	
	CH_2SiMe$_3$	0.16 d, 0.60 d	J_{CH} = 11
	(CH_3)$_3$P	0.71 d	$^2J_{PH}$ = 3.8
	ScCH_3	-0.45	
(^{31}P: toluene-d_8, 36.2MHz)	(CH_3)$_3P$	-51	
(^{tBu}CpSiNR)(PMe$_3$)ScC_6H_5 (17a)[c]	[C_5H_3(C(CH$_3$)$_3$)Si]	6.6 m, 6.5 m, 5.9 m	
(^{1}H: C_6D_6, 400MHz)	[C_5H_3(C(CH_3)$_3$)Si]	1.27 s	
	(CH_3)$_3$CN	1.15 s	
	(CH_3)$_2$Si	0.81 s, 0.59 s	
	(CH_3)$_3$P	0.68 d	$^2J_{PH}$ = 5.2
	ScC_6H_5	7.49 d, 7.29 t, 7.22 ≈t	
(^{tBu}CpSiNR)(PMe$_3$)ScC_6H_5 (17b)[c]	[C_5H_3(C(CH$_3$)$_3$)Si]	6.6 m, 6.3 m, 5.9 m	
(^{1}H: C_6D_6, 400MHz)	[C_5H_3(C(CH_3)$_3$)Si]	1.46 s	
	(CH_3)$_3$CN	1.29 s	
	(CH_3)$_2$Si	0.59[b] s	
	(CH_3)$_3$P	0.68 d	$^2J_{PH}$ = 5.2
	ScC_6H_5	7.49 d, 7.29 t, 7.22 ≈t	

[a] ^{1}H and ^{31}P NMR spectra were obtained at ambient temperature unless otherwise stated. ^{1}H chemical shifts (δ) are reported in ppm using either tetramethylsilane or residual protons in the solvent as an internal reference. ^{31}P spectra are referenced to an H_3PO_4 external standard.

[b] Other resonance for (CH_3)$_2$Si believed to be obscured by P(CH_3)$_3$.

[c] Chemical shift data for both diastereomers are reported. Isomer a is the kinetically formed isomer and is isolated from the reaction of 13 with PhLi. Isomer b is the thermodynamically preferred isomer (*ca* 13:1), which has not been isolated but is formed upon heating a in solution.

Table IV. Crystal and Intensity Collection Data for $[(Cp^*SiNR)(PMe_3)ScH]_2$ (4).

Formula: $ScPSiNC_{18}H_{37}\cdot C_7H_8$	Formula Weight: 463.66
Crystal Color: pale yellow	Habit: irregular
$a = 21.238(3)$Å	
$b = 11.470(2)$Å	$\beta = 113.16(1)^\circ$
$c = 22.253(3)$ Å	
$v = 4984.0(14)$ Å^3	$z = 8$ (4 dimers)
density = 1.24 g cm^{-3}	
$\lambda = 0.71073$ Å	T: 22°
Graphite monochromator	
Space group: C2/c	Absences: hkl, $h+k=2n+1$; h0l, $l=2n+1$
Crystal Size: .11×.13×.23 mm	$\mu = 4.26$ cm^{-1} ($\mu r_{max} = 0.122$)
CAD-4 Diffractometer	ω scan
2θ range: 2°-40°	Octants collected: $\pm h, \pm k, l$
Number reflections measured: 8166	
Number of independent reflections: 2313	
Number with $F_o^2 > 0$: 2164	
Number with $F_o^2 > 3\sigma(F_o^2)$: 1678	
Goodness of fit for merging data: 0.97	
Final R-index: 0.051	
Final goodness of fit: 1.53	

Table V. Final Parameters for Compound 4

x, y, z and $U_{eq}{}^{a} \times 10^{4}$

Atom	x	y	z	U_{eq} or B
Sc	847(.3)	599(.6)	2859(.3)	387(2)
Si	2032(1)	−263(1)	2662(1)	594(3)
P	1073(.5)	258(.9)	4263(.5)	556(3)
N	1388(1)	−858(2)	2803(1)	443(8)
C1	1782(2)	1286(3)	2676(2)	438(11)
C2	1831(2)	1883(3)	3278(2)	456(12)
C3	1346(2)	2758(3)	3104(2)	466(12)
C4	989(2)	2703(3)	2395(2)	479(13)
C5	1251(2)	1809(3)	2132(2)	463(11)
C7	2370(3)	1772(7)	3972(3)	714(19)
C8	1330(4)	3688(6)	3599(4)	812(22)
C9	477(3)	3558(6)	1973(4)	796(20)
C10	1021(4)	1547(7)	1383(3)	767(20)
C11	2874(3)	−548(7)	3314(5)	1197(32)
C12	2096(5)	−685(7)	1844(5)	1055(24)
C13	1827(3)	−418(9)	4870(4)	924(22)
C14	464(3)	−656(6)	4404(3)	722(17)
C15	1011(4)	1562(5)	4724(3)	793(19)
C16	1282(2)	−2130(4)	2815(3)	618(13)
C17	835(4)	−2364(5)	3186(4)	855(22)
C18	959(4)	−2604(6)	2088(4)	936(23)
C19	1923(3)	−2791(6)	3201(5)	1127(28)

Table V. (Cont'd)

C20	5041(10)	1007(9)	359(6)	1949(48)
C21	5555(6)	585(12)	276(7)	1664(45)
C22	5529(7)	−379(14)	−98(6)	1433(40)
C23	5997(9)	−843(14)	−225(8)	1711(63)
HSc	−28(12)	588(20)	2971(12)	3.3(6) *

* $U_{eq} = \frac{1}{3}\sum_i \sum_j [U_{ij}(a_i^* a_j^*)(\vec{a}_i \cdot \vec{a}_j)]$

*Isotropic displacement parameter, B

Table VI. Hydrogen Parameters for Compound 4.

x, y and $z \times 10^4$

Atom	x	y	z	B
H7A	2745(21)	2088(34)	3972(20)	6.8(13)*
H7B	2484(21)	1079(34)	4125(21)	6.8(17)*
H7C	2282(20)	2110(34)	4383(20)	8.3(14)*
H8A	1658(21)	4254(42)	3700(21)	9.2(15)*
H8B	1134(29)	3501(48)	3876(27)	13.9(25)*
H8C	1104(18)	4148(33)	3399(18)	1.9(13)*
H9A	434(21)	4158(39)	2263(21)	9.1(17)*
H9B	83(26)	3302(42)	1733(25)	10.1(21)*
H9C	557(22)	3854(40)	1604(22)	9.8(18)*
H10A	635(27)	1862(47)	1120(26)	11.8(24)*
H10B	932(27)	777(45)	1293(26)	11.5(23)*
H10C	1313(19)	1686(33)	1216(19)	6.3(13)*
H11A	3116(21)	−9(35)	3346(23)	6.9(16)*
H11B	3001(25)	−1220(46)	3181(26)	12.0(21)*
H11C	2884(25)	−581(47)	3813(23)	11.4(23)*
H12A	1665(25)	−779(46)	1449(26)	12.6(26)*
H12B	2282(24)	−1333(41)	1907(25)	9.1(19)*
H12C	2295(22)	−147(37)	1685(23)	8.9(16)*
H13A	2159(25)	136(39)	4933(23)	9.8(18)*
H13B	1894(29)	−1021(47)	4690(28)	11.9(29)*
H13C	1815(20)	−628(37)	5304(21)	9.0(15)*
H14A	576(20)	−689(34)	4885(21)	7.9(14)*
H14B	501(24)	−1389(38)	4305(23)	8.5(19)*
H14C	35(21)	−346(35)	4097(20)	8.3(15)*
H15A	1353(21)	2066(38)	4774(22)	8.3(16)*
H15B	1077(19)	1329(35)	5206(21)	8.6(14)*
H15C	611(24)	1963(42)	4477(23)	10.3(19)*
H17A	1055(23)	−2301(36)	3668(21)	7.8(18)*
H17B	707(19)	−3187(36)	3148(20)	7.8(13)*
H17C	461(19)	−1925(35)	2990(19)	6.9(14)*
H18A	550(26)	−2180(44)	1774(27)	12.2(24)*
H18B	873(21)	−3394(37)	2081(22)	8.9(16)*
H18C	1224(21)	−2520(32)	1852(22)	6.4(15)*
H19A	2135(24)	−2805(39)	2888(23)	9.2(18)*
H19B	1829(18)	−3562(35)	3248(19)	6.7(13)*
H19C	2101(29)	−2494(48)	3733(29)	14.4(28)*
H20	5059	1712	586	18.3
H21	5983	967	488	15.8
H22	5925	−595	−172	13.6
H23A	5827	−1209	−633	16.7
H23B	6240	−1398	114	16.7
H23C	6327	−245	−217	16.7

Table VII. Anisotropic Displacement Parameters for Compound 4.

Atom	U_{11}	U_{22}	U_{33}	U_{12}	U_{13}	U_{23}
Sc	319(4)	406(4)	462(5)	−29(4)	183(4)	−28(4)
Si	430(7)	559(8)	877(10)	−6(6)	347(7)	−90(7)
P	479(7)	687(9)	499(7)	14(6)	189(6)	44(6)
N	340(17)	384(21)	652(23)	−20(14)	245(16)	−40(16)
C1	303(23)	508(26)	559(30)	−71(20)	231(23)	−64(25)
C2	311(24)	476(29)	558(34)	−111(22)	146(24)	−33(25)
C3	400(27)	378(26)	690(38)	−128(22)	290(27)	−117(26)
C4	341(27)	499(28)	651(38)	−81(21)	253(27)	37(26)
C5	412(26)	523(28)	543(34)	−141(22)	285(26)	−57(25)
C7	501(35)	897(51)	706(46)	−165(35)	196(33)	−11(39)
C8	794(45)	483(43)	1283(64)	−110(39)	541(46)	−191(45)
C9	560(40)	802(46)	1010(53)	143(33)	293(41)	245(43)
C10	619(42)	1131(58)	646(46)	−226(38)	351(37)	−77(39)
C11	411(33)	834(54)	2150(105)	41(36)	293(43)	−261(62)
C12	1376(69)	712(50)	1663(80)	−110(48)	1228(69)	−212(51)
C13	596(37)	1327(68)	757(47)	129(42)	168(33)	303(50)
C14	667(38)	850(48)	741(47)	10(35)	375(35)	195(40)
C15	905(48)	848(44)	660(45)	−107(40)	345(38)	−169(35)
C16	559(30)	459(29)	996(42)	26(25)	478(30)	30(30)
C17	887(52)	558(42)	1296(72)	−18(34)	618(53)	135(40)
C18	1137(61)	677(48)	1225(69)	−259(40)	712(57)	−341(44)
C19	875(50)	602(43)	2060(105)	312(37)	745(60)	410(56)
C20	1841(107)	1161(86)	1757(83)	104(100)	−462(93)	8(63)
C21	1529(87)	727(66)	1707(87)	−239(59)	−471(72)	225(73)
C22	1593(107)	1208(98)	1155(65)	164(66)	171(65)	221(59)
C23	2501(211)	1473(146)	1715(146)	168(129)	1425(156)	−77(110)

The form of the displacement factor is:

$$\exp -2\pi^2(U_{11}h^2a^{*2} + U_{22}k^2b^{*2} + U_{33}l^2c^{*2} + 2U_{12}hka^*b^* + 2U_{13}hla^*c^* + 2U_{23}klb^*c^*)$$

Table VIII. Complete Distances and Angles for Compound 4.

Distance(Å)				Angle(°)			
Se	-P	2.996(1)		P	-Se	-Si	108.7(0)
Se	-N	2.058(3)		N	-Se	-P	95.3(1)
Se	-C1	2.314(4)		Cp*	-Se	-P	112.4(0)
Se	-C2	2.424(4)		HSe	-Se	-P	68.8(7)
Se	-C3	2.665(4)		HSe′	-Se	-P	134.0(7)
Se	-C4	2.688(4)		HSe	-Se	-N	125.4(7)
Se	-C5	2.523(4)		HSe′	-Se	-N	104.2(7)
Se	-Cp*	2.216(3)		HSe	-Se	-Cp*	129.8(7)
Se	-HSe	1.97(3)		HSe′	-Se	-Cp*	102.3(7)
Se	-HSe′	1.98(3)		HSe	-Se	-HSe′	65.9(10)
Si	-N	1.663(3)		C1	-Si	-N	97.3(2)
Si	-C1	1.858(4)		C11	-Si	-N	113.3(3)
Si	-C11	1.836(9)		C12	-Si	-N	116.2(3)
Si	-C12	1.941(10)		C11	-Si	-C1	110.7(3)
P	-C13	1.812(8)		C12	-Si	-C1	112.4(3)
P	-C14	1.786(7)		C12	-Si	-C11	106.8(4)
P	-C15	1.847(7)		C13	-P	-Se	124.5(3)
P	-HSe	2.93(3)		C14	-P	-Se	115.4(2)
N	-C16	1.478(5)		C15	-P	-Se	117.1(2)
C1	-C2	1.471(6)		C14	-P	-C13	96.1(3)
C1	-C5	1.423(6)		C15	-P	-C13	99.6(3)
C2	-C3	1.381(6)		C15	-P	-C14	99.4(3)
C2	-C7	1.523(8)		Si	-N	-Se	101.4(1)
C3	-C4	1.459(6)		C16	-N	-Se	135.0(3)
C3	-C8	1.543(9)		C16	-N	-Si	123.4(3)
C4	-C5	1.400(6)		C2	-C1	-Si	122.8(3)
C4	-C9	1.490(8)		C5	-C1	-Si	121.6(3)
C5	-C10	1.570(8)		C5	-C1	-C2	109.2(3)
C16	-C17	1.507(9)		C3	-C2	-C1	107.7(4)
C16	-C18	1.585(10)		C7	-C2	-C1	129.9(4)
C16	-C19	1.496(10)		C7	-C2	-C3	121.7(4)
C20	-C21	1.27(2)		C4	-C3	-C2	106.6(4)
C20	-C22	1.33(2)		C8	-C3	-C2	121.7(5)
C21	-C22	1.37(2)		C8	-C3	-C4	130.8(5)
C22	-C23	1.25(2)		C5	-C4	-C3	111.1(4)
HSe	-HSe′	2.15(4)		C9	-C4	-C3	126.3(4)
				C9	-C4	-C5	122.0(4)
				C4	-C5	-C1	105.3(4)
				C10	-C5	-C1	129.4(4)
				C10	-C5	-C4	125.1(4)
				C22′	-C20	-C21	114.6(14)
				C22	-C21	-C20	124.2(14)
				C23	-C22	-C20′	109.7(15)
				C23	-C22	-C21	129.3(15)
				C21	-C22	-C20′	121.0(14)

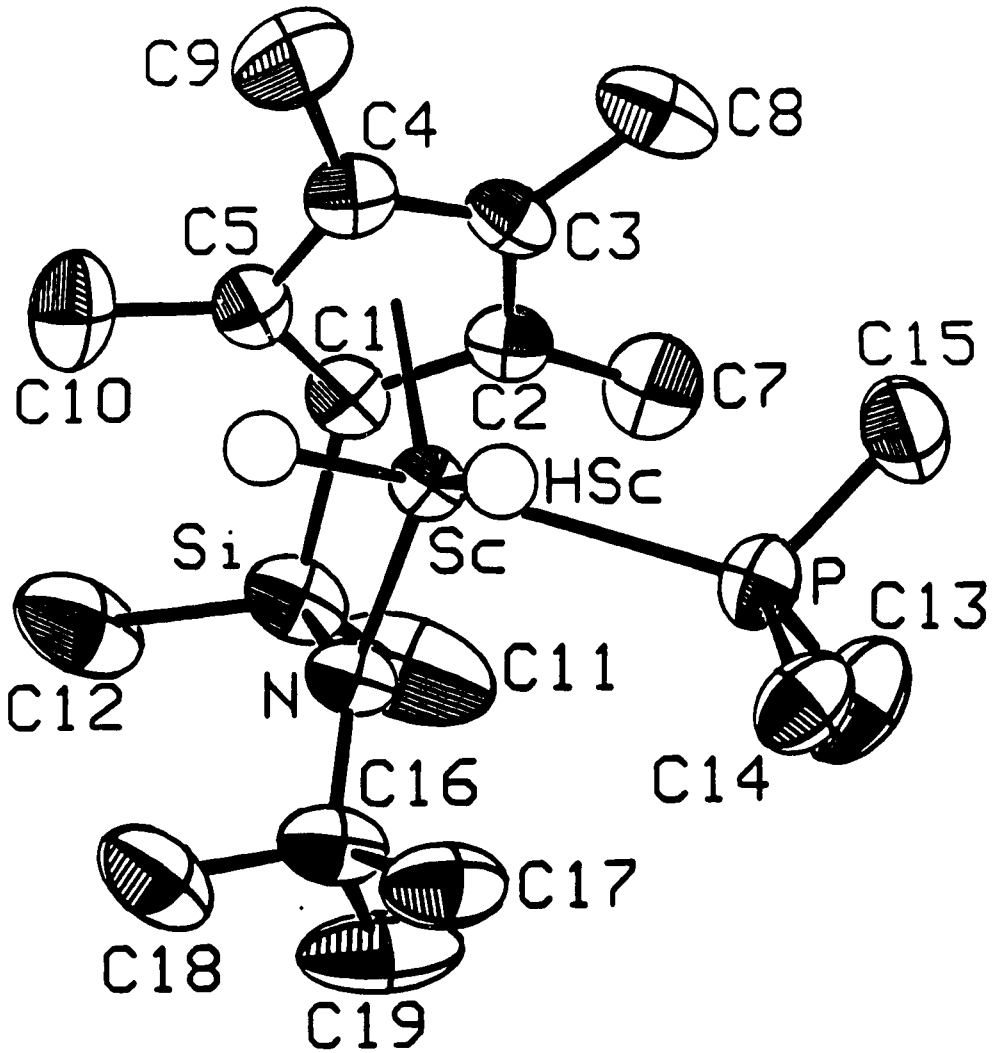

Figure 1.8. ORTEP drawing of $[(Cp^*SiNR)(PMe_3)ScH]_2$ (4) showing the atom labeling.

Table IX. Crystal and Instensity Collection Data for $[(Cp^*SiNR)Sc]_2(\mu,\eta^2,\eta^2\text{-}C_2H_4)$ (5).

Formula: $Sc_2Si_2P_2N_2C_{45}H_{84}$	Formula Weight: 861.22
Crystal Color: pale yellow	Habit: Hexagonal Prisms
$a = 23.706(5)$ Å	
$b = 11.342(2)$ Å	$\beta = 111.57(1)^\circ$
$c = 21.141(3)$ Å	
$v = 5286.2(7)$ Å^3	$z = 4$
$\lambda = 0.71073$ Å	T: 23°
Graphite monochromator	
Space group: C2/c	Absences: hkl, h + k odd; h0l, l odd
Crystal Size: ~ .35 x .4 x.4 mm	$\mu = 4.03 cm^{-1}$ ($\mu r_{max} = 0.13$)
CAD-4 Diffractometer	ω scan
2θ range: 2°-40°	Octants collected: $\pm h, \pm k, -l$

Number reflections measured: 5205

Number of independent reflections: 2475

Number with $F_o^2 > 0$: 2291

Number with $F_o^2 > 3\sigma(F_o^2)$: 1757

Goodness of fit for merging data: 0.97

Final R-index: 0.086

Final goodness of fit: 3.84

Table X. Final Parameters for Compound 5.

x, y, z and $U_{eq}{}^{a} \times 10^{4}$

Atom	x	y	z	U_{eq} or B	
Sc	1008(1)	485(1)	2979(1)	452(4)	
P	1128(1)	157(2)	4347(1)	729(8)	
Si	2091(1)	−386(2)	2729(1)	653(7)	
N	1478(2)	−988(5)	2863(3)	4.2(1)	*
C 1	1866(3)	1190(6)	2751(4)	4.1(2)	*
C 2	1361(3)	1717(6)	2237(4)	4.3(2)	*
C 3	1114(3)	2607(6)	2520(4)	4.4(2)	*
C 4	1449(3)	2635(7)	3213(4)	4.6(2)	*
C 5	1905(3)	1803(7)	3368(4)	4.7(2)	*
C 6	1132(4)	1412(7)	1489(4)	789(27)	
C 7	630(4)	3457(8)	2129(5)	953(30)	
C 8	1379(4)	3564(8)	3687(5)	977(30)	
C 9	2414(4)	1660(8)	4052(4)	894(30)	
C10	28(4)	466(9)	2174(4)	4.3(2)	*
C11	2174(5)	−766(8)	1914(5)	1142(34)	
C12	2857(4)	−720(8)	3374(6)	1168(37)	
C13	1349(4)	−2256(8)	2846(5)	744(29)	
C14	848(5)	−2513(8)	3064(6)	1283(41)	
C15	1854(6)	−2940(11)	3234(11)	2730(102)	
C16	1129(10)	−2664(11)	2124(10)	3066(106)	
C17	1019(5)	1443(10)	4784(5)	1218(38)	
C18	553(4)	−767(9)	4465(4)	1044(33)	
C19	1810(4)	−482(11)	4955(5)	1424(43)	

Table X. (Cont'd)

H10A	−7(28)	1130(58)	3045(32)	6.2(20) *
H10B	−91(23)	−234(49)	3016(27)	3.8(15) *

[a] $U_{eq} = \frac{1}{3}\sum_i \sum_j [U_{ij}(a_i^* a_j^*)(\vec{a}_i \cdot \vec{a}_j)]$

*Isotropic displacement parameter, B

Table XI. Assigned Parameters for Compound 5.

x, y, z and $U_{eq}{}^{a} \times 10^{4}$

Atom	x	y	z	U_{eq} or B	
C21	5008	829	487	12.0	*
C22	5543	530	399	12.0	*
C23	5536	−300	−88	12.0	*
C24	6124	−626	−184	12.0	*
H 6A	795	1908	1217	7.0	*
H 6B	994	603	1391	7.0	*
H 6C	1446	1514	1291	7.0	*
H 7A	433	3851	2382	7.0	*
H 7B	301	3049	1746	7.0	*
H 7C	779	4054	1891	7.0	*
H8A1	1641	4245	3715	7.0	*
H8A2	1464	3287	4136	7.0	*
H8A3	965	3881	3519	7.0	*
H8B1	1731	3655	4091	7.0	*
H8B2	1036	3414	3817	7.0	*
H8B3	1303	4345	3462	7.0	*
H 9A	2804	1953	4059	7.0	*
H 9B	2486	843	4208	7.0	*
H 9C	2339	2088	4419	7.0	*
H11A	1795	−1050	1586	7.0	*
H11B	2478	−1343	1971	7.0	*
H11C	2283	−66	1715	7.0	*
H12A	3148	−152	3360	7.0	*
H12B	2993	−1490	3294	7.0	*
H12C	2847	−728	3827	7.0	*
H14A	966	−2436	3571	7.0	*
H14B	705	−3335	2978	7.0	*
H14C	504	−2019	2871	7.0	*
H15A	2213	−2766	3078	7.0	*
H15B	1801	−3783	3153	7.0	*
H15C	2016	−2801	3705	7.0	*
H16A	753	−2889	1992	7.0	*
H16B	1405	−3378	2152	7.0	*
H16C	1246	−2096	1883	7.0	*
H17A	1394	1979	4900	7.0	*
H17B	1002	1269	5220	7.0	*
H17C	693	1916	4529	7.0	*
H18A	577	−778	4926	7.0	*
H18B	611	−1603	4352	7.0	*
H18C	154	−556	4174	7.0	*
H19A	2167	39	5006	7.0	*
H19B	1900	−1226	4840	7.0	*
H19C	1796	−496	5410	7.0	*

* $U_{eq} = \frac{1}{3} \sum_i \sum_j [U_{ij} (a_i^* a_j^*)(\vec{a}_i \cdot \vec{a}_j)]$

*Isotropic displacement parameter, B

Table XII. Anisotropic Displacement Parameters for Compound 5.

Atom	U_{11}	U_{22}	U_{33}	U_{12}	U_{13}	U_{23}
Sc	428(9)	504(10)	440(9)	−50(8)	177(7)	−24(8)
P	653(16)	1032(21)	484(15)	−85(15)	188(12)	55(14)
Si	512(15)	692(18)	825(18)	5(14)	327(13)	−73(15)
C 6	802(64)	979(72)	611(60)	−200(54)	289(51)	28(52)
C 7	849(70)	847(69)	1268(84)	97(57)	512(65)	270(61)
C 8	1311(84)	675(65)	1248(86)	−291(58)	828(73)	−334(59)
C 9	714(64)	1157(80)	745(67)	−286(55)	192(54)	−81(56)
C11	1505(93)	834(76)	1546(100)	−118(65)	1102(83)	−243(66)
C12	655(65)	1074(82)	1716(103)	107(58)	367(68)	−54(75)
C13	788(68)	533(65)	1014(76)	40(55)	451(61)	76(56)
C14	1248(92)	726(75)	2279(134)	−170(65)	1125(95)	41(77)
C15	987(105)	991(104)	5807(361)	139(83)	771(156)	1410(160)
C16	6416(409)	979(112)	3070(227)	−1992(182)	3165(264)	−1073(134)
C17	1666(106)	1348(94)	821(77)	−152(80)	669(76)	−219(68)
C18	1052(77)	1391(93)	670(63)	−280(66)	293(57)	169(60)
C19	1027(81)	2288(130)	839(74)	56(86)	203(66)	597(82)

The form of the displacement factor is:

$$\exp -2\pi^2(U_{11}h^2a^{*2} + U_{22}k^2b^{*2} + U_{33}\ell^2c^{*2} + 2U_{12}hka^*b^* + 2U_{13}h\ell a^*c^* + 2U_{23}k\ell b^*c^*)$$

Table XIII. Complete Distances and Angles for Compound 5.

Distance(Å)		Distance(Å)		Angle(°)			
Se -P	2.825(3)	C 6 -H 6A	0.974(8)	Se -C10	-C10'	73.6(5)
Se -N	2.071(6)	C 6 -H 6B	0.971(8)	C10 -Se	-C10'	35.7(3)
Se -C 1	2.395(7)	C 6 -H 6C	0.985(8)	Se -P	-C17	116.2(4)
Se -C 2	2.464(8)	C 7 -H 7A	0.943(9)	Se -P	-C18	114.9(3)
Se -C 3	2.641(8)	C 7 -H 7B	1.007(9)	Se -P	-C19	120.6(4)
Se -C 4	2.628(8)	C 7 -H 7C	0.983(9)	Se -N	-Si	102.9(3)
Se -C 5	2.481(8)	C 8 -H8A1	0.980(9)	Se -N	-C13	132.6(5)
Se -C10	2.320(9)	C 8 -H8A2	0.947(9)	C 5 -C 1	-C 2	104.1(6)
Se -C10'	2.357(9)	C 8 -H8A3	0.982(9)	C 3 -C 2	-C 1	110.1(7)
C10 -C10'	1.433(12)	C 8 -H8B1	0.955(9)	C 6 -C 2	-C 1	125.5(7)
C10 -H10A	0.88(7)	C 8 -H8B2	0.963(9)	C 6 -C 2	-C 3	124.3(7)
C10 -H10B	0.93(6)	C 8 -H8B3	0.990(9)	C 4 -C 3	-C 2	107.3(7)
Si -N	1.722(6)	C 9 -H 9A	0.978(9)	C 7 -C 3	-C 2	125.7(7)
Si -C 1	1.871(8)	C 9 -H 9B	0.977(9)	C 7 -C 3	-C 4	126.5(7)
Si -C11	1.855(11)	C 9 -H 9C	0.984(9)	C 5 -C 4	-C 3	109.3(7)
Si -C12	1.865(10)	C17 -H17A	1.028(11)	C 8 -C 4	-C 3	124.0(7)
C11 -H11A	0.967(10)	C17 -H17B	0.957(11)	C 8 -C 4	-C 5	126.1(7)
C11 -H11B	0.948(10)	C17 -H17C	0.933(11)	C 4 -C 5	-C 1	109.2(7)
C11 -H11C	0.976(10)	C18 -H18A	0.955(9)	C 9 -C 5	-C 1	125.0(7)
C12 -H12A	0.953(10)	C18 -H18B	0.999(9)	C 9 -C 5	-C 4	125.4(7)
C12 -H12B	0.968(10)	C18 -H18C	0.948(9)	C14 -C13	-N	112.1(8)
C12 -H12C	0.967(10)	C19 -H19A	1.005(11)	C15 -C13	-N	113.6(10)
N -C13	1.469(11)	C19 -H19B	0.925(11)	C16 -C13	-N	108.7(10)
C13 -C14	1.453(15)	C19 -H19C	0.976(11)	C15 -C13	-C14	108.9(10)
C13 -C15	1.41(2)	C21 -C22	1.390(0)	C16 -C13	-C14	104.1(11)
C13 -C16	1.49(2)	C21 -C23	1.391(0)	C16 -C13	-C15	109.1(12)
C14 -H14A	1.007(11)	C22 -C23	1.390(0)	C23 -C21	-C22	120.2
C14 -H14B	0.965(11)	C23 -C24	1.526(0)	C23 -C22	-C21	120.0
C14 -H14C	0.947(11)			C22 -C23	-C21	119.8
C15 -H15A	1.037(17)			C24 -C23	-C21	120.3
C15 -H15B	0.972(17)			C24 -C23	-C22	119.9
C15 -H15C	0.939(17)					
C16 -H16A	0.87(2)			C13 -N	-Si	124.41(5)
C16 -H16B	1.03(2)					
C16 -H16C	0.93(2)					
P -C17	1.796(11)					
P -C18	1.806(10)					
P -C19	1.807(11)					
C 1 -C 2	1.419(11)					
C 1 -C 5	1.450(11)					
C 2 -C 3	1.405(11)					
C 2 -C 6	1.513(11)					
C 3 -C 4	1.388(11)					
C 3 -C 7	1.493(12)					
C 4 -C 5	1.381(11)					
C 4 -C 8	1.505(12)					
C 5 -C 9	1.513(12)					

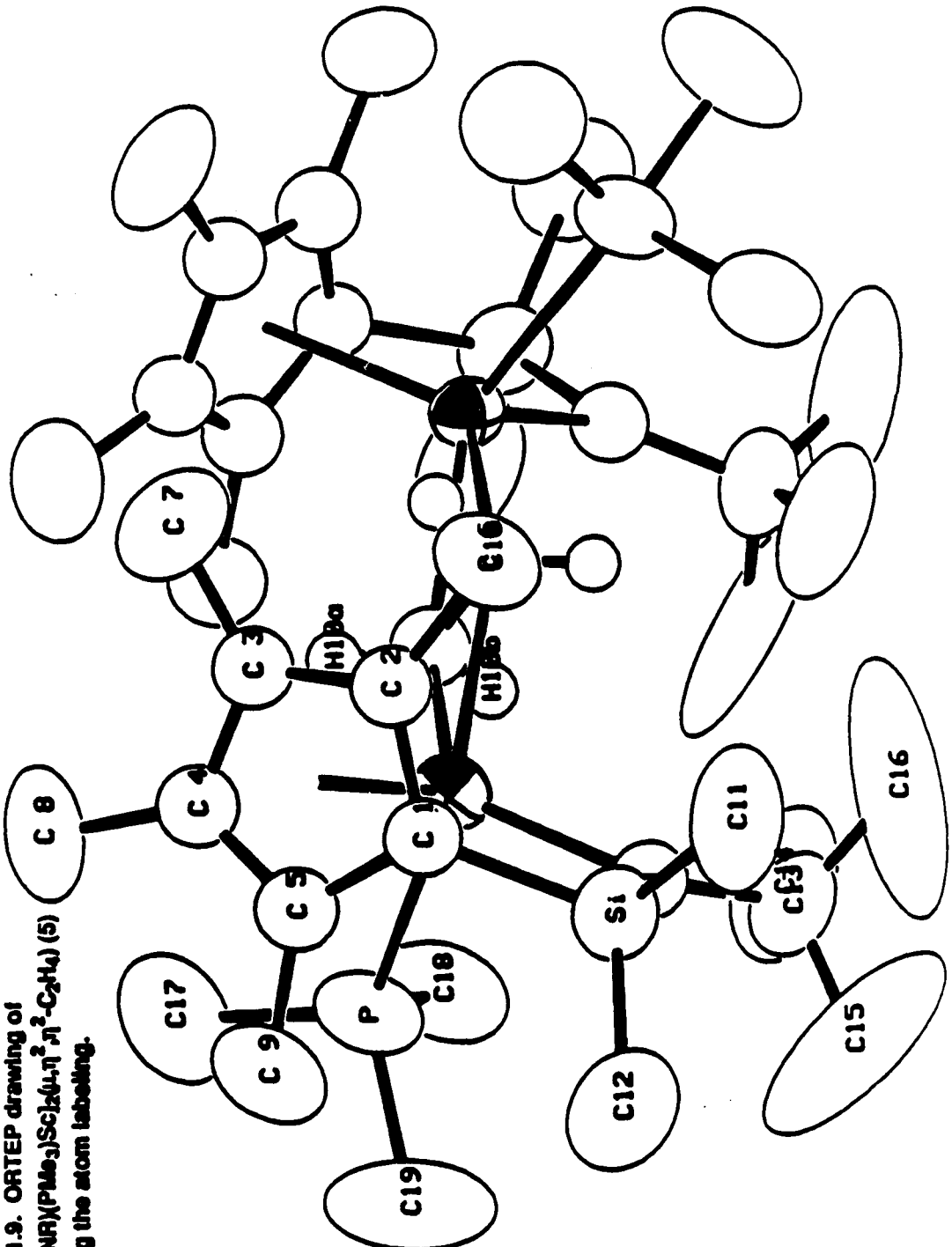

Figure 1.9. ORTEP drawing of $[(Cp'SiNR)(PMe_3)Sc]_2(\mu,\eta^2,\eta^2\text{-}C_2H_4)$ (5) showing the atom labeling.

Table XIV. Crystal and Intensity Collection Data for [(Cp*SiNR)Sc]$_2$(μ-$CH_2CH_2CH_3$) (6).

Crystal Color: pale yellow	Crystal Habit: irregular plates
a = 9.429(2)Å	
b = 21.937(5)Å	β = 99.39(2)°
c = 9.826 (2)Å	
T = 21°C	λ = 0.71073 Å
CAD-4	2θ range: 3° - 40°
ω scan	Octants of data collected: $\pm h, \pm k, l$
Graphite monochromator: yes	μ = 4.28cm^{-1} μr_{max} = 0.16

Crystal Size: .2 x .2 x .8mm

Total Number Reflections: 4082

Total Independent Reflections: 1863

GOF for Merging: 0.977

(R merge for reflections with exactly 2 observations) 0.041

Number of Reflections used in Refinement: 1863

Number of Reflections with $F_o^2 > 0$ used in R: 1706

Number of Reflections with $F_o^2 > 3\sigma(F_o^2)$: 1231

(R for reflections with $F_o^2 > 3\sigma(F_o^2)$: 0.0579

Table XV. Final Parameters for Compound 6.

x, y, z and U_{eq}[a] $\times 10^4$

Atom	x	y	z	U_{eq}
Sc	−85(2)	748(1)	5192(1)	460(4)
C1	464(8)	1783(3)	5817(8)	463(21)
C2	1742(9)	1557(3)	5417(8)	503(24)
C3	2422(8)	1151(3)	6419(9)	522(25)
C4	1560(10)	1115(3)	7452(8)	558(26)
C5	368(8)	1499(3)	7083(9)	521(25)
C7	2394(8)	1745(3)	4169(9)	868(27)
C8	3929(9)	912(3)	6481(10)	987(32)
C9	1952(9)	799(4)	8863(8)	974(31)
C10	−747(9)	1620(4)	7995(9)	878(27)
Si	−1108(2)	2023(1)	4535(2)	597(7)
C11	−2527(8)	2423(4)	5348(9)	1079(31)
C12	−609(9)	2594(3)	3292(10)	1046(32)
N	−1537(5)	1300(2)	3923(5)	419(16)
C13	−2684(8)	1166(3)	2711(8)	556(26)
C14	−3253(10)	537(4)	2865(10)	739(33)
C15	−3939(9)	1615(4)	2611(10)	698(31)
C16	−1995(11)	1205(5)	1386(10)	813(41)
C20	885(8)	111(3)	3677(8)	591(23)
C21	2222(10)	−173(4)	3397(9)	920(31)
C22	2646(9)	−64(4)	1971(9)	1080(33)

[a] $U_{eq} = \frac{1}{3} \sum_i \sum_j [U_{ij} (a_i^* a_j^*) (\vec{a}_i \cdot \vec{a}_j)]$

Table XVI. Assigned Parameters for Compound 6.

	x, y and $z \times 10^4$			
Atom	x	y	z	B
C14a	−4101	1054	3277	10.3
C15a	−2274	597	1980	10.3
C16a	−2852	1714	1752	10.3
H7a	1718	1668	3374	8.0
H7b	3239	1499	4161	8.0
H7c	2647	2158	4262	8.0
H8a	4050	760	5614	8.9
H8b	4101	600	7167	8.9
H8c	4587	1242	6746	8.9
H9a	2526	1079	9474	9.6
H9b	2490	448	8742	9.6
H9c	1103	705	9203	9.6
H10a	−536	1998	8433	8.2
H10b	−683	1299	8665	8.2
H10c	−1657	1619	7437	8.2
H11a	−2058	2692	6045	10.1
H11b	−3062	2134	5721	10.1
H11c	−3110	2659	4648	10.1
H12a	−1473	2810	2893	9.8
H12b	−201	2400	2610	9.8
H12c	40	2883	3792	9.8
H14a	−3689	516	3612	12.1
H14b	−2429	270	2918	12.1
H14c	−3877	458	2011	12.1
H15a	−4317	1594	3422	11.3
H15b	−4617	1472	1838	11.3
H15c	−3583	1996	2429	11.3
H16a	−1974	1623	1175	13.3
H16b	−2687	1000	703	13.3
H16c	−1139	1016	1552	13.3
H20a	1110	546	3652	5.6
H20b	189	37	2825	5.6
H21a	2048	−581	3542	8.7
H21b	2896	−4	4102	8.7
H22a	1970	−253	1305	9.9
H22b	3569	−246	2032	9.9
H22c	2701	361	1823	9.9

Table XVII. Anisotropic Displacement Parameters for Compound 6.

Atom	U_{11}	U_{22}	U_{33}	U_{12}	U_{13}	U_{23}
Sc	567(10)	332(8)	449(10)	22(8)	−9(8)	19(8)
C1	564(56)	371(46)	478(55)	10(40)	154(44)	56(42)
C2	593(60)	349(48)	562(60)	−55(44)	82(52)	−38(44)
C3	458(57)	385(51)	670(64)	60(44)	−67(53)	−77(47)
C4	722(65)	392(51)	490(61)	−91(48)	−109(55)	−24(46)
C5	660(64)	323(48)	606(64)	−56(45)	183(54)	−208(46)
C7	878(66)	712(58)	1081(78)	−101(49)	357(61)	−10(56)
C8	685(63)	649(57)	1532(89)	28(50)	−101(62)	−237(58)
C9	1445(83)	706(59)	627(57)	45(59)	−262(58)	69(54)
C10	1056(73)	773(60)	841(68)	−32(55)	265(61)	−218(53)
Si	684(17)	346(12)	730(17)	68(12)	23(14)	50(12)
C11	1017(72)	875(64)	1246(86)	437(54)	−112(66)	−341(61)
C12	1245(75)	528(53)	1237(81)	−14(50)	−181(66)	470(56)
N	493(41)	290(32)	471(39)	74(28)	74(34)	56(29)
C13	685(59)	338(50)	572(59)	16(45)	−116(50)	10(44)
C14	819(76)	452(63)	804(79)	29(55)	−287(66)	−4(55)
C15	547(67)	532(60)	905(81)	89(55)	−210(60)	−41(59)
C16	910(83)	1197(92)	324(65)	−143(69)	80(61)	−85(62)
C20	545(51)	379(46)	856(64)	−21(41)	139(48)	−184(43)
C21	1066(78)	993(76)	678(69)	−190(59)	77(61)	42(56)
C22	954(69)	1606(91)	740(69)	269(67)	316(58)	355(65)

The form of the displacement factor is:

$$\exp -2\pi^2(U_{11}h^2a^{*2} + U_{22}k^2b^{*2} + U_{33}l^2c^{*2} + 2U_{12}hka^*b^* + 2U_{13}hla^*c^* + 2U_{23}klb^*c^*)$$

Table XVIII. Complete Distances and Angles for Compound 6.

Distance(Å)

Sc	-N	2.083(5)
Sc	-C20	2.334(7)
Sc	-C20	2.372(7)
Sc	-Sc	3.310(2)
C20	-C20	3.346(10)
Sc	-Cp*	2.210
Si	-N	1.720(5)
Si	-C1	1.858(7)
Si	-C11	1.885(8)
Si	-C12	1.862(8)
C20	-C21	1.472(11)
C21	-C22	1.538(12)
C1	-C2	1.417(10)
C1	-C5	1.407(10)
C2	-C3	1.403(11)
C2	-C7	1.515(11)
C3	-C4	1.403(11)
C3	-C8	1.507(11)
C4	-C5	1.403(11)
C4	-C9	1.539(11)
C5	-C10	1.513(11)
N	-C13	1.501(9)
C13	-C14	1.497(11)
C13	-C15	1.530(11)
C13	-C16	1.550(12)
C13	-C14A	1.548(7)
C13	-C15A	1.521(7)
C13	-C16A	1.520(7)

Angle(°)

C9	-C4	-C5	124.6(7)
C4	-C5	-C1	109.3(7)
C10	-C5	-C1	126.6(7)
C10	-C5	-C4	123.9(7)
C11	-Si	-C1	112.8(3)
C12	-Si	-C1	112.1(3)
N	-Si	-C1	95.3(3)
C12	-Si	-C11	103.7(4)
N	-Si	-C11	115.8(3)
N	-Si	-C12	117.5(3)
C13	-N	-Si	123.8(4)
Sc	-N	-C13	132.8(4)
Sc	-N	-Si	103.4(2)
Sc	-C20	-C21	144.0(5)
Sc	-C20	-Sc	89.4(2)
Sc	-C20	-C21	95.7(5)
N	-Sc	-Cp*	102.5
C20	-Sc	-C20	90.6(2)
C22	-C21	-C20	117.5(7)
Cp*	-Sc	-C20	119.6
Cp*	-Sc	-C20	118.5
Cp*	-C1	-Si	155.6
Sc	-Cp*	-C1	82.8
C5	-C1	-C2	105.7(6)
C3	-C2	-C1	109.8(7)
C7	-C2	-C1	127.3(7)
C7	-C2	-C3	122.8(7)
C4	-C3	-C2	106.9(7)
C8	-C3	-C2	124.7(7)
C8	-C3	-C4	127.3(7)
C5	-C4	-C3	108.3(7)
C9	-C4	-C3	126.5(7)
C9	-C4	-C5	124.6(7)
C4	-C5	-C1	109.3(7)
C10	-C5	-C1	126.6(7)
C10	-C5	-C4	123.9(7)
C14	-C13	-N	108.9(6)
C15	-C13	-N	112.0(6)
C16	-C13	-N	108.0(6)
C14A	-C13	-N	107.4(5)
C15A	-C13	-N	109.2(5)
C16A	-C13	-N	109.0(5)
C15	-C13	-C14	108.3(6)
C16	-C13	-C14	110.0(7)
C16	-C13	-C15	109.6(6)
C15A	-C13	-C14A	109.8(4)
C16A	-C13	-C14A	109.9(4)
C16A	-C13	-C15A	111.4(4)
C22	-C21	-C20	117.5(7)
C5	-C1	-C2	105.7(6)
Si	-C1	-C2	122.1(5)
Si	-C1	-C5	124.5(5)
C3	-C2	-C1	109.8(7)
C7	-C2	-C1	127.3(7)
C7	-C2	-C3	122.8(7)
C4	-C3	-C2	106.9(7)
C8	-C3	-C2	124.7(7)
C8	-C3	-C4	127.3(7)
C5	-C4	-C3	108.3(7)
C9	-C4	-C3	126.5(7)

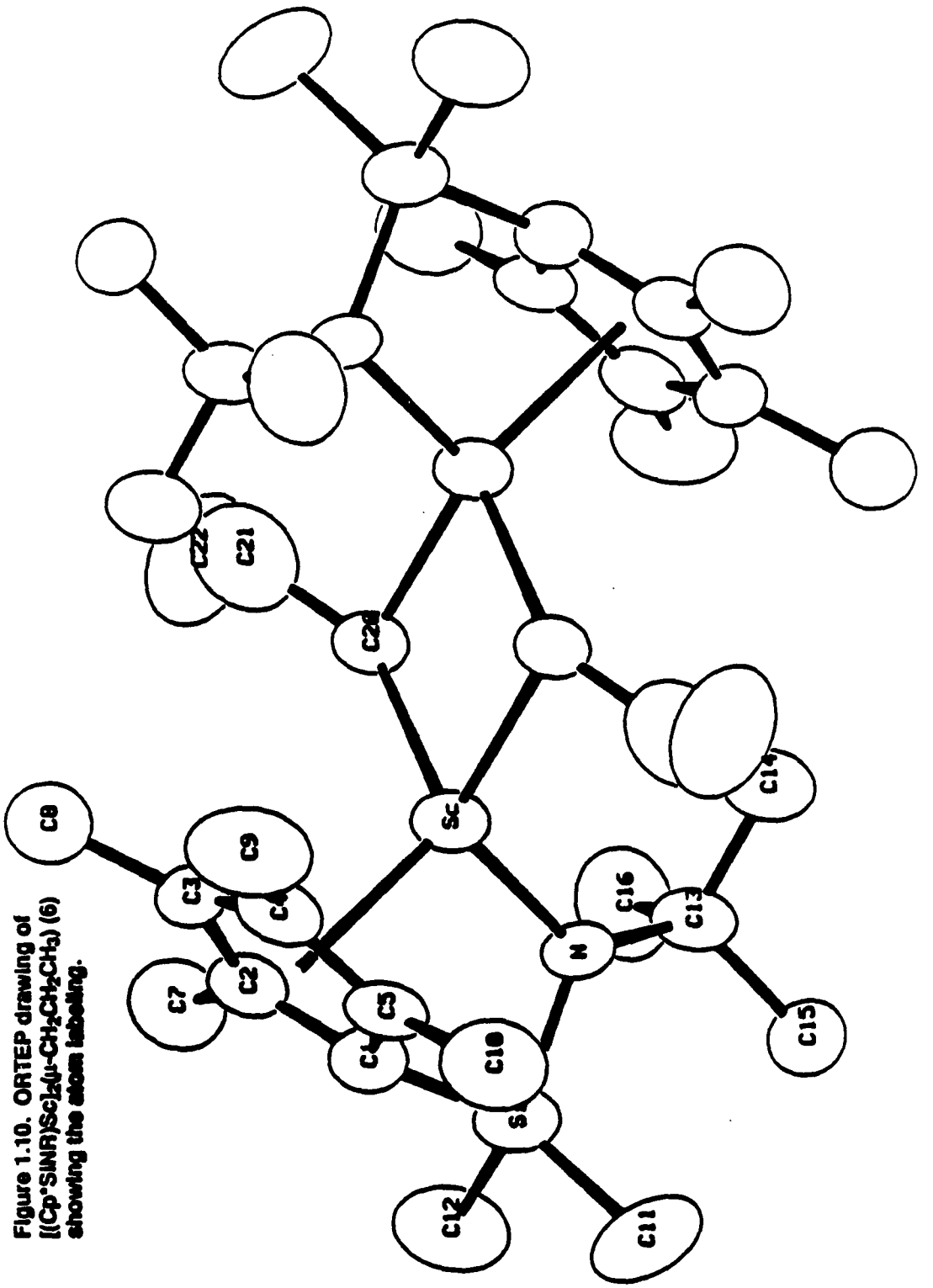

Figure 1.10. ORTEP drawing of [(Cp'SiNR)Sc]$_2$(μ-$CH_2CH_2CH_2CH_3$) (6) showing the atom labeling.

Table XIX. Crystal and Intensity Collection Data for (Cp*SiNR)(PMe_3)$ScCH_2TMS$ (16).

$a = 11.181(4)$Å	Crystal Color: clear
$b = 18.206(5)$Å	Crystal Habit: irregular
$c = 15.250(6)$Å	2θ range: 2° - 40°
$\beta = 108.25(3)°$	Octants of data collected: $\pm h, \pm k, l$
$\lambda = 0.71073$ Å	$\mu = 3.95 cm^{-1}$

T= 23°C

CAD-4

ω scan

Graphite monochromator: yes

$\mu r_{max} = 0.15$

Absences: h 0 l, h + l odd; 0 k 0, k odd.

Crystal Size: 0.14 x 0.26 x 0.67mm

Total Number Reflections: 8508

Total Independent Reflections: 5186

GOF for Merging: 0.94
(R merge for reflections with exactly 2 observations: 0.039)

Number of Reflections used in Refinement: 5186

Number of Reflections with $F_o^2 > 0$ used in R: 4307

Number of Reflections with $F_o^2 > 3\sigma(F_o^2)$: 2101

(R for reflections with $F_o^2 > 3\sigma(F_o^2)$: 0.0533)

Table XX. Final Parameters for Compound 16.

x, y, z and U_{eq}[a] $\times 10^4$

Atom	x	y	z	U_{eq}
Sc	5569(.6)	1832(.4)	2742(.5)	489(2)
P	5936(1)	1887(1)	1031(1)	734(4)
Si1	7502(1)	948(1)	4101(1)	712(4)
Si2	2285(1)	1868(1)	2735(1)	769(4)
N	6135(3)	794(2)	3196(2)	567(9)
C1	7450(4)	1960(2)	4019(3)	589(12)
C2	6549(4)	2416(2)	4246(3)	586(12)
C3	6296(4)	3048(2)	3692(3)	571(12)
C4	7017(4)	2983(2)	3101(3)	652(13)
C5	7716(3)	2345(3)	3299(3)	616(13)
C6	3494(3)	2056(2)	2189(3)	661(12)
C7	4911(5)	1427(3)	71(3)	1172(20)
C8	5828(5)	2806(3)	586(3)	1325(22)
C9	7428(5)	1566(4)	955(4)	1880(30)
C10	8983(4)	603(3)	3912(4)	1079(17)
C11	7515(5)	657(3)	5277(4)	1242(20)
C12	1261(5)	1074(3)	2170(4)	1304(20)
C13	2980(5)	1619(3)	3994(4)	1135(17)
C14	1230(5)	2670(3)	2686(4)	1322(20)
C15	5536(5)	3718(2)	3792(4)	811(16)

Table XX. (Cont'd)

Atom	x	y	z	U_{eq}
C16	4571(5)	3542(3)	4261(4)	1222(20)
C17	4862(6)	4058(3)	2846(5)	1428(24)
C18	6456(5)	4297(3)	4371(4)	1271(21)
C19	5596(5)	66(2)	2916(3)	751(15)
C20	4921(10)	−213(4)	3537(6)	2722(42)
C21	6444(6)	−475(4)	2802(8)	2933(48)
C22	4577(8)	123(3)	2026(6)	2163(38)

* $U_{eq} = \frac{1}{3} \sum_i \sum_j [U_{ij}(a_i^* a_j^*)(\vec{a}_i \cdot \vec{a}_j)]$

Table XXI. Assigned Hydrogen Parameters for Compound 16.

x, y and $z \times 10^4$

Atom	x	y	z	B
H2	6178	2307	4714	5.5
H4	7030	3325	2632	6.1
H5	8296	2188	2996	5.7
H6a	3221	1798	1619	6.1
H6b	3436	2570	2072	6.1
H7a	5061	1495	−465	11.0
H7b	4801	922	207	11.0
H7c	4007	1637	−23	11.0
H8a	5964	2790	0	12.3
H8b	5021	2992	522	12.3
H8c	6456	3096	998	12.3
H9a	7427	1619	336	17.9
H9b	8079	1859	1349	17.9
H9c	7537	1072	1137	17.9
H10a	9672	711	4442	10.1
H10b	8913	88	3818	10.1
H10c	9084	837	3388	10.1
H11a	8313	769	5705	11.5
H11b	6875	909	5434	11.5
H11c	7374	142	5272	11.5
H12a	653	995	2478	12.3
H12b	862	1185	1545	12.3
H12c	1773	650	2228	12.3
H13a	2308	1527	4239	10.5
H13b	3475	1192	4044	10.5
H13c	3474	2014	4310	10.5
H14a	630	2542	2980	12.4
H14b	1727	3070	2999	12.4
H14c	827	2793	2063	12.4
H16a	4127	3979	4302	11.5
H16b	4004	3187	3907	11.5
H16c	4984	3358	4859	11.5
H17a	4396	4473	2936	13.5
H17b	5463	4203	2565	13.5
H17c	4304	3706	2477	13.5
H18a	5984	4718	4433	12.3
H18b	6877	4099	4957	12.3
H18c	7039	4427	4063	12.3
H20a	4632	−697	3343	26.0

Table XXI. (Cont'd)

Atom	*x*	*y*	*z*	*B*
H20b	5555	−264	4151	26.0
H20c	4303	96	3563	26.0
H21a	5992	−919	2619	28.7
H21b	6777	−315	2334	28.7
H21c	7091	−537	3363	28.7
H22a	4253	−359	1861	20.5
H22b	3957	435	2099	20.5
H22c	4931	302	1581	20.5

Table XXII. Anisotropic Displacement Parameters for Compound 16.

Atom	U_{11}	U_{22}	U_{33}	U_{12}	U_{13}	U_{23}
Sc	474(5)	507(5)	514(5)	−10(4)	194(4)	30(4)
P	583(7)	1105(10)	550(8)	59(8)	231(7)	67(8)
Si1	756(9)	667(9)	678(9)	138(7)	174(8)	109(7)
Si2	605(8)	717(9)	1116(12)	5(8)	457(8)	1(9)
N	559(21)	488(22)	651(24)	6(17)	187(19)	0(18)
C1	553(27)	645(29)	512(27)	−9(25)	85(22)	21(25)
C2	666(29)	576(29)	539(28)	−58(24)	222(24)	−42(25)
C3	616(28)	442(29)	625(29)	−58(23)	149(24)	−25(25)
C4	672(30)	626(34)	644(31)	−128(26)	184(26)	71(25)
C5	441(27)	713(33)	698(34)	−70(24)	185(25)	−93(27)
C6	509(26)	707(31)	779(32)	−16(22)	220(24)	9(24)
C7	1363(48)	1412(48)	662(37)	4(38)	203(35)	−101(34)
C8	1671(56)	1496(52)	772(40)	−314(44)	331(39)	262(37)
C9	904(41)	3956(101)	913(44)	900(54)	474(37)	127(56)
C10	771(34)	985(38)	1364(49)	300(29)	167(35)	27(34)
C11	1731(56)	1124(44)	764(38)	26(38)	236(38)	259(33)
C12	1095(45)	1309(47)	1685(58)	−410(37)	690(43)	−128(43)
C13	1438(49)	1080(42)	1202(47)	36(34)	868(41)	93(34)
C14	918(40)	1212(44)	2043(66)	364(35)	762(44)	277(44)
C15	988(39)	529(32)	894(40)	−26(30)	264(34)	−31(29)
C16	1064(43)	903(40)	1848(63)	93(33)	672(46)	−372(40)
C17	1720(59)	835(40)	1508(60)	469(40)	188(49)	156(41)
C18	1261(47)	743(38)	1819(62)	−166(34)	496(45)	−455(39)
C19	821(35)	598(33)	847(41)	−25(29)	281(33)	−71(29)
C20	5083(155)	1510(67)	2457(94)	−2143(89)	2455(110)	−929(64)
C21	1031(50)	1306(56)	6293(188)	46(43)	904(79)	−2150(85)
C22	2510(88)	828(46)	2241(89)	−676(53)	−565(76)	−250(52)

$U_{i,j}$ values have been multiplied by 10^4
The form of the displacement factor is:

$$\exp -2\pi^2(U_{11}h^2a^{*2} + U_{22}k^2b^{*2} + U_{33}l^2c^{*2} + 2U_{12}hka^*b^* + 2U_{13}hla^*c^* + 2U_{23}klb^*c^*)$$

Table XXIII. Complete Distances and Angles for Compound 16.

	Distance(Å)		Distance(Å)
Sc -Cp	2.208	C8 -H8c	0.944
Sc -P	2.767(1)	C9 -H9a	0.949
Sc -N	2.044(3)	C9 -H9b	0.950
Sc -C1	2.389(4)	C9 -H9c	0.939
Sc -C2	2.454(4)	C10 -H10a	0.946
Sc -C3	2.632(4)	C10 -H10b	0.949
Sc -C4	2.600(4)	C10 -H10c	0.943
Sc -C5	2.467(4)	C11 -H11a	0.948
Sc -C6	2.244(4)	C11 -H11b	0.942
Sc -H13a	4.901	C11 -H11c	0.950
Sc -H13b	3.701	C12 -H12a	0.951
Sc -H13c	3.851	C12 -H12b	0.939
P -C7	1.810(5)	C12 -H12c	0.949
P -C8	1.796(6)	C13 -H13a	0.952
P -C9	1.804(7)	C13 -H13b	0.945
Si1 -N	1.731(3)	C13 -H13c	0.942
Si1 -C1	1.846(4)	C14 -H14a	0.944
Si1 -C10	1.876(5)	C14 -H14b	0.949
Si1 -C11	1.866(5)	C14 -H14c	0.944
Si2 -C6	1.829(4)	C15 -C16	1.504(8)
Si2 -C12	1.876(6)	C15 -C17	1.533(8)
Si2 -C13	1.887(5)	C15 -C18	1.543(7)
Si2 -C14	1.864(6)	C16 -H16a	0.951
N -C19	1.464(6)	C16 -H16b	0.946
C1 -C2	1.431(6)	C16 -H16c	0.944
C1 -C5	1.410(6)	C17 -H17a	0.952
C2 -C3	1.403(6)	C17 -H17b	0.941
C2 -H2	0.951	C17 -H17c	0.947
C3 -C4	1.390(6)	C18 -H18a	0.952
C3 -C15	1.521(6)	C18 -H18b	0.942
C4 -C5	1.379(6)	C18 -H18c	0.945
C4 -H4	0.952	C19 -C20	1.472(10)
C5 -H5	0.951	C19 -C21	1.415(9)
C6 -H6a	0.951	C19 -C22	1.478(9)
C6 -H6b	0.950	C20 -H20a	0.953
C7 -H7a	0.950	C20 -H20b	0.986
C7 -H7b	0.943	C20 -H20c	0.901
C7 -H7c	0.945	C21 -H21a	0.947
C8 -H8a	0.952	C21 -H21b	0.948
C8 -H8b	0.940	C21 -H21c	0.939

Table XXIII. (Cont'd)

			Angle(°)				Angle(°)
H6a	-C6	-Si2	104.6	H13b	-C13	-Si2	108.8
H6b	-C6	-Si2	104.7	H13c	-C13	-Si2	109.1
H6b	-C6	-H6a	109.4	H13b	-C13	-H13a	109.8
H7a	-C7	-P	108.6	H13c	-C13	-H13a	110.0
H7b	-C7	-P	109.0	H13c	-C13	-H13b	110.7
H7c	-C7	-P	108.8	H14a	-C14	-Si2	108.8
H7b	-C7	-H7a	110.1	H14b	-C14	-Si2	108.5
H7c	-C7	-H7a	109.8	H14c	-C14	-Si2	108.8
H7c	-C7	-H7b	110.5	H14b	-C14	-H14a	110.0
H8a	-C8	-P	108.3	H14c	-C14	-H14a	110.5
H8b	-C8	-P	108.9	H14c	-C14	-H14b	110.1
H8c	-C8	-P	108.7	C16	-C15	-C3	112.5(4)
H8b	-C8	-H8a	110.2	C17	-C15	-C3	110.8(4)
H8c	-C8	-H8a	109.8	C18	-C15	-C3	108.1(4)
H8c	-C8	-H8b	110.8	C17	-C15	-C16	108.6(4)
H9a	-C9	-P	108.6	C18	-C15	-C16	108.8(4)
H9b	-C9	-P	108.5	C18	-C15	-C17	107.8(4)
H9c	-C9	-P	109.1	H16a	-C16	-C15	108.6
H9b	-C9	-H9a	109.6	H16b	-C16	-C15	109.1
H9c	-C9	-H9a	110.5	H16c	-C16	-C15	109.1
H9c	-C9	-H9b	110.5	H16b	-C16	-H16a	109.8
H10a	-C10	-Si1	108.8	H16c	-C16	-H16a	109.9
H10b	-C10	-Si1	108.6	H16c	-C16	-H16b	110.3
H10c	-C10	-Si1	108.9	H17a	-C17	-C15	108.3
H10b	-C10	-H10a	109.9	H17b	-C17	-C15	109.3
H10c	-C10	-H10a	110.4	H17c	-C17	-C15	108.8
H10c	-C10	-H10b	110.1	H17b	-C17	-H17a	110.1
H11a	-C11	-Si1	108.8	H17c	-C17	-H17a	109.6
H11b	-C11	-Si1	109.2	H17c	-C17	-H17b	110.6
H11c	-C11	-Si1	108.8	H18a	-C18	-C15	108.4
H11b	-C11	-H11a	110.3	H18b	-C18	-C15	109.1
H11c	-C11	-H11a	109.6	H18c	-C18	-C15	109.1
H11c	-C11	-H11b	110.1	H18b	-C18	-H18a	110.0
H12a	-C12	-Si2	108.6	H18c	-C18	-H18a	109.7
H12b	-C12	-Si2	109.2	H18c	-C18	-H18b	110.6
H12c	-C12	-Si2	108.7	C19	-N	-Si1	124.0(3)
H12b	-C12	-H12a	110.3	C20	-C19	-N	111.8(5)
H12c	-C12	-H12a	109.5	C21	-C19	-N	115.8(5)
H12c	-C12	-H12b	110.5	C22	-C19	-N	109.4(4)
H13a	-C13	-Si2	108.5	C21	-C19	-C20	109.8(6)

Table XXIII. (Cont'd)

Distance(Å)		Angle(°)	
C22 -H22a	0.952	Cp -Sc -N	104.1
C22 -H22b	0.930	Cp -Sc -P	106.9
C22 -H22c	0.943	Cp -Sc -C6	126.3
		Sc -P -C7	118.4(2)
		Sc -P -C8	112.2(2)
		Sc -P -C9	117.5(2)
		C8 -P -C7	100.2(2)
		C9 -P -C7	102.8(3)
		C9 -P -C8	103.3(3)
		Sc -N -C19	133.1(3)
		Sc -N -Si1	102.9(2)
		Sc -C6 -Si2	128.3(2)
		C1 -Si1 -N	96.1(2)
		C10 -Si1 -N	115.2(2)
		C11 -Si1 -N	117.3(2)
		C10 -Si1 -C1	109.5(2)
		C11 -Si1 -C1	109.8(2)
		C11 -Si1 -C10	108.1(2)
		C12 -Si2 -C6	111.5(2)
		C13 -Si2 -C6	112.4(2)
		C14 -Si2 -C6	112.5(2)
		C13 -Si2 -C12	106.3(2)
		C14 -Si2 -C12	107.3(3)
		C14 -Si2 -C13	106.4(2)
		Si1 -C1 -Cp	154.1
		C2 -C1 -Si1	124.9(3)
		C5 -C1 -Si1	122.6(3)
		C5 -C1 -C2	103.7(3)
		C3 -C2 -C1	110.8(4)
		H2 -C2 -C1	124.4
		H2 -C2 -C3	124.8
		C4 -C3 -C2	105.8(4)
		C15 -C3 -C2	127.7(4)
		C15 -C3 -C4	126.1(4)
		C5 -C4 -C3	109.5(4)
		H4 -C4 -C3	125.4
		H4 -C4 -C5	125.1
		C4 -C5 -C1	110.2(4)
		H5 -C5 -C1	124.8
		H5 -C5 -C4	125.0

Table XXIII. (Cont'd)
Angle(°)

C22	-C19	-C20	102.3(5)
C22	-C19	-C21	106.8(5)
H20a	-C20	-C19	108.1
H20b	-C20	-C19	106.4
H20c	-C20	-C19	111.6
H20b	-C20	-H20a	106.3
H20c	-C20	-H20a	113.5
H20c	-C20	-H20b	110.5
H21a	-C21	-C19	108.2
H21b	-C21	-C19	108.3
H21c	-C21	-C19	109.0
H21b	-C21	-H21a	109.9
H21c	-C21	-H21a	110.7
H21c	-C21	-H21b	110.6
H22a	-C22	-C19	107.3
H22b	-C22	-C19	108.8
H22c	-C22	-C19	108.0
H22b	-C22	-H22a	111.0
H22c	-C22	-H22a	109.8
H22c	-C22	-H22b	111.8

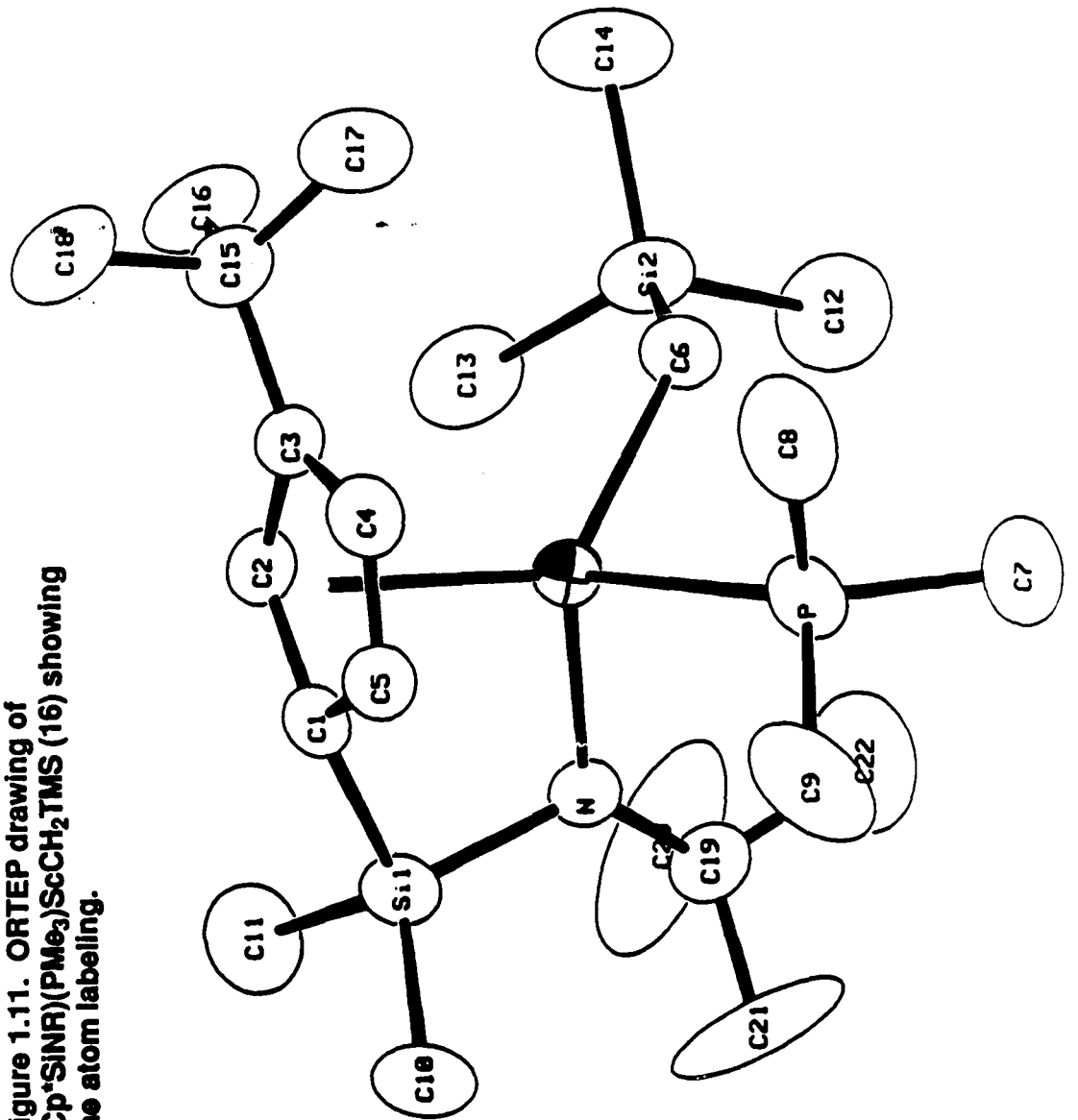

Figure 1.11. ORTEP drawing of $(Cp^*SiNR)(PMe_3)ScCH_2TMS$ (16) showing the atom labeling.

EXPERIMENTAL SECTION

General Considerations. All manipulations were performed by using glovebox and high-vacuum line techniques as described elsewhere.[26] Solvents were dried by standard techniques and further purified by vacuum transfer from titanocene[27] or sodium benzophenone. Argon and hydrogen were purified by passage over MnO on vermiculite and activated 4Å molecular sieves.

NMR spectra were recorded on Varian EM-390 (^{1}H, 90MHz), JEOL FX90Q (^{1}H, 89.56 MHz; ^{13}C, 22.50 MHz; ^{31}P, 36.23 MHz), JEOL GX400Q (^{1}H, 399.78 MHz;^{13}C, 100.38 MHz) and Bruker AM500 (^{1}H, 500.13 MHz) spectrometers. Infrared spectra were recorded on a Beckman 4240 spectrometer and a Perkin-Elmer 1600 series FTIR spectrometer and peak positions are reported in cm^{-1}. Elemental analyses were performed by F. Harvey of the Caltech Analytical Laboratory. Where indicated, oxidant (V_2O_5 and WO_3) was added to the compound to facilitate burning.

Reagents. Propene, ethylene and HCl (Matheson) were freeze-pump-thawed at least twice prior to use. PMe_3 was either prepared as described elsewhere[28] or purchased from Aldrich. Butyllithium (1.6M soln. in hexanes) and Me_2SiCl_2 were used as obtained from Aldrich. Methyllithium and trimethylsilylmethyllithium (Aldrich) were used as solids obtained by drying their ether solutions. $ScCl_3(THF)_3$,[1b] $Li(C_5Me_4H)$,[7] $LiCH(SiMe_3)_2$,[29] and $LiCH_2PMe_2$[30] were prepared as reported elsewhere.

$Li_2(Cp^*SiNR)$ (1). $Li(C_5Me_4H)$ (23.1 g, 0.2 mol) was suspended in 250mL tetrahydrofuran. While cooling the mixture to -78°C, Me_2SiCl_2 (24.1 mL, 0.2 mol) was added *via* syringe. The mixture was allowed to warm to room temperature and stirred overnight. The tetrahydrofuran was removed *in vacuo*, leaving $(C_5Me_4)SiMe_2Cl$ as a non-volatile, clear, colorless liquid, which was dissolved in 100 mL petroleum ether and filtered to remove LiCl. The petroleum ether was removed *in vacuo*, the $(C_5Me_4)SiMe_2Cl$ was dissolved in 250 mL

THF and Li(Me_3CNH) powder was added gradually with stirring to the solution at room temperature (exothermic). The mixture was stirred for two hours at room temperature, and the THF was removed *in vacuo* and replaced with 100 mL petroleum ether. LiCl was filtered off and the petroleum ether was removed *in vacuo* to afford H_2Cp^*SiNR as an orange oil. The oil was dissolved in 100 mL diethyl ether and cooled to -78°C. n-Butyllithium (1.6M in hexanes, 250 mL, 0.4 mol) was added via syringe and the reaction was allowed to warm to room temperature. After stirring the reaction overnight, the precipitated $Li_2(Cp^*SiNR)$ was collected by filtration as a tan powder (45.2 g, 80.7% yield).

(Cp^*SiNR)ScCl (2). $Li_2(Cp^*SiNR)$ (16.8 g, 64 mmol) and $ScCl_3(THF)_3$ (23.5 g, 64 mmol) were combined with 250 mL toluene and stirred overnight at room temperature. The resulting solution was filtered and the toluene was removed *in vacuo*, leaving an orange oil. Addition of petroleum ether (*ca* 100 mL) precipitated a white solid. Three crops were obtained. The solid was loaded into a flask and heated at 100°C under dynamic vacuum overnight to remove the THF. The product was then extracted away from the LiCl with hot toluene. The toluene was removed *in vacuo*, and petroleum ether was added to the resulting orange oil to precipitate 1 as a white powder (10.4 g, 51% yield). Elemental Anal. Found(Calcd) C, 54.14(54.45); H, 7.90(8.22); N, 4.23(3.93). IR(Nujol): 2733, 2686, 1465, 1372, 1349, 1320, 1244, 1198, 1122, 1076, 1046, 1029, 849, 826, 802, 756, 692, 552, 500.

(Cp^*SiNR)ScCH{$Si(CH_3)_3$}$_2$ (3). Compound 2 (3.0 g, 9.1mmol) and $LiCH(TMS)_2 \cdot 1/2Et_2O$ (1.85g, 9.1mmol) were combined in 150 mL toluene and stirred at 80°C for approx. 1hr, then overnight at room temperature. The toluene was removed *in vacuo* and the residue was redissolved in petroleum ether and filtered to remove the LiCl. The product was then precipitated at -78°C as a white microcrystalline solid (3.12 g, yield 76%). Elemental Anal. Found(Calcd) C, 58.0(58.1); H, 10.0(10.2), N 3.0(3.1). IR(Nujol): 2756, 2663, 1453, 1372, 1360, 1302, 1232, 1186, 1023, 860, 837, 814, 790, 767, 756, 721, 663, 599, 581, 535, 488.

[(Cp*SiNR)(PMe_3)Sc]$_2$(μ-H)$_2$ (4). Compound 3 (1.04 g, 2.3 mmol) was partially dissolved in 30 mL of petroleum ether in a thick-walled glass vessel, and 0.23 mL PMe_3 (2.3 mmol) was added by vacuum transfer. H_2 (4 atm) was added to the vessel and the reaction mixture was stirred at room temperature. After 15 min the solid was completely dissolved, leaving a yellowish solution. Upon continued stirring, a white precipitate formed. The reaction was stirred overnight and 4 was collected by filtration as a white powdery precipitate (0.71 g, 83% yield). Elemental Anal. Found(Calcd) C, 58.6(58.0); H, 9.8(10.0); N, 3.2(3.8). IR(Nujol): 2704, 2670, 1459, 1375, 1352, 1335, 1328, 1279, 1240, 1299, 1226, 1200, 1152, 1130, 1031, 1014, 950, 936, 837, 814, 795, 738, 671, 662, 623.

[(Cp*SiNR)(PMe_3)Sc]$_2$(μ, η^2, η^2-C_2H_4 (5). Compund 4 (0.308g, 0.414mmol) was dissolved in 10 mL of toluene in a thick-walled glass vessel. Two equiv. of ethylene (148 Torr, 104.3 mL), one equiv. per scandium, were condensed into the reaction mixture at -196°C. The reaction was thawed at -80°C and then stirred at 0°C for 2hrs. The resulting yellow solution was warmed to RT and then transferred to a flask attached to a swivel frit assembly in a nitrogen-filled glovebox. The solution was concentrated to *ca* 5mL and cooled to -80°C for 3 hr to afford orange-yellow crystals of 5 (0.170g, 53%). Elemental Anal. (oxidant added, two sets of data reported): Found C, 61.53, 63.64; H, 9.31, 9.71; N 3.07, 3.19 Calcd. C, 62.8; H, 9.8; N, 3.25.

[(Cp*SiNR)Sc]$_2$(μ-$CH_2CH_2CH_3$)$_2$ (6). Compound 4 (0.531 g, 0.787mmol) was dissolved in 20 mL of toluene in a thick walled glass vessel. Two equiv. of propene (256 Torr, 104.3 mL), one equiv. per scandium, were condensed into the reaction mixture at -196°C. After warming slowly to 25°C, the reaction was stirred for 15 minutes. The solution was then transferred to a flask attached to a swivel frit assembly in an N_2-filled glovebox. The solvent was removed under reduced pressure and the resulting white solid was suspended in 5 mL petroleum ether, filtered and washed once with another portion of petroleum ether to afford a white powder (0.156 g, 32%). Elemental Anal. (oxidant added, two sets of data reported):

Found C, 64.87, 63.13; H, 10.07, 9.76; N, 4.56, 4.40; Calcd. C, 64.0; H, 10.2; N, 4.1. IR(Nujol): 2720, 1455, 1375, 1350, 1320, 1240, 1190, 1120, 1035, 1010, 840, 815, 790, 760, 740, 470.

[(Cp*SiNR)Sc]$_2$(μ-$CH_2CH_2CH_2CH_3$)$_2$ (7). The same procedure was used as is described above for **6**, except that 1-butene (192 Torr, 104.3 mL) was added to a toluene solution of **4** (0.4 g, 0.54 mmol). The resulting white solid was redissolved in 10 mL toluene and the volatiles were then removed *in vacuo*. This cycle was repeated three times to ensure complete removal of PMe_3 from the product. Yield 0.173 g, 37.6%. Elemental Anal. Found(Calcd) C, 64.91(64.9); H, 10.09(10.3), N 4.16(4.0). IR(Nujol): 2720, 1455, 1378, 1355, 1320, 1243, 1226, 1196, 1126, 1096, 1079, 1038, 1014, 944, 838, 814, 797, 762, 744, 668, 532, 497, 480.

(Cp*SiNR)(PMe_3)$ScCH_2CH(CH_3)CH_2CH_2CH_3$ (8). 2.2 equiv. of 2-methyl-1-pentene (251 Torr, 104.3 mL) were condensed into a solution of **3** (0.50 g, 1.3 mmol) in 15 mL toluene at -196°C. The reaction mixture was warmed to RT and stirred for 2 days. Removal of the solvent under reduced pressure afforded a golden brown oil, which was dissolved in 2-3 mL pentane and cooled to -78°C to afford white crystals (0.298 g, 50.3%). Elemental Anal. Found(Calcd) C, 62.7(63.3); H, 10.4(10.8), N 2.8(3.1). IR(Nujol): 2708, 1461, 1372, 1355, 1308, 1284, 1237, 1196, 1138, 1126, 1032, 1014, 961, 950, 891, 838, 814, 785, 756, 738, 662, 532, 520, 497, 479.

(Cp*SiNR)(PMe_3)$ScCH(C_6H_5)CH_2CH_2CH_2C_6H_5$ (9). To a solution of compound **4** (0.20 g, 0.54 mmol) in 15 mL toluene were added 125 μL (1.1 mmol) styrene by syringe under the N_2 atmosphere of a glove box. The reaction was stirred at RT for 1 hour. The volatiles were removed from the resulting orange-yellow solution under reduced pressure, leaving a yellow solid that was redissolved in petroleum ether. Cooling the solution to -78°C afforded a bright, canary-yellow, microcrystalline solid (2 crops: 0.253 g, 81%). Elemental Anal. Found(Calcd) C, 70.22(70.4); H, 8.96(9.2), N 2.2(2.4). IR(Nujol): 2750, 2700, 1584, 1455,

1376, 1352, 1308, 1258, 1199, 1093, 1026, 838, 811, 800, 747, 697, 597, 565, 535, 523, 500, 479.

$(C_5H_4CMe_3)SiMe_2Cl$ (10). $(C_5H_4CMe_3)Li$ (21.7g, 0.169 moles) was dissolved in 300 mL THF. The solution was cooled to -78°C and Me_2SiCl_2 was added *via* syringe against a flow of argon. The reaction was warmed to RT and stirred overnight. The THF was removed under reduced pressure and the product was dissolved in 100 mL petroleum ether and filtered to remove LiCl. Removal of the petroleum ether *in vacuo* afforded a clear, light yellow, non-volatile liquid (33.1g, 91%).

Li_2(tBuCpSiNR) (11). Compound 10 was added dropwise by pipet to a solution of $Li(Me_3CNH)$ in 300 mL THF with stirring (slightly exothermic) in a nitrogen-filled glove box. The reaction was stirred overnight at room temperature. The THF was removed under reduced pressure, and the resulting yellow-orange liquid was dissolved in 250 mL petroleum ether and filtered away from the LiCl. The petroleum ether solution of the ligand was cooled to -78°C and 116 mL of a 1.6M solution of nBuLi in hexanes were syringed into the solution under an argon flow. The solution was warmed to slightly above RT, at which point the evolution of gas was observed. The yellow reaction solution became tan colored and viscous. After 5 hr the petroleum ether was removed *in vacuo* to afford a tan, glassy solid (26g, 106% theoretical yield). Impurities resulting from the crude method of work-up probably account for the excess yield.

(^{tBu}CpSiNR)ScCl(THF) (12). $ScCl_3(THF)_3$ (20.0g. 0.054 moles) and 11 (14.4g, 0.054 moles) were combined in a flask and 250 mL toluene were added to the solids. The reaction mixture was stirred at RT overnight. The resulting dark-brown solution was filtered to remove LiCl. Removal of toluene *in vacuo* afforded a sticky, brown residue from which a solid precipitated upon addition of petroleum ether. The solid was suspended in 100 mL petroleum ether and collected by filtration. Repeated washings with petroleum ether to remove the soluble, brown impurities afforded a white solid (15.68 g, 87%). The solid may

be purified by recrystallization from toluene. Elemental Anal. Found(Calcd) C, 57.3(56.8); H, 8.71(8.8), N 3.22(3.5). IR(Nujol): 2720, 2661, 1455, 1373, 1243, 1202, 1179, 1073, 1032, 1011, 938, 920, 859, 832, 808, 790, 762, 738, 685, 672, 532, 491.

(^{tBu}CpSiNR)ScCH$_2$PMe$_2$ (13). A flask was charged with compound 12 (3.0 g, 7.5 mmol) and LiCH$_2$PMe$_2$ (0.61 g, 7.5 mmol). Toluene (60 mL) was condensed onto the solids at -78°C, and the reaction mixture was warmed to RT and stirred overnight to afford a white powder, which coprecipitated with the LiCl co-product (2.66 g, 95%). Elemental Anal. Found(Calcd) C, 51.8(52.5); H, 8.2(8.6), N 3.1(3.4).

(^{tBu}CpSiNR)(PMe$_3$)ScCl (14). A thick walled glass vessel was charged with compound 13 (6.9g, 0.017 moles). Toluene (100 mL) was condensed onto the solid at -78°C. The mixture was then frozen at -196°C and 1 equiv. of HCl (272 Torr, 1.5 L) was condensed into the vessel. The reaction mixture was warmed to RT and stirred overnight. The solution was filtered through a pad of celite to remove the fine LiCl precipitate and then dried *in vacuo* to a foam. Recrystallization from petroleum ether afforded and off-white, microcrystalline solid (4.33 g, 64%). Elemental Anal. Found(Calcd) C, 53.37(53.2); H, 8.83(8.9), N 3.48(3.4).

(^{tBu}CpSiNR)ScCl (15). Heating 14 to 120°C for 5 hr under vacuum liberates PMe$_3$ to afford 14 cleanly as a foam. Elemental Anal. Found(Calcd) C, 54.01(54.6); H, 8.23(8.2), N, 4.25(4.2). IR(Nujol): 2719, 2672, 1455, 1372, 1296, 1243, 1196, 1173,1079, 1014, 955, 938, 914, 832, 808, 785, 767, 750, 685, 673, 538, 491.

(^{tBu}CpSiNR)(PMe$_3$)ScCH$_2$TMS (16). Compound 14 (1.0g, 2.5 mmol) and LiCH$_2$TMS (0.23 g, 2.5 mmol) were dissolved in 15 mL toluene, and the reaction was stirred for 1 hr at RT. The toluene was removed under reduced pressure, and the product was dissolved in 3-5 mL pentane. Cooling the solution to -78°C afforded white crystals (0.82 g, 87.4%). Elemental Anal. Found(Calcd) C, 57.9(57.7); H, 10.0(10.3), N, 3.3(3.1). IR(Nujol): 2720, 2672, 1455,

1377, 1364, 1353, 1305, 1286, 1239, 1198, 1176, 1082, 1053, 1030, 1018, 1004, 955, 940, 921, 832, 764, 746, 720, 662, 598, 537, 496.

[(^{tBu}CpSiNR)ScMe]$_x$ (17). Compound 14 (0.50g, 1.52 mmol) and MeLi (0.035 g, 1.54 mmol) were measured into a flask and 20 mL toluene were condensed onto the solids at -78°C. The reaction was warmed to RT and stirred for 2 hrs. The solution was filtered to remove LiCl, and the toluene was removed under reduced pressure. The residue was dissolved in 10 mL pentene and cooled to -78°C to afford a fluffy precipitate, which was isolated as an off-white solid (0.264 g, 56%). Elemental Anal. Found(Calcd) C, 62.06(62.1); H, 9.94(9.8); N, 3.98(4.5) . IR(Nujol): 2719, 2672, 1455, 1372, 1296, 1243, 1196, 1173, 1073, 1020, 955, 932, 914, 832, 808, 785, 761, 744, 726, 685, 673, 532, 491.

(^{tBu}CpSiNR)(PMe_3)ScC_6H_5 (18). Toluene, 50mL, was added to compound 13 (2.0g, 5.3 mmol) in a thick walled glass vessel. One equivalent of HCl gas (942 Torr, 104.3mL) was admitted to the vessel at -196°C and the reaction was stirred overnight at room temperature. The resulting solution was transferred to a flask containing 0.67g (8.0mmol) phenyl lithium in a nitrogen-filled glove box. The flask was attached to a frit assembly and the reaction was stirred overnight. The toluene was removed under reduced pressure, and the product was dissolved in pentane and filtered to remove insoluble salts. Concentration of the solution and cooling to -80°C afforded 0.433g (20% yield) of a tan solid. The product is extremely soluble and the reaction yield has not been optimized.

Toepler experiment to determine amount of ethane produced in formation of 5

Compound 4 (45.5mg, 0.0612mmol) was dissolved in 2.5mL toluene in a small glass vessel (5mL "oligomerizer"). 0.12mmol of ethylene (57 Torr, 40.1 mL) was admitted to the frozen reaction mixture at -196°C. The reaction mixture was thawed at -80°C, stirred at 0°C for one hour and then at 25°C for 15 min. The volatiles from the reaction, including solvent, were vacuum transferred to a larger volume (*ca* 25mL) thick walled vessel and were kept at

-8°C during the Toepler measurement. The amount of gas measured (43±1Torr, 25.2mL; 0.58±.02mmol) corresponds to 95.5% the theoretical amount of ethane expected. IR analysis of the gas confirmed its identity as ethane.

X-ray Crystal Structure Determination of $[(Cp^*SiNR)(PMe_3)Sc]_2(\mu\text{-}H)_2$ (4)

A crystal grown from a concentrated toluene-d_8 solution of 4 in an NMR tube was placed in a capillary in a nitrogen atmosphere and mounted on the diffractometer. Unit-cell dimensions and an orientation matrix were obtained from the setting angles of 25 reflections with $19° < 2\theta < 21°$. The compound crystallizes in the monoclinic system, in space group C2/c (#15), with a = 21.238(3)Å, b = 11.470(2)Å , c = 22.253(3)Å, β = 113.16(1)°, volume = 4984.0(14)Å^3; z = 8 (4 dimers), and density = 1.26 g cm^{-3}. Two complete data sets were collected; the data were corrected for a slight decay, but not for absorption (μr_{max} = 0.122, so neglect of this could have led to maximum errors of 1.3% in F). Lorentz and polarization factors were applied and the data were merged and then put on an approximate absolute scale by Wilson's method. The position of the scandium atom was found from a Patterson map, and the rest of the molecule was located in a subsequent Fourier map. A few cycles of isotropic refinement lowered R to 0.2, and a difference map then showed the toluene molecule, disordered at a center of symmetry. Anisotropic refinement of all the heavy atoms reduced R to 7%, but the goodness of fit was 2.55. Hydrogen atoms were introduced at positions found on the maps calculated in their planes or (for the deuteriums of the toluene molecule) at calculated positions. Their positions and isotropic thermal parameters were refined (but not the parameters of the toluene deuterium atoms, which were repositioned once near the end of the refinement and were assigned isotropic B's 20% greater than those of the carbon atoms they are bonded to). The final refinement involved 383 parameters in a single matrix; the largest shift/esd in the last cycle was 1.38 for z of C8; shifts for all other atoms, including the hydrogens (except those on C8) were less than 0.2 esd. The hydrogen atoms at C8 were poorly defined in difference maps, which probably leads to their poor

refinement. Further cycles of refinement did not change the situation significantly. The final difference map showed maximum excursions of ±0.24eÅ-3; the final R-index for those reflections with $Fo^2>3\sigma(Fo^2)$ was 0.034.

The labeling scheme is given in Figure 1.8, a summary of the data collection information is given in Table IV, coordinates and U_{eqs} for non-hydrogen atoms are listed in Table V, parameters for the hydrogen atoms are listed in Table VI, anisotropic thermal parameters are in Table VII, and complete distances and angles are given in Table VIII.

X-ray Crystal Structure Determination of [(Cp*SiNR)(PMe_3)Sc]$_2$(μ, η^2, η^2-C_2H_4) (5)

Orange-yellow crystals were grown from a toluene solution of 5 cooled at -60°C. A roughly cubic crystal was cut with a razor blade from a large hexagonal prism and held inside a 0.5 mm capillary with some hydrocarbon grease. The crystal was centered on the diffractometer and 25 reflections with $18°<2\theta<21°$ were found and centered. Preliminary cell dimensions and the orientation matrix were obtained from their setting angles; final cell dimensions were calculated from the setting angles of 25 different reflections with $32°<2\theta<40°$. The compound crystallizes in the monoclinic system in space group C2/c(#15), with a = 23.706(5), b = 11.342(2), c = 21.141(3)Å, β = 111.57(1)°, and volume = 5286.2(17)Å^3; z = 4. Two equivalent sets of data were collected and merged to give the final data set; the R-factor for merging was 0.055. The data were corrected for a slight (0.2%) decay, but no absorption correction was applied because μr_{max} was so small, and the grease obscured the edges of the crystal. The structure was solved by MULTAN and refined by full matrix least squares. A toluene solvent molecule was found early on, disordered about a center of symmetry, and its carbon atoms were included as constant contributions to the structure factors, but their parameters were not refined. Hydrogen atoms attached to the methyl groups were positioned at idealized positions based on difference maps calculated in their planes; of the 12 methyl groups, 11 showed clearly 3 hydrogen atoms in reasonable positions. The last, C8, had 6 possible locations, so two sets of half-hydrogens were

introduced there. All these were fixed in position, with arbitrary (7.0Å^2) thermal parameters. The two hydrogen atoms on the bridging ethylene molecule were located in a difference map, and their positional and thermal parameters were refined. The refinement converged quickly; the final R-index for reflections with $F_o^2>3\sigma(F_o^2)$ is 0.069. The final goodness of fit, 3.84, is rather high; this probably reflects problems in modeling the disordered toluene solvate, because the three highest peaks, and 6 of the top 9, in the final difference map are in this region (0.7, 0.7 and 0.5 eÅ^{-3}); the next highest peaks are less than 0.5eÅ^{-3}, two near the Cp* ring and one near the t-butyl group on nitrogen. All other peaks are less than 0.4eÅ^{-3}. There are 4 negative peaks in the difference map with magnitude greater than 0.4eÅ^3; all are in the solvent region, the largest, -0.8eÅ^{-3}, near C21. Unfortunately, the peaks and holes do not suggest a different model for this region.

The labeling scheme is given in Figure 1.9, a summary of the data collection information is given in Table IX, coordinates and U_{eqs} for non-hydrogen atoms are listed in Table X, parameters for the hydrogen atoms are listed in Table XI, anisotropic thermal parameters are in Table XII, and complete distances and angles are given in Table XIII.

X-ray Crystal Structure Determination of [(Cp*SiNR)Sc]$_2$(μ-CH$_2$CH$_2$CH$_3$)$_2$ (6)

Crystals of 6 were grown from a benzene solution cooled to ca 5°C and mounted in glass capillary tubes. Most were twinned, but one was found whose rotation photograph was acceptable. The capillary was large and the crystal was obscured by grease inside it, so we could not determine its size or shape precisely. The crystal was centered on the diffractometer and unit cell dimensions plus an orientation matrix were calculated from the setting angles of 25 reflections with $2\theta\approx20$ °. Final unit-cell dimensions were obtained later from 24 reflections with 31°<2θ<35°. The crystal was monoclinic, space group $P2_1/n$ (#14), with a = 9.429(2)Å, b = 21.937(5)Å, c = 9.826(2)Å, β = 99.39(2)°, and volume = 2005.2(7)Å^3; Z = 2. Two equivalent sets of data were collected; there was no decay in the crystal as measured by the three check reflections that we monitored during data collection. The data

were corrected for background, Lorentz and polarization factors were applied, and the data were merged to give one set that was put on an approximately absolute scale by Wilson's method. The locations of the scandium and silicon atoms were found by MULTAN and the remainder of the atoms were located in a subsequent Fourier map. Full matrix least squares, first with isotropic and then with anisotropic thermal parameters for the non-hydrogen atoms, converged with an R-index of about 15%. A disorder in the methyl atoms of the t-butyl group was noted and an alternate orientation of those three carbon atoms was added, with the population fixed at 20% of the total. Hydrogen atoms were added, either at calculated positions or based on difference maps calculated in their planes, on all carbon atoms except C20, the bridging atom, and the minor component of the t-butyl group. The hydrogen atoms were given isotropic thermal parameters 20% greater than the equivalent isotropic thermal parameter of the bonded carbon atom; neither their positions nor their thermal parameters, nor the parameters of the t-butyl component (whose isotropic thermal parameters were fixed at the average of the equivalent isotropic thermal parameters of the three major carbon atoms) were refined. Further refinement converged with an R-index of about 9% and a goodness of fit of 2.65. Most peaks in the difference map (maximum height $\pm 0.62 e\text{Å}^{-3}$) were in the region of the bridging n-propyl group, but a chemically reasonable model for an alternate bridging group could not be found. The two hydrogen atoms on the bridging carbon atom C20 were located, included as fixed contributions along with the rest of the hydrogen atoms (repositioned) and the minor component of the t-butyl group, and the refinement was completed. The final R-index is 0.0854; for those reflections with $F_o^2 > 3\sigma(F_o^2)$, R = 0.0579. The goodness of fit is 2.36. The final difference map had excursions of +0.48 and -0.45 $e\text{Å}^{-3}$. The largest peak is about equidistant from the three atoms of the bridging propyl group, still suggesting that the model is inadequate, but the small size of the residual peaks indicates that whatever disorder exists in this region is minor.

The labeling scheme is given in Figure 1.10, a summary of the data collection information is given in Table XIV, coordinates and U_{eqs} for non-hydrogen atoms are listed in Table XV, assigned parameters for the hydrogen atoms and disordered t-butyl carbons are listed in Table XVI, anisotropic displacement parameters are in Table XVII, and complete distances and angles are given in Table XVIII.

X-ray Crystal Structure Determination of (Cp*SiNR)(PMe_3)$ScCH_2TMS$ (16)

Crystals of 16 were grown from a petroleum ether solution cooled at -80°C and mounted in thin-walled glass capillaries. Preliminary photos of one crytal showed that it was single, with monclinic symmetry. Unit cell dimensions and an orientation matrix were calculated from the setting angles of 25 reflections with $13°<2\theta<16°$. The compound crystallizes in space group $P2_1/n$, #14, with a = 11.181(4), b = 18.206(5), c = 15.250(6)Å, β = 108.25(3)°, and volume = 2948.2(18)$Å^3$; Z = 4. Two complete data sets were collected out to 2θ = 40°; the data were corrected for a slight decay, Lorentz and polarization factors were applied and they were put on an approximately absolute scale by Wilson's method. No correction for absorption was made because μr_{max} is small, and the two data sets merged together well. The structure was solved by direct methods, phasing the reflections by hand; and the E map calculated with about 300 reflections revealed the Sc, P, and Si atoms. MULTAN had great difficulty with the data. Once the Sc, P and Si atoms were located, the remaining heavy atoms were found in Fourier maps and were refined by six cycles of least squares. Hydrogen atoms were then introduced at calculated positions (C-H = 0.95Å, with isotropic thermal parameters 20% greater than those of the bonded carbon atom), assuming staggered geometries at the methyl groups, as constant contributions to the structure factors. They were repositioned once, just before the final cycles of full matrix refinement, which adjusted the positional and anisotropic thermal parameters of all the non-hydrogen atoms and a scale factor (244 parameters). The final R-index for 4307 reflections with $F_o^2>0$ is 0.1298, somewhat high, but for the 2101 reflections with $F_o^2>3\sigma(F_o^2)$ it is 0.0533, a more

acceptable number. The value for all reflections is high because of the large number of weak reflections (59% of the total). The final difference map had maxima of ±0.65eÅ^3, with no discernible pattern to them. The largest positive peak was near C20, a methyl carbon with large, apparent thermal motion.

The labeling scheme is given in Figure 1.11, a summary of the data collection information is given in Table XIX, coordinates and U_{eqs} for non-hydrogen atoms are listed in Table XX, assigned parameters for the hydrogen atoms are listed in Table XXI, anisotropic displacement parameters are in Table XXII, and complete distances and angles are given in Table XXIII.

Calculations were done with programs of the CRYM Crystallographic Computing System and ORTEP. Scattering factors and corrections for anomalous scattering were taken from a standard reference (International Tables for X-ray Crystallography, Vol. IV, p.71, p. 149; Birmingham, Kynoch Press, 1974). $R = \Sigma||F_o|-|F_c||/\Sigma Fo$, for only $Fo^2>0$, and goodness of fit = $[\Sigma w(Fo2-Fc2)2/(n-p)]^{1/2}$, where n is the number of data and p the number of parameters refined. The function minimized in least squares was $\Sigma w((Fo^2-Fc^2)^2$, where $w = 1/\sigma^2(Fo^2)$. Variances of the individual reflections were assigned on the basis of counting statistics plus an additional term $0.014I^2$. Variances of the merged reflections were determined by standard propagation of error plus another additional term, $0.014<I>^2$.

References

1. a) Thompson, M. E.; Bercaw, J. E. *Pure Appl. Chem.* **1984**, *56*, 1. b) Thompson, M.E.; Baxter, S. M.; Bulls, A. R.; Burger, B. J.; Nolan, M. C.; Santarsiero, B. D.; Schaefer, W. P.; Bercaw, J. E. *J. Am. Chem. Soc.* **1987**, *109*, 203.

2. a) McKenzie, T. C.; Sanner, R. D.; Bercaw, J. E. *J. Organomet. Chem.* **1975**, *102*, 457. b) Bercaw, J. E. *Advances in Chemistry Series* **1978**, *167*, 136. c) Gibson, V. C.; Bercaw, J. E.; Bruton, W. J.; Sanner, R. D. *Organometallics*, **1986**, *5*, 976

3. a) Lappert, M. F.; Holton, J.; Ballard, D. G. H.; Pearce, R.; Atwood, J. L.; Hunter, W. E. *J. Chem. Soc., Dalton Trans.* **1979**, 45. b) Lappert, M. F.; Holton, J.; Ballard, D. G. H.; Pearce, R.; Atwood, J. L.; Hunter, W. E. *J. Am. Chem. Soc., Dalton Trans.* **1979**, 54. c) Lappert, M. F.; Singh, A.; Atwood, J. L.; Hunter, W. E. *J. Chem. Soc., Chem. Commun.* **1983**, 206. d) Atwood, J. L.; Smith, K. D. *J. Chem. Soc., Dalton Trans.*, **1973**, 2487.

4. Burger, B. J.; Thompson, M. E.; Cotter, W. D.; Bercaw, J. E. *J. Am. Chem. Soc.* **1990**, *112*, 1566.

5. Parkin, G.; Bunel, E.; Burger, B. J.; Trimmer, M. S.; van Asselt, A.; Bercaw, J. E. *J. Mol. Catal.* **1987**, *41*, 21.

6. The ebulliometric molecular-weight analysis gave molecular weights of 583 g/mole and 559 g/mole on two separate occasions (theoretical MW for monomer is 454.8 g/mole).

7. Bunel, E. Ph.D. Thesis, California Institute of Technology, **1988**.

8. Pauling, L. *The Nature of the Chemical Bond*, 3rd ed.; Cornell Press: Ithaca, 1960; Chapter 7.

9. Ghotra, J. S.; Hursthouse, M. B.; Welch, A. J. *J. Chem. Soc., Chem. Commun.* **1973**, 66.

10. a) Brauer, D. J.; Bürger, H.; Essig, E.; Geschwandtner, W. *J. Organomet. Chem.* **1980**, 343. b) Planalp, R. P.; Andersen, R. A.; Zalki, A. *Organometallics*, **1983**, l2 , 16. c) Planalp, R. P.; Andersen, R. A. *Organometallics*, **1983**, 2, 1675.

11. Lappert, M. F.; Pedley, J. B.; Sharp, G. J.; Bradley, D. C. *J. Chem. Soc., Dalton Trans.* **1976**, 1737.

12. Harris, R. K. *Nuclear Magnetic Resonance Spectroscopy*; Pitman: Marshfield, 1983; p. 232.

13. Evans, W. J.; Meadows, J. H.; Wayda, A. L.; Hunter, W. G.; Atwood, J. L. *J. Am. Chem. Soc.* **1982**, *104*, 2008.

14. Jordan, R. F.; Bajgur, C. S.; Dasher, W. E. *Organometallics*, **1987**, *6*(5), 1041.

15. For other examples of μ, η^2, η^2-olefin-bridged dimers see: b) Cotton, F. A.; Kibula, P. A. *Polyhedron*, **1987**, *6*, 645. c) Evans, W. J.; Ulibarri, T. A.;

Ziller, J. W. *J. Am. Chem. Soc.* 1990, *112*, 219. d) Burns, C. J.; Andersen, R. A. *J. Am. Chem. Soc.* 1987, *109*, 915. e) Ref. 17

16. Schultz, A. J.; Brown, R. K.; Williams, J. M.; Schrock, R. R. *J. Am. Chem. Soc.* 1981, *103*, 169 and references therein.

17. Kaminsky, W.; Vollmer, H. J.; Heins, E.; Sinn H. *Makromol. Chem.* 1974, *175*, 443. b) Heins, V. E.; Hinck, H.; Kaminsky, W.; Oppermann, G.; Raulinat, P. *Makromol. Chem.* 1970, *134*, 1.

18. Kaminsky, W.; Kopf, J.; Sinn, H.; Vollmer, H. J. *Angew. Chem., Int. Ed. Engl.* 1976, *15*(10), 629.

19. Holton, J.; Lappert, M. F.; Ballard, D. G. H.; Pearce, R.; Atwood, J. L.; Hunter, W. E. *J. Chem. Soc., Dalton Trans.* 1979, 54.

20. Anderson, G. A.; Almenningen, A.; Forgaard, F. R.; Haaland, A. *J. Chem. Soc., Chem. Commun.* 1971, 480.

21. Huffman, J. C.; Streib, W. E. *J. Chem. Soc., Chem. Commun.* 1971, 911.

22. Burger, B. J. Ph.D. Thesis, California Institute of Technology, 1987.

23. Doherty, N. M.; Bercaw, J. E. J. Am. Chem. Soc., 1985, 107, 2670.

24. In the reaction of triisobutylaluminum with styrene to form tris-(phenethyl)aluminum, 22-44% of the 2-phenethyl substituents were found in the products. This may be compared to a similar reaction with 1-hexene, in which n-hexyl products prevail. Natta, G.; Pino, P.; Mazzanti, P.; Longi, P.; Bernardini, F. J. Am. Chem. Soc., 1959, 2561.

25. a) Ewen, J. A. *J. Am. Chem. Soc.* 1984, *106*, 6355. b) Kaminsky, W.; Külper, K.; Brintzinger, H. H.; Wild, F. R. W. P. *Angew. Chem. Int. Ed. Engl.* 1985, *24*, 6. c) Kaminsky, W.; Bark, A.; Spiehl, R.; Möller-Lindenhof, N.; Niedoba, S. In *Transition Metals and Organometallics as Catalysts for Olefin Polymerization*/ Kaminsky, W., Sinn H., Eds.; Springer-Verlag: Berlin, 1988; p. 291. d) Ewen, J. A.; Haspeslagh, L.; Elden, M. J.; Atwood, J. L.; Zhang, H.; Cheng, H. N. In Transition Metals and Organometallics as Catalysts for Olefin Polymerization/ Kaminsky, W., Sinn H., Eds.; Springer-Verlag: Berlin, 1988; p. 281.

26. Burger, B. J.; Bercaw, J. E. In *New Developments in the Synthesis, Manipulation and Characterization of Organometallic Compounds* Wayda, A. L., Darensbourg, M. Y. *Eds.; ACS Symposium Series, 357* (1987).

27. Marvich, R. H.; Brintzinger, H. H. *J. Am. Chem. Soc.* 1971, 93, 203.

28. a) Sharp, P. R. *Organometallics*, 1984, *3*, 1217. b) Wolfsberger, W.; Schmidbauer, H. *Synth. React. Inorg. Met-Org. Chem.* 1974, *4*, 149.

29. a) Cowley, A. H.; Kemp, R. A. *Synth. React. Inorg. Met.-Org. Chem.* 1981, *11*(6), 591. b) Davidson, P. J.; Harris, D. H.; Lappert, M. F. *J. Chem. Soc., Dalton, Trans.* 1976, 2268.

30. Karsch, H. H.; Schmidbaur, H. *Z. Naturforsch., B: Anorg. Chem., Org. Chem.* **1977**, *32*, 762.

Chapter 2

Investigations of the α-Olefin Polymerization Activity and Mechanism for Monocyclopentadienyl Scandium Amido Complexes

Introduction

Identifying the active species involved in industrially important catalytic processes is usually difficult and often impossible. For instance, the Fischer-Tropsch process for hydrocarbon synthesis,[1a] the Haber process for the reduction of N_2 to ammonia[1b] and the ammoxidation of propene to acrylonitrile[1c] are examples of processes whose mechanisms remain uncertain because the conditions of the reactions preclude direct characterization of the active catalyst species. The Ziegler-Natta olefin polymerization process is no exception. As mentioned in the general introduction, the catalyst centers are ill-defined because of their multicomponent, heterogeneous composition and the fact that usually only a small percentage of the transition metal centers are active. Even in homogeneous Ziegler-Natta systems based on mixtures of group IV metallocenes and an alkyl aluminum or aluminoxane cocatalyst, the active species are unidentifiable because of the presence of complex equilibria in the former case[2] and the overwhelming amount of aluminum cocatalyst (1000 fold!) necessary in the latter case.[3] One solution to better understanding the mechanisms of such hard-to-get-at catalyst systems is to develop well-defined, soluble, unimolecular complexes that undergo discrete reactions pertinent to the catalysis and are easily characterized by structurally informative methods such as NMR spectroscopy and x-ray crystallography. In fact, the development and investigation of such model complexes has been one of the mainstays of synthetic and mechanistic organometallic chemistry. There are now several well-defined, early transition metal and lanthanide complexes which, by virtue of their olefin insertion activity, serve as models for Ziegler Natta catalyst systems. The structural simplicity of these model systems serves to facilitate their mechanistic investigation. The permethylscandocene system is especially conducive to mechanistic study since its derivatives are monomeric and all activity is constrained to occur in the "equatorial wedge" between the cyclopentadienyl rings, where the frontier molecular orbitals are located.[4] In increasing the activity of the scandium by progressing from the bis-

pentamethylcyclopentadienyl ligand framework to the monocyclopentadienyl amido ligand framework we sacrifice some of this simplicity. As a result of the decreased steric demand of the monocylopentadienyl amido ligand system, the scandium complexes tend to oligomerize and require coordinating ligands for stabilization. Our isolated, structurally characterized complexes are no longer the actual catalysts but *precatalysts* for the polymerization. It behooved us to determine the nature of the active catalyst (i.e., monomer *vs.* dimer, phosphine-bound *vs.* phosphine-free) if we were to understand our systems any better than the complex catalyst mixtures we were trying to model. We therefore set out to determine through kinetic analysis the nature of the active catalyst species derived from these precatalyst complexes. The results of these experiments are described within. All evidence points to a monomeric, Lewis-base free, 12e- scandium alkyl as the active chain propagating species. Other aspects of the polymerization reactions such as the molecular weights and polydispersities of the polymer products and the regioselectivity and stereospecificity of the polymerization are also discussed. In essence, this chapter presents our efforts to characterize the α-olefin polymerization activity of the complexes described in Chapter 1.

Results and Discussion

General Features of Olefin Polymerization by [(Cp*SiNR)(PMe_3)Sc]$_2$(μ-H)$_2$(4).

The α-olefin polymerizing activity of the (Cp*SiNR)Sc system was initially discovered with the scandium hydride complex (4). Most of the features of the polymerization using this precatalyst are summarized in Scheme I. As can be seen, the turnover rate of this system is rather slow. As a result, although the polymerization of propene may be observed in an NMR tube, the relatively low solubility of propene in toluene at 25°C causes the synthesis of polypropene at monomer pressures of <5 atm. to be rather sluggish and impractical. Only modest molecular weight polymers are obtained from the polymerizations of 1-pentene and 1-butene at 25°C. The molecular weights listed in

Scheme I.

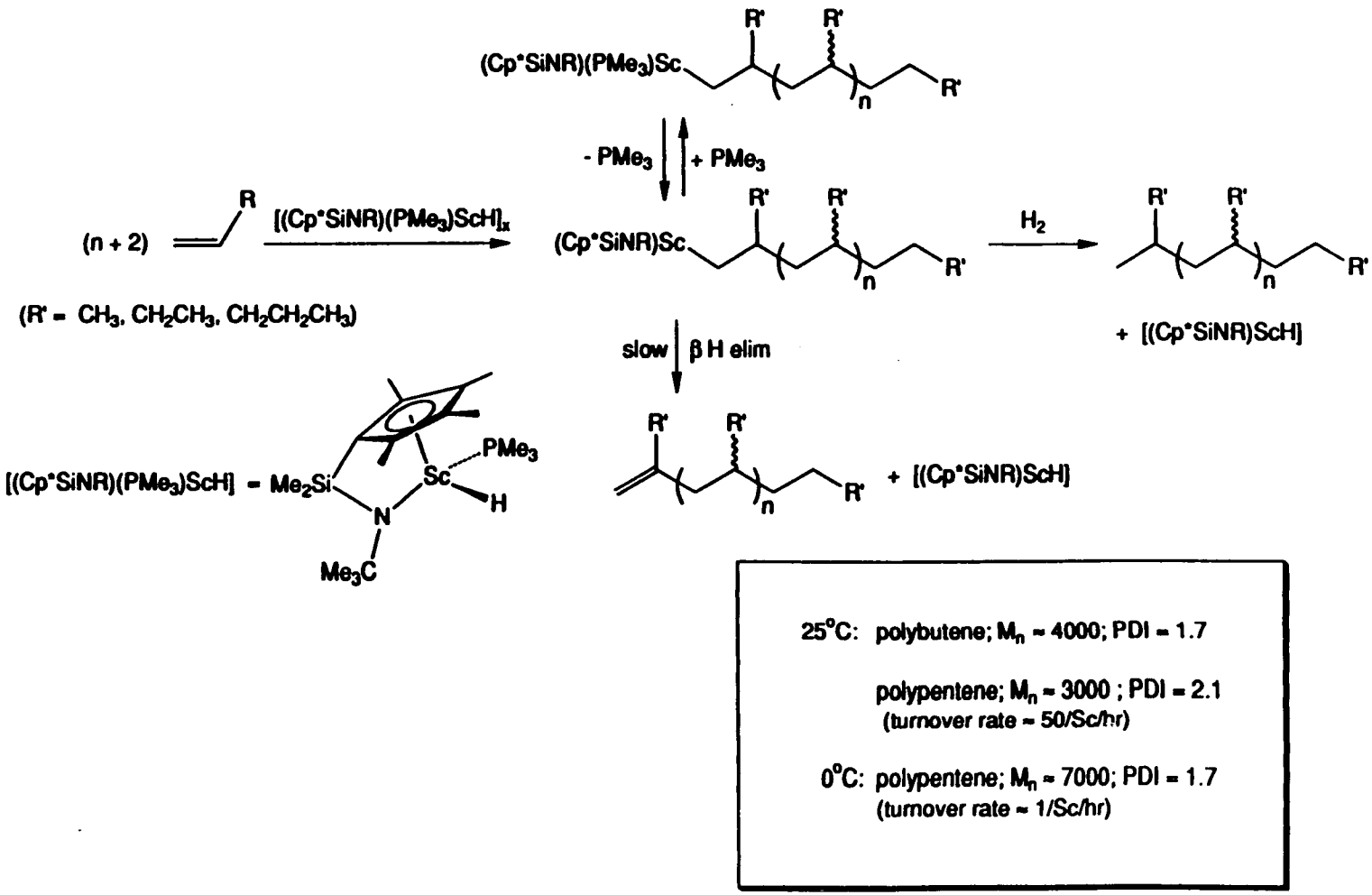

25°C: polybutene; M_n = 4000; PDI = 1.7

polypentene; M_n = 3000 ; PDI = 2.1
(turnover rate = 50/Sc/hr)

0°C: polypentene; M_n = 7000; PDI = 1.7
(turnover rate = 1/Sc/hr)

Scheme I were measured by GPC relative to polystyrene. The 1-butene and 1-pentene polymers are colorless, sticky oils, and resonances for vinylidene chain ends are observed in their ^{1}H NMR spectra, implicating β-H elimination as a principal chain-transfer pathway. Cooling the reaction results in an increase in the molecular weight of the polymer product and a slight reduction in the polydispersity index. This trend is expected since lowering the temperature at which the polymerization is performed should favor the intermolecular insertion reaction relative to intramolecular β-H elimination. The sluggishness of the polymerization reaction prohibits cooling the reaction below 0 °C, thus keeping us from our goal of eliminating chain transfer completely (as in a "living" system).

As mentioned above, resonances that correspond to gem-disubstituted olefin (vinylidene) chain ends are observed in the ^{1}H NMR spectra of polymers produced at room temperature by 4, consistent with chain transfer by β-H elimination. We have found that gem disubstituted olefins (cf. 2-methyl-1-pentene) react slowly (1 day) with 4 in a stoichiometric fashion. This indicates that chain transfer by β-H elimination in this catalyst system is only slowly reversed, and reinsertion of the chain end does not compete effectively with the much faster addition of α-olefin. Also, branching of the polymer caused by the combination of vinylidene chain ends does not occur.

Chain transfer by β-alkyl elimination would lead to vinylic chain ends, which are not observed in the ^{1}H NMR spectrum of polymers produced at room temperature. Such vinylic chain ends would not be observed, however, if they react in the same way as other α-olefins and are combined to form branched polymer. This possibility deserves investigation. A pattern in the olefin region of the ^{1}H NMR spectrum that is diagnostic of *vinylic* chain ends is observed for polypropene prepared at 80 °C with 4. Thus, β-alkyl elimination is evident at least at elevated temperatures. The scandium catalyst is not stable at this temperature, however, forming a new species that crystallizes from the solution as it cools. The structure of this decomposition product could not be elucidated from either its ^{1}H or ^{13}C NMR

spectrum, although the activation of PMe_3 C-H bonds is apparent. Efforts to obtain a crystal structure have been unsuccessful so that the identity of this decomposition product is still unknown. Further investigation is necessary to establish the importance of β-alkyl elimination as a chain-transfer mechanism in this system. A search for this type of reactivity in model scandium complexes (cf. $(Cp^*SiNR)(PMe_3)ScCH_2CH(CH_3)CH_2CH_2CH_3$ (8)) could be informative.

The reactivity of 4 toward other unsaturated substrates has been examined briefly. Conjugated dienes are at least oligomerized with this system, albeit slowly and only at elevated temperatures (80°C).[5] As will be discussed, the phosphine-free systems, such as the scandium propyl dimer (6), are more efficient catalysts for polymerizing α-olefins and are better catalysts for the polymerization of conjugated dienes as well. The reactivity of 4 toward gem-disubstituted olefins has already been discussed in Chapter 1. Internal olefins, allene, terminal and internal alkynes react only stoichiometrically with 4, and the identities of the reaction products were not pursued.

Analysis of Propene Oligomer Molecular Weight Distributions

Two primary concerns associated with studying a catalyst system such as 4 are that a) only a minor component of the mixture is responsible for the catalysis, and b) more than one active species is present. Clearly, either of these situations would present severe limitations to our ability to describe the system.

Certain observations with regard to polymerization catalysis by 4 served to diminish these two concerns. That all of the scandium is involved in the polymerization is indicated by the disappearance of signals characteristic of 4 in the ^1H NMR spectrum upon addition of olefin; these resonances are regenerated when the reaction mixture is hydrogenated. Also, the PDI's of the polymers produced by 4, as determined by GPC, are approximately 2, indicating that the catalyst mixture is homogeneous.[6]

Nevertheless, a more reliable method was needed for demonstrating that our catalyst system was well behaved, i.e., that all of the scandium centers were acting alike. Therefore, as a more careful check, the molecular weight distributions of propene oligomers produced by **4** were examined at low monomer conversion, where chain transfer by β-H elimination is essentially absent. Given that the rate of initiation is at least as fast as the rate of subsequent insertions and that all of the scandium centers are active and inserting monomer at a uniform rate (conditions for a "living"[7] system), the molecular weight distribution of oligomers produced by **4** should be adequately modeled by a Poisson function based on the ratio of monomer consumed to scandium present.[8]

The oligomerization reactions were carried out as described in the experimental section. The resulting scandium alkyls were cleaved with H_2 and the molecular weight distributions of the saturated oligomers were analyzed by GC. Since, with the exception of the propene trimer, 2,4-dimethylhexane, authentic standards were not available for comparison with the oligomers, the identities of the oligomers out to C_{27} were verified first by GC/MS analysis. In determining the relative amounts of oligomers in the GC traces, the response factors of the oligomers were assumed to scale linearly with their carbon number.

In Figure 2.1, two representative oligomer distributions are compared with the calculated Poisson distributions on the basis ofthe amount of monomer consumed *assuming that all scandium centers are active*. Good agreement is observed between the experimental and the calculated distributions, *indicating that most, if not all, of* the scandium centers are participating in the polymerization and are propagating at a similar rate.

An interesting sidelight to this experiment was our finding that the maximum theoretical number of separable head-to-tail (*vide infra*) stereoisomers could be observed by capillary GC for the shorter propene oligomers, two for the tetramer, 2,4,6-trimethylnonane, four for the pentamer, 2,4,6,8-tetramethylundecane, and eight for the hexamer, 2,4,6,8,10-tetramethyltridecane (Figure 2.2). Apart from the physical characteristics of the polymers

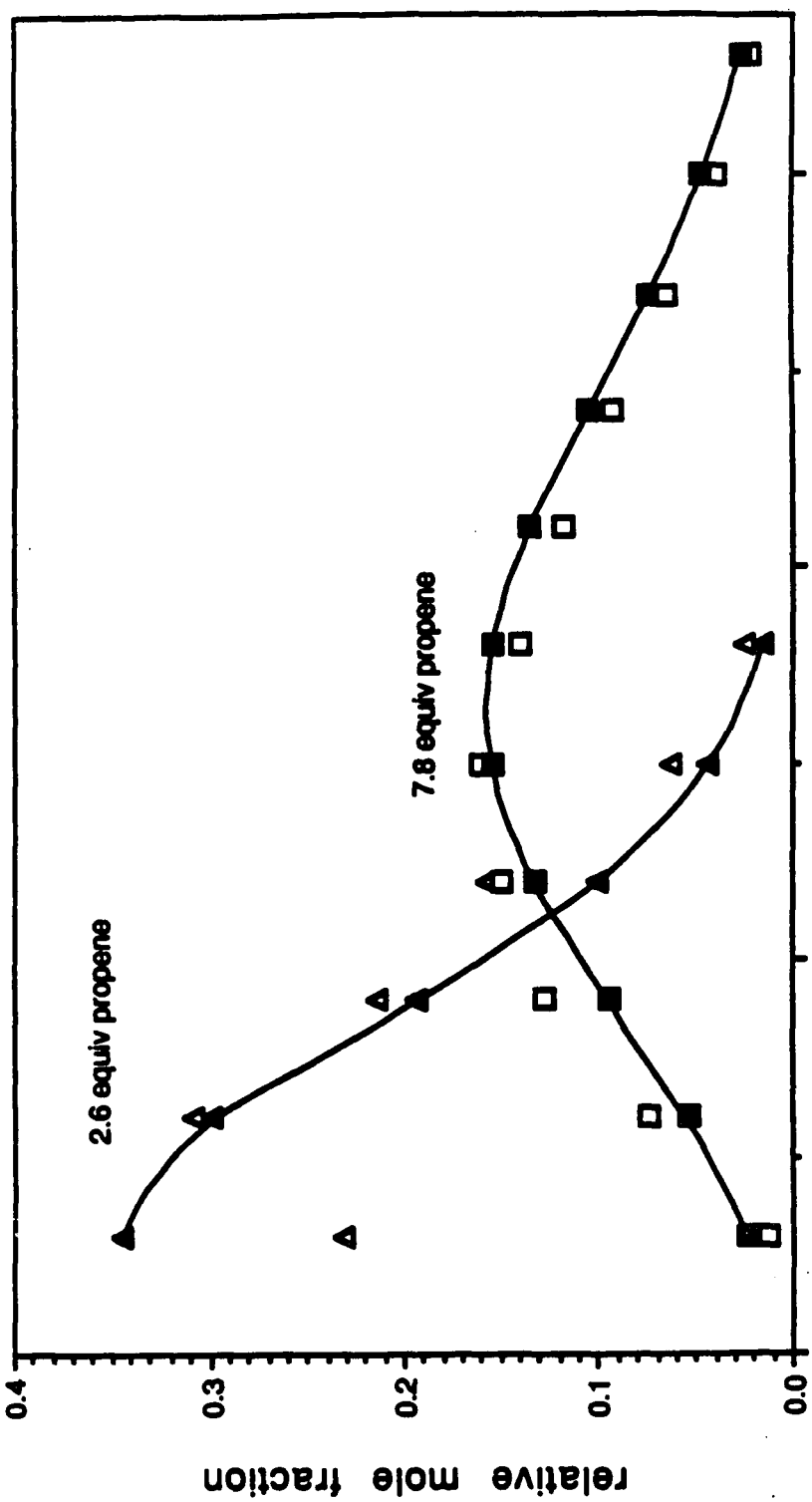

Figure 2.1. Experimental (open symbols) vs. calculated Poisson (solid symbols) oligomer distributions for the reactions of $[(Cp^*SiNR)(PMe_3)ScH]_2$ with 2.6 equiv of propene (triangles) and with 7.8 equiv of propene (squares).

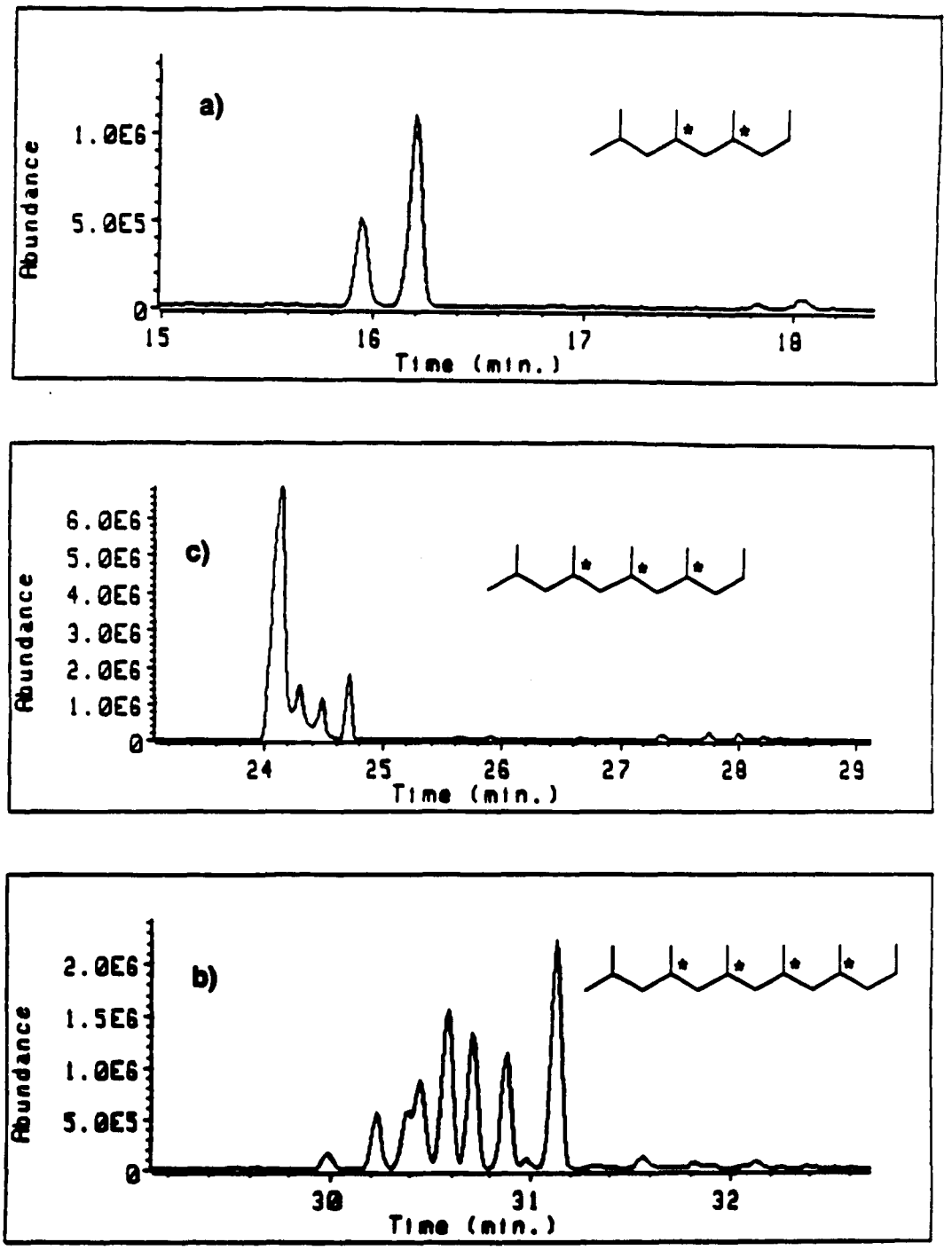

Figure 2.2. GC analysis of a mixture of propene oligomers prepared with $[(Cp^*SiNR)(PMe_3)ScH]_2$. Expanded regions show peaks corresponding to the maximum number of separable stereoisomers for: a) 2,4,6-trimethylnonane, b) 2,4,6,8-tetramethylundecane and c) 2,4,6,8,10-pentamethyltridecane.

produced by **4**, this was the first evidence that atactic polymer is produced by this catalyst system. Results from the examination of polymer tacticity by ^{13}C NMR are presented later in this chapter.

Kinetic Analysis of 1-Pentene Polymerization by 4

Confident that **4** was indeed the catalyst precursor and that the system was well behaved, we proceeded to examine the kinetics of the polymerization in order to elucidate the nature of the active chain carrying scandium species. Since the concentration of catalyst centers is constant during the polymerization, assuming that the rate of olefin insertion is independent of the size of the alkyl chain on the scandium, the disappearance of olefin monomer can be monitored to determine a value for k_{obs} in the rate expression for the reaction (Equations 1 and 2). A series of kinetic experiments were carried out in this manner by monitoring the rate of disappearance of 1-pentene by ^1H NMR. The concentration of scandium and the concentration of PMe_3 were varied separately to determine their effect on k_{obs}, thereby revealing whether the active species was monomeric or dimeric and whether phosphine loss was a prerequisite for olefin insertion.

$$(1)\quad [ScR] + CH_2{=}CHR' \xrightarrow{k_1} [ScCH_2CHRR'] + CH_2{=}CHR' \xrightarrow{k_1} \textit{etc.}$$

$$(2)\quad \text{Rate} = k_1[ScR]\,[CH_2{=}CHR'] = k_{obs}[CH_2{=}CHR']$$

We began by varying the concentration of **4** in the reaction to determine its effect on k_{obs}. As shown by the plots in Figure 2.3, the reaction was monitored for six different concentrations of **4**, ranging from 0.017M to 0.072M in scandium. Clean first-order disappearance of monomer was observed over 3-4 half lives, confirming the assumption that the rate of propagation is independent of the size of the alkyl chain on the metal. The k_{obs} corresponding to each concentration of **4** is obtained from the slope of each line. When these values for k_{obs} are plotted against [ScH] (Figure 2.4), instead of increasing linearly

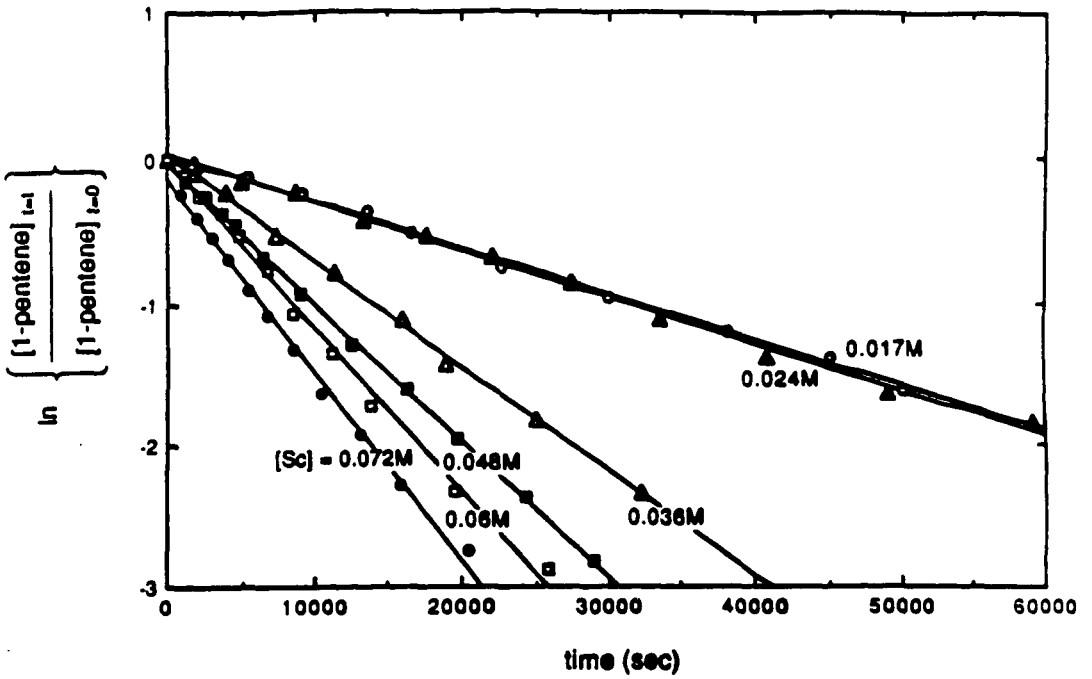

Figure 2.3

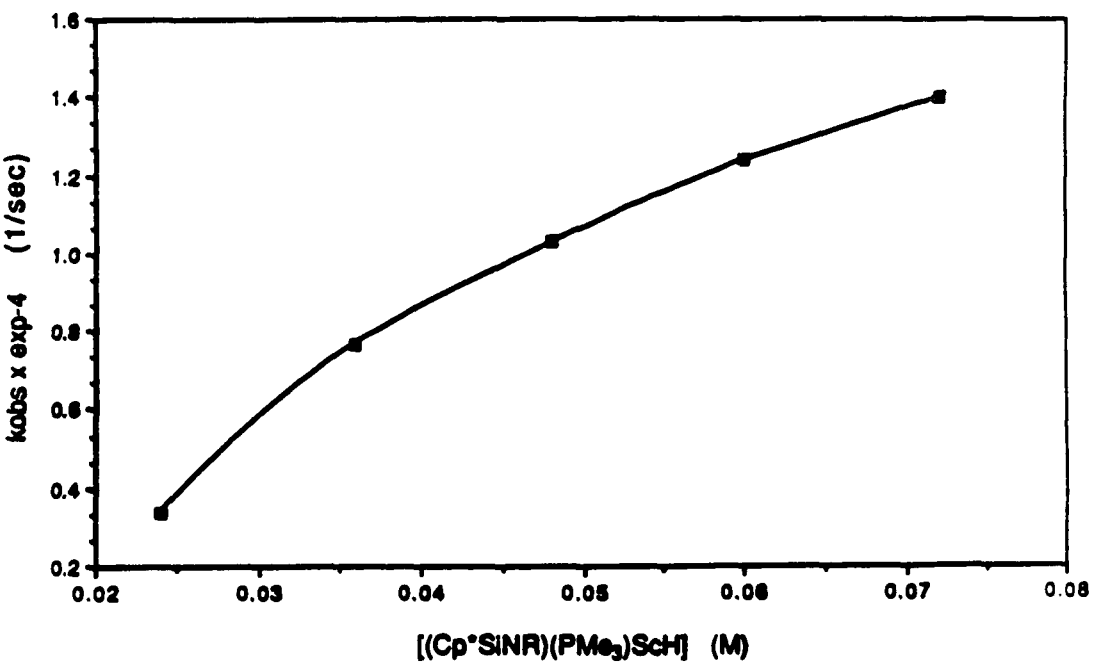

Figure 2.4

with the concentration of scandium, they level off gradually. This behavior signifies a dissociative pre-equilibrium in the generation of the active species.

The proposed mechanistic model for the polymerization (shown in Figure 2.5) involves a dissociative pre-equilibrium to afford the active catalyst (Cp*SiNR)ScR. This model is consistent with behavior observed in other Ziegler-Natta model systems. For example, kinetic studies of the insertion of propene by $Cp^*_2LuCH_3 \cdot L$ revealed a dissociative pre-equilibrium to afford the active species $Cp^*_2LuCH_3$.[9] The monomeric nature of the active species was confirmed by kinetic analysis of the reaction of $[Cp^*_2LuCH_3]_2$ with propene. Likewise, Jordan has shown that the active species in ethylene polymerization by $[Cp_2Zr(CH_3)(THF)^+]$ is the "naked alkyl", $[Cp_2Zr(CH_3)^+]$.[10]

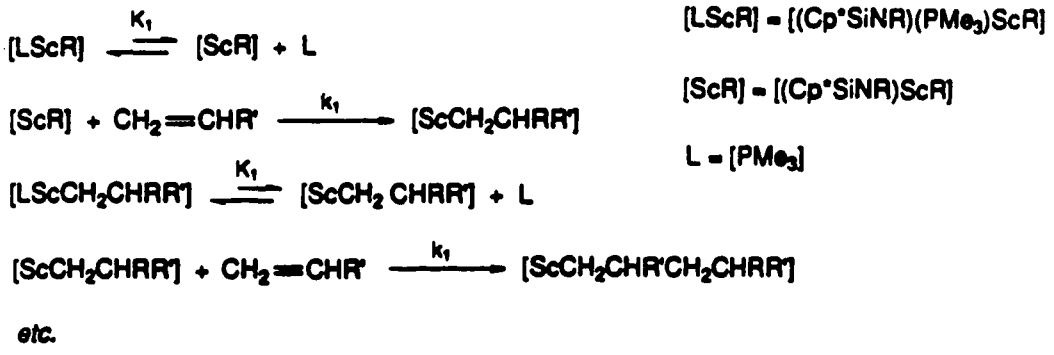

Figure 2.5. Mechanism of Olefin Polymerization by (Cp*SiNR)(PMe$_3$)ScR

We were already aware of the inhibitory effect of phosphine on the rate of olefin polymerization in that adding excess phosphine to the catalyst system slows the polymerization and the phosphine-free Sc-alkyl dimers are much more active than 4. To check the validity of the above model and to determine values for K_1 and k_1, the kinetics of 1-pentene polymerization by 4 was measured at 32°C for different concentrations of added PMe_3, with the concentration of scandium held constant. Once again, clean first-order

disappearance of olefin was observed (Figure 2.6).

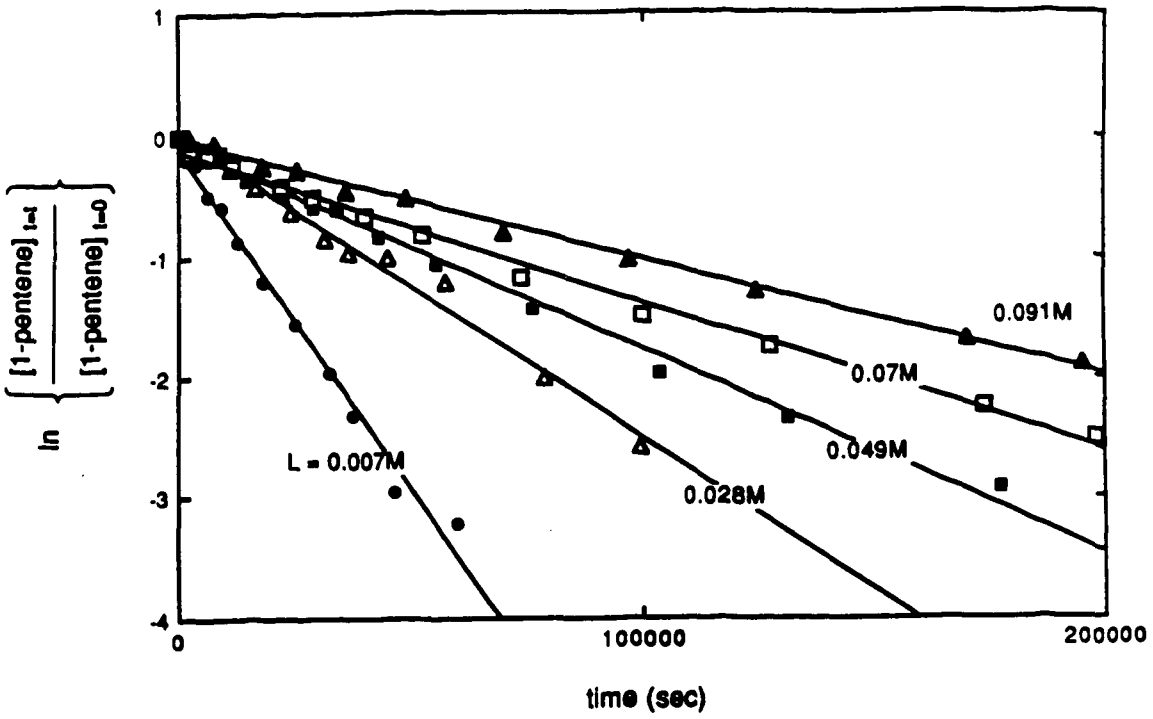

Figure 2.6

If we assume that the amount of dissociated phosphine is negligible relative to added phosphine, we obtain the expression for K_1 shown in Equation 3. Given this assumption, a plot of $1/k_{obs}$ vs. [PMe_3 added] should afford a straight line (Figure 2.7). The second-order rate constant, k_1, is evaluated from the intercept of the line as $0.0015M^{-1}sec^{-1}$. Using this value for k_1, a value for K_1 of 0.0085M is determined from the slope of the line. While an inverse dependence of k_{obs} on phosphine concentration is clearly indicated from the plot of $1/k_{obs}$ vs. [PMe_3 added], the degree of phosphine dissociation indicated by the size of K_1 is higher than initially estimated, too high for dissociated phosphine to be neglected in our calculations.[11]

Including dissociated phosphine into the equilibrium expression gives a more complex dependence of k_{obs} on added phosphine (Equations 6 and 7). This time, a non-

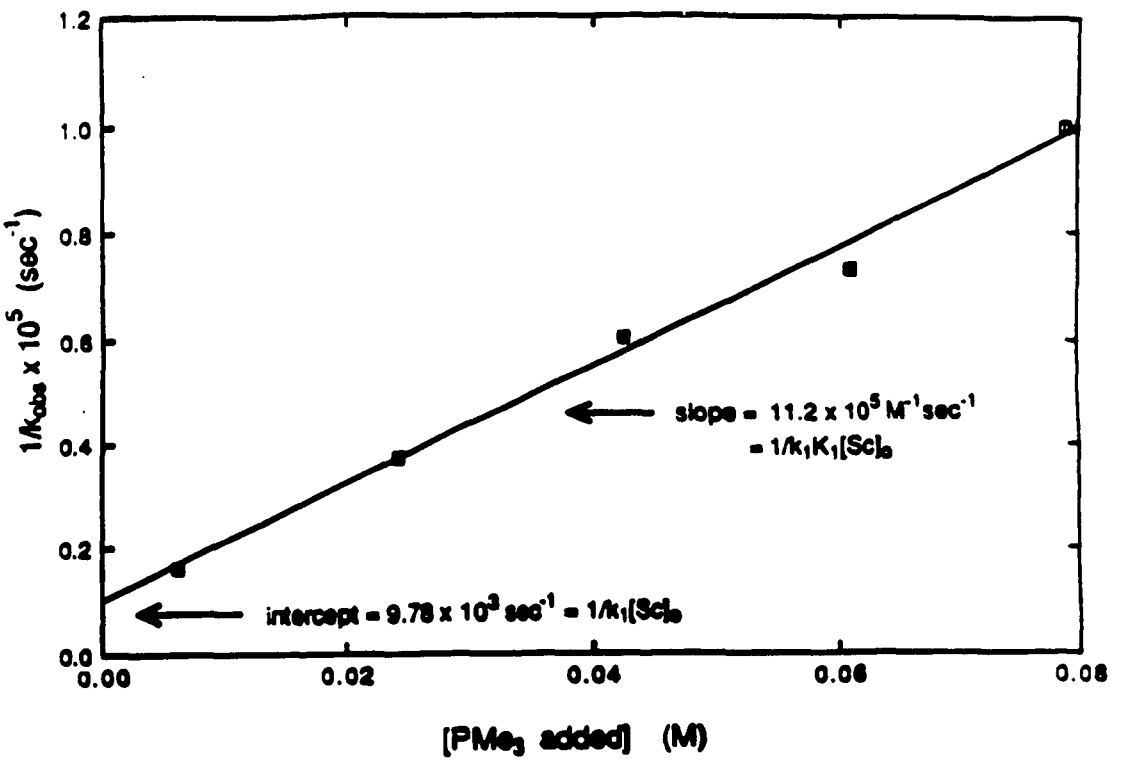

Figure 2.7

(3) $$K_1 = \frac{[(Cp^*SiNR)ScR]\,[L]}{[Sc]_o - [(Cp^*SiNR)ScR]}$$

$[L] = [PMe_3 \text{ added}]$

$[Sc]_o = [\text{total scandium}]$

(4) $$k_{obs} = k_1[(Cp^*SiNR)ScR] = \frac{k_1K_1[Sc]_o}{K_1 + [L]}$$

(5) $$\frac{1}{k_{obs}} = \frac{1}{k_1[Sc]_o} + \frac{L}{k_1K_1[Sc]_o}$$

linear, least-squares fit of the data gives a smaller value for K of 0.0012(5)M along with a second-order rate constant k_1 of 0.0094(40) $M^{-1}sec^{-1}$.[12] A plot of the data (k_{obs} vs. [PMe_3 added]) with the corresponding curve fit is shown in Figure 2.8.

$$K_1 = \frac{[ScR]\,([ScR] + [L])}{[Sc]_o - [ScR]} \qquad (6)$$

$$k_{obs} = k_1[ScR] = (k_1/2)\,(-([L] + K_1) + \{([L] + K_1)^2 + 4K_1[Sc]_o\}^{0.5}) \qquad (7)$$

Although an excellent fit with the kinetic data is obtained with this model, it was of concern to us that the value for k_1 determined at 32°C from these experiments is essentially the same size as the value for k_1 (0.016$M^{-1}sec^{-1}$) determined for 1-pentene polymerization at -6°C by the phosphine-free scandium propyl complex (6)(*vide infra*). Theoretically, if the same active intermediate is involved, the value for k_1 at 32°C, using precatalyst 4, should be about a factor of ten greater than k_1 at -6°C, using precatalyst 6.[13] We considered the possibility that our active catalyst was actually the phosphine-coordinated scandium species; however, the behavior of k_{obs} expected from this model is completely different from what is observed.

Yet another refinement was added to our mechanistic model in order for it to be complete and in order to improve our estimates of the parameters K_1 and k_1. We included in our model the monomer/dimer equilibrium for (Cp*SiNR)ScR (Equation 8), which was revealed in the kinetic analysis of 1-pentene polymerization by 6 (*vide infra*).

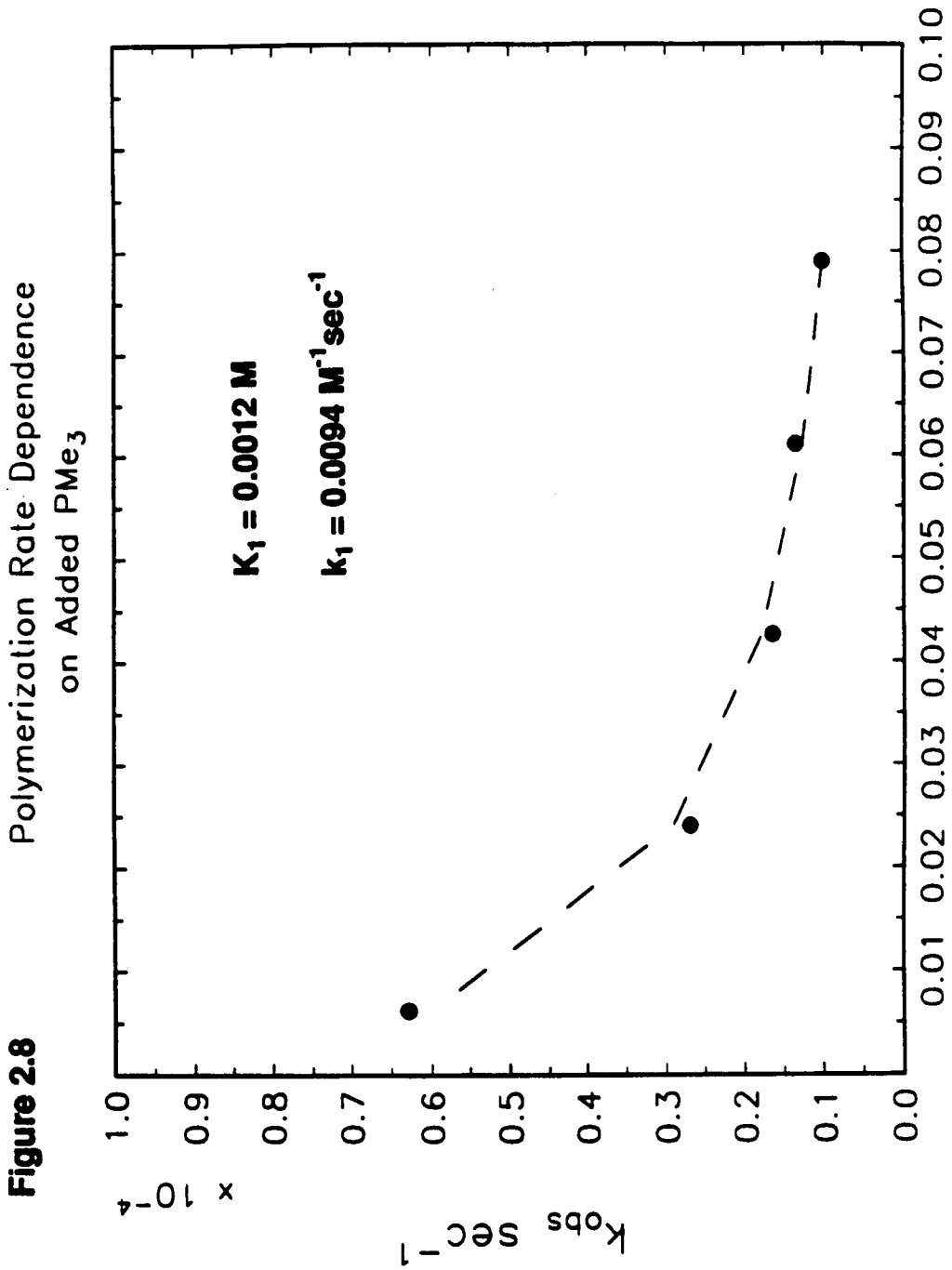
Polymerization Rate Dependence
on Added PMe3
K1 = 0.0012 M
k1 = 0.0094 M-1sec-1
kobs sec-1
x 10-4
1.0
0.9
0.8
0.7
0.6
0.5
0.4
0.3
0.2
0.1
0.0
0.01 0.02 0.03 0.04 0.05 0.06 0.07 0.08 0.09 0.10
Conc. Added PMe3 (M)

Figure 2.8

$$[\,(ScR)_2\,] \overset{K_2}{\rightleftharpoons} 2\,[ScR] \qquad (8)$$

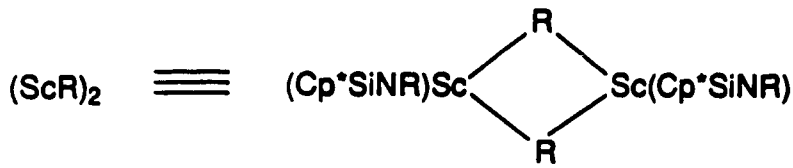

A cubic equation (Equation 9) was derived, which involves a third parameter, K_2, to describe the new dependence of k_{obs} on added phosphine.

$$[Sc]_o = [ScR] + [(ScR)_2] + [ScRL]$$

$$= \frac{[ScR]([Sc]_o + [L])}{(K_2 + [ScR])} + \frac{2[ScR]^2}{K_1} + [ScR]$$

$$= \frac{[k_1/k_{obs}]([Sc]_o + [L])}{(K_2 + [k_1/k_{obs}])} + \frac{2[k_1/k_{obs}]^2}{K_1} + [k_1/k_{obs}] \qquad (9)$$

Given the limited set of data, a non-linear, least-squares fit to all three parameters was not feasible; therefore, a reasonable value for K_2 at 32°C was calculated and included in the least squares analysis to estimate k_1 and K_1. A value for K_2 at 32°C of 0.039M was extrapolated from the value of 0.006M measured at -6°C by assuming a ΔS for dimer dissociation of 20 eu. Inclusion of the monomer/dimer equilibrium in the analysis serves to increase k_1 to 0.018(15)$M^{-1}sec^{-1}$ and to reduce K_1 to 0.0006(5)M. The data and new curve fit are shown in Figure 2.9.

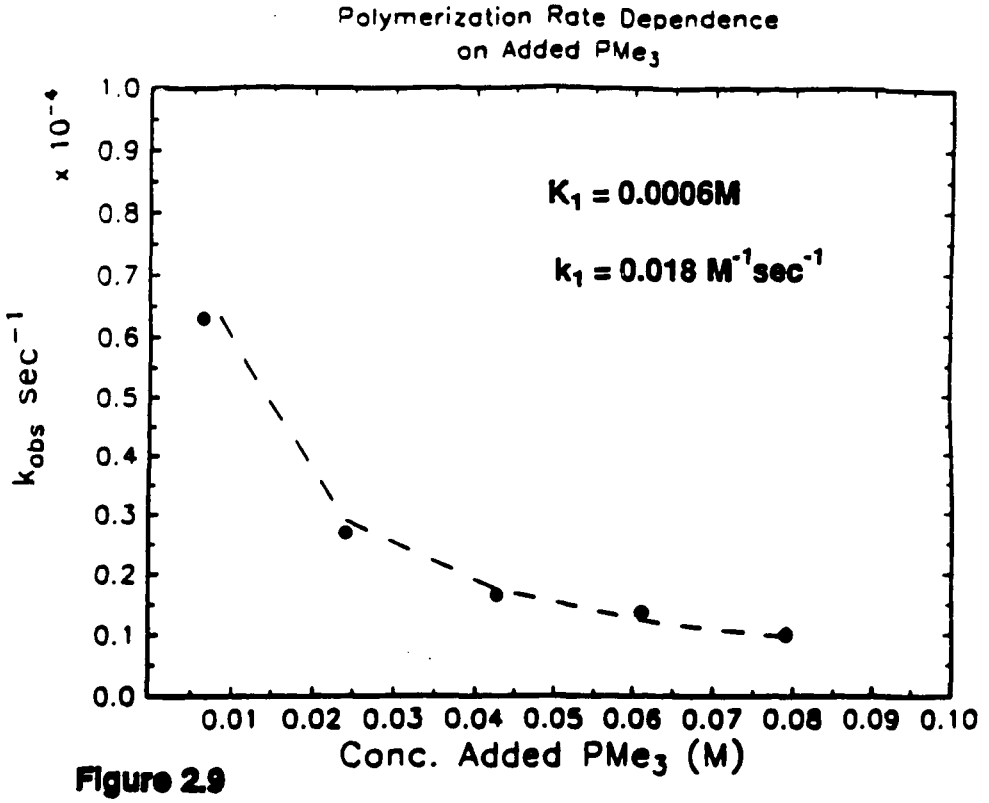

Figure 2.9

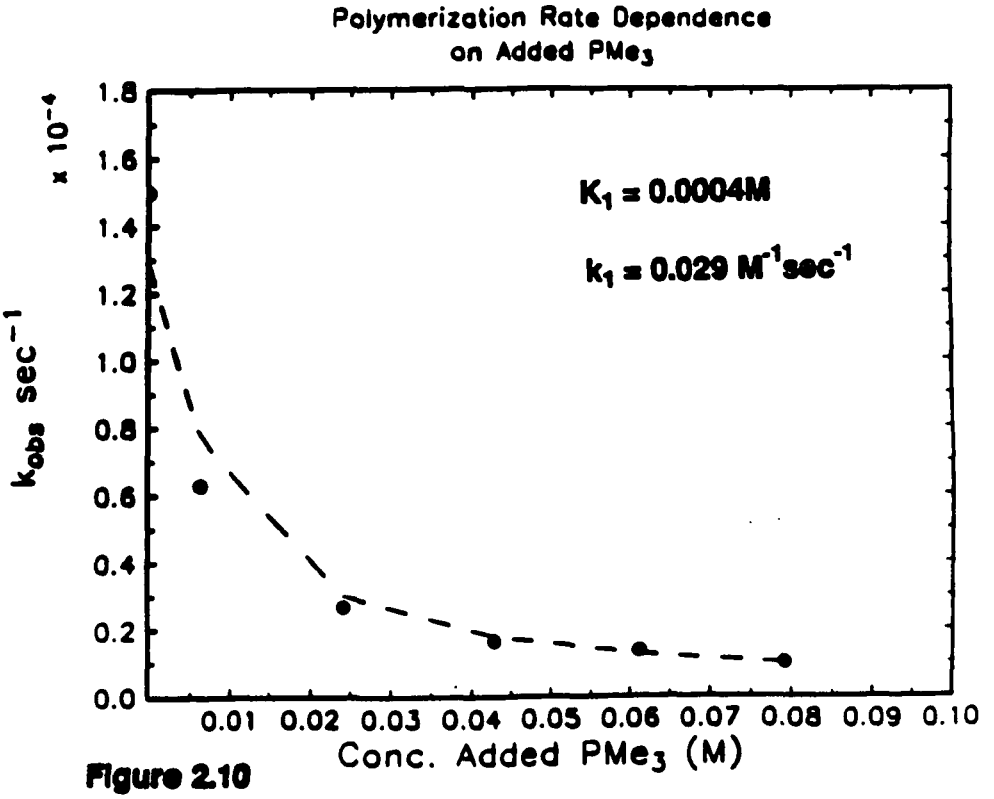

Figure 2.10

Despite our refinement of the model, the value for k_1 had not increased significantly. When another point is added to the data set, (the rate of 1-pentene polymerization by system 4 in the absence of added phosphine determined in a separate experiment), the value for k_1 determined from the non-linear, least-squares fit increases to $0.029(13)M^{-1}sec^{-1}$ (Figure 2.10). While this value is fairly stable to changes in the value for scandium concentration, it is quite sensitive to changes in the concentrations of added phosphine. Changing the value for K_2 has a noticeable effect on k_1 as well.[14]

Although we were not able to resolve the discrepancy in the values for k_1 determined at the two temperatures, there are a number of assumptions and numerous sources of error in this experiment that could contribute to the analysis of k_1. Nevertheless, a pre-equilibrium for phosphine dissociation is clearly indicated. The same monomeric, phosphine-free scandium-alkyl species responsible for the polymerization by 6 (below) is, most likely, also the active intermediate in the polymerization by precatalyst 4.

General Features of the Olefin Polymerization by $[(Cp^*SiNR)Sc]_2(\mu\text{-alkyl})_2$ (6 and 7)

Not only is an enhanced rate of olefin polymerization observed when the phosphine-free, scandium alkyl dimers 6 and 7 are the precatalysts instead of 4, but higher molecular weight polymer is obtained as well (Figure 2.11). Significant polymerization activity is still observed at temperatures as low as -10°C with the scandium propyl system. While lowering the temperature of the polymerization results in the formation of higher molecular weight polymer, we were disappointed to find that the molecular weight polydispersity of the polymer does not improve with the decrease in temperature.

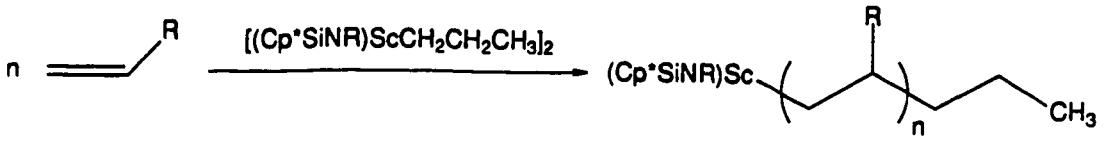

polypentene: *ca.* 25°C; Mn = 6,000; PDI = 1.5
[neat pentene]

polypropene: *ca.* 25°C; Mn = 5,200; PDI = 2.8
(*ca.* 25 v/v% in toluene)

ca. -11°C; Mn = 12,700; PDI = 2.2
(*ca.* 25 v/v % in toluene)

Figure 2.11

When the polymerization is monitored by ^{1}H NMR, after the consumption of several equivalents of olefin relative to scandium, a considerable amount of the starting complex is unreacted. Thus, slow initiation relative to propagation could broaden the molecular weight distribution of the polymer. To confirm that it was indeed a leftover starting complex that we were observing in these polymerizations and not simply a generic spectrum for all phosphine-free scandium alkyls, a reaction mixture obtained from **6** and ten equivalents of propene was hydrogenolyzed and the volatiles were vacuum transferred to another NMR tube in order to measure the amount of propane liberated. Using hexamethyldisiloxane as a standard to quantify the propane by ^{1}H NMR, a 0.44 equivalent of propane relative to scandium was measured, indicating that 44% of the scandium propyl complex was unreacted after the ten equivalents of propene had been consumed. We attribute this slow rate of initiation relative to propagation to the stability of the alkyl bridges of the dimer complex, which must cleave to form the active 12e- scandium-alkyl monomer.

While following the kinetics of 1-pentene polymerization by **6**, a uniform decay in the activity of the catalyst systems over time was observed. This catalyst decay would also tend

to broaden the molecular weight distribution of the polymer. The cause of this decay in activity has not yet been determined. Activation of the toluene solvent by the scandium was ruled out as the cause, since similar behavior was observed in methylcyclohexane and in cyclohexane. No olefin resonances that were due to β-H elimination were apparent in the ^{1}H NMR of polypropene produced by **6**. Either the olefin chain ends are too dilute relative to the size of the polymer to be observed, or alternate forms of chain transfer and chain termination are more important in this system.

Unfortunately, even the phosphine-free (Cp*SiNR)ScR complexes are not potential "living" catalysts for the polymerization of α-olefins. Nevertheless, the enhanced activity of these systems has allowed the preparation of polypropene for microstructure analysis (*vide infra*) as well as the polymerization of substrates, such as conjugated dienes,[7] which are only poorly polymerized by **4**.

As will be discussed in the next section, and has been alluded to earlier, these complexes have also allowed us to complete our mechanistic picture of the polymerization by enabling the dependence of the rate on the concentration of scandium to be measured in the absence of phosphine.

Kinetic Analysis of 1-Pentene Polymerization by 6

The kinetic analysis of 1-pentene polymerization by **4** established an inverse dependence of the rate on PMe_3 concentration. Because of the complexity of the system, however, meaningful information could not be extracted from these data about the dependence of the rate on scandium concentration in order to determine the molecularity of the catalyst. The PMe_3-free scandium-alkyl dimers provided us with this opportunity. The problem of slow initiation by these systems had to be circumvented in order to ensure that activity from all of the scandium centers was being measured. Bulkier olefins such as neohexene and 3-methyl-1-butene were investigated as substrates which, by slowing the

polymerization, could narrow the gap between the rate of initiation and the rate of propagation in addition to making the reaction slower and easier to monitor. Interestingly, neohexene was unreactive toward these systems. 3-Methyl-1-pentene reacts with **6** and **7** but is not polymerized, so its use as a monomer was not pursued. Our ultimate approach was to use highly dilute catalyst solutions (*ca* 0.03M to 0.07M in scandium dimer) to favor scandium-monomer formation and a large excess of olefin (100 to 400 equivalents), so there would be plenty of olefin left over after all of the starting dimer complex had reacted.

Upon monitoring the reaction at 32°C, instead of the usual first-order disappearance in monomer, we found that the rate of the polymerization decayed over time. The source of this decay in catalyst activity was not determined, although it was slowed sufficiently at -6°C so that polymerization rates could be obtained. The first order disappearance in olefin over 2-3 half-lives is plotted for three different concentrations of scandium in Figure 2.12. A less than first-order dependence of k_{obs} on scandium concentration is evident from these data as well as from the plot of k_{obs} vs. [Sc-dimer] (Figure 2.13). In fact, the observed behavior corresponds to a monomer-dimer pre-equilibrium prior to olefin insertion modeled by Equation 10. This establishes the 12e-, monomeric scandium alkyl as the active species in the polymerization reaction. The non-linear, least-squares fit to the data gave values for the parameters k_1 and K_2 of $0.016 M^{-1}sec^{-1}$ and 0.008M respectively.

A Brief Look at Olefin Polymerization by (^{tBu}CpSiNR)ScR

Because of the recent development of the (^{tBu}CpSiNR)Sc system, our examination of its polymerization activity has been only preliminary. As mentioned in Chapter1, only the PMe_3-free species are active, and $[(^{tBu}CpSiNR)ScMe]_x$ is one complex we have managed to isolate for examination. Qualitatively, this system was found to polymerize olefins as slowly as the catalyst system based on **4**. The dissociation of the scandium methyl oligomers to monomeric species is probably rate determining. Nevertheless, we were able to prepare polypropene with this system for stereochemical analysis (*vide infra*). GPC analysis of the

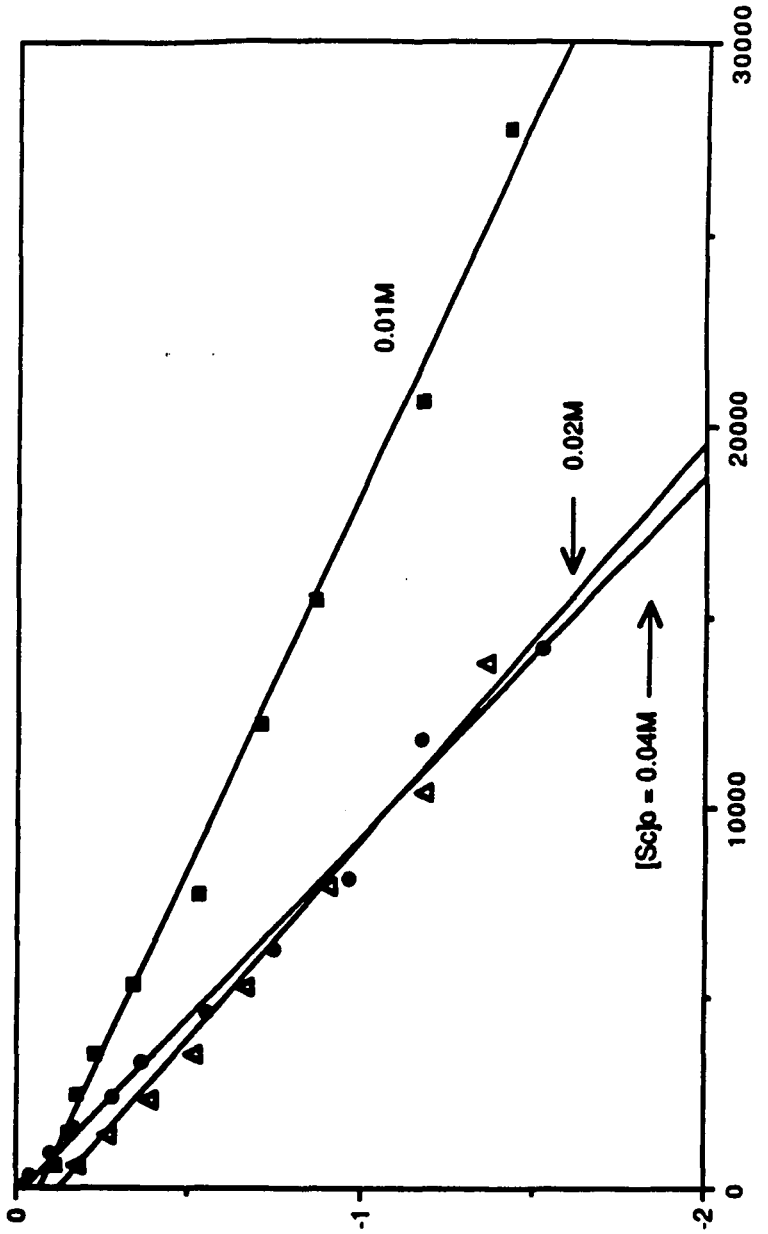
0.01M
0.02M
[Scp = 0.04M
time (sec)
0
10000
20000
30000
0
-1
-2
ln {[1-pentene] t=t / [1-pentene] t=0}

Figure 2.12

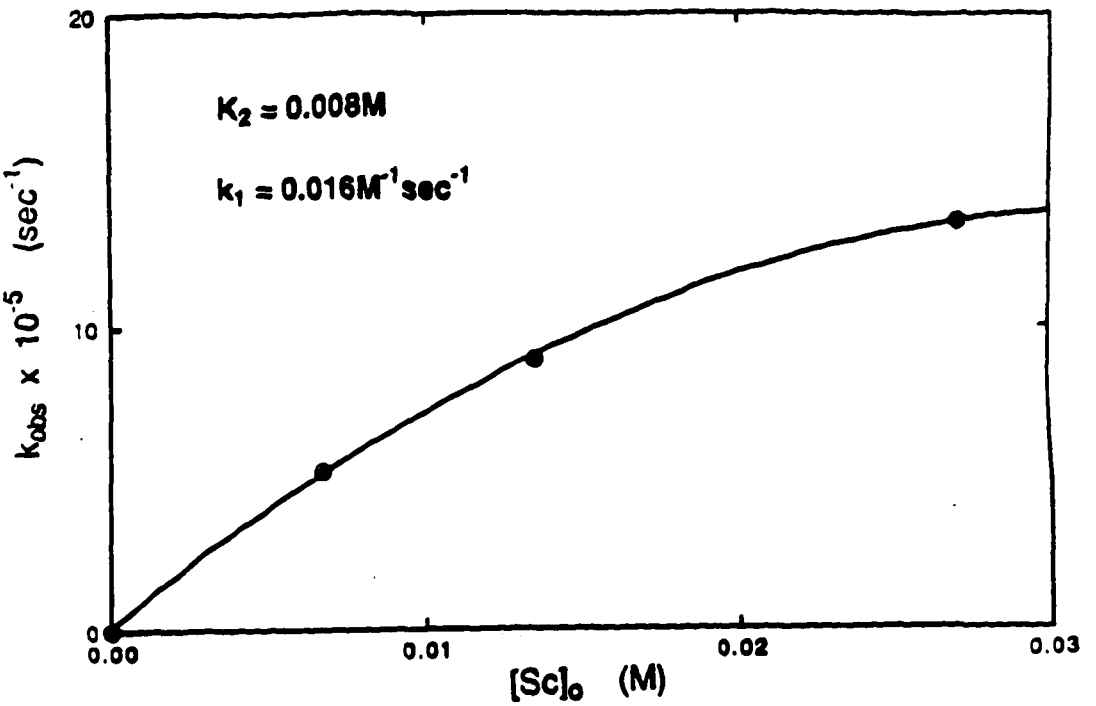

Figure 2.13

$$[(ScR)_2] \underset{}{\overset{K_2}{\rightleftharpoons}} 2\,[ScR]$$

$$[ScR] + |CH_2{=}CHR'| \xrightarrow{k_1} [ScCH_2CHRR']$$

$$[(ScCH_2CHRR')_2] \underset{}{\overset{K_2}{\rightleftharpoons}} 2\,[ScCH_2CHRR']$$

$$[ScCH_2CHRR'] + |CH_2{=}CHR'| \xrightarrow{k_1} [ScCH_2CHR'CH_2CHRR']$$

etc.

$$\text{Rate} = k_1[ScR]\,|CH_2{=}CHR'|$$

$$k_{obs} = k_1[ScR]$$

$$[Sc]_o = (2/K_2k_1^2)(k_{obs})^2 + (1/k_1)(k_{obs}) \qquad (10)$$

polypropene produced at room temperature over two days by this catalyst revealed a fairly low number-average molecular weight of 3000 and a PDI of 2.15.

Regio- and Stereochemistry of Olefin Insertion

High regio- and stereospecificity are distinguishing features of Ziegler-Natta catalyst systems that have allowed the synthesis of commercially important, crystalline poly-α-olefins.[15] Since the regio- and sterocontrol of the polymerization is intimately linked with the mechanism of olefin insertion by Ziegler-Natta systems, current mechanistic models for both heterogeneous and homogeneous systems have relied heavily on the analysis of polymer microstructure.[16] As a result, significant advances have been made in the elucidation of polymer microstructure, especially through ^{1}H and ^{13}C NMR spectroscopy.[17]

Described below are our efforts to characterize the regiochemistry and the stereochemistry of α-olefin polymerization by our monocyclopentadienyl scandium amido systems. The results obtained can be rationalized within the context of the behavior observed with other Ziegler Natta catalyst systems, and they contribute to our understanding of how ligand steric environments can influence selectivity.

Regioselectivity

It is difficult to sort out the importance of electronic vs. steric effects in deciding the origin of regioselectivity in Ziegler-Natta systems. As a result, this aspect of the polymerization reaction has been somewhat taken for granted. In general, most heterogeneous and homogeneous Ziegler-Natta systems, including the group IV metallocene systems, are highly head-to-tail regioselective.[18] It is not surprising, therefore, that our organoscandium model systems are highly head-to-tail regioselective as well. In the catalytic α-olefin dimerization by the silylene-bridged scandocene systems, $\{(\eta^5\text{-}C_5Me_4)_2SiMe_2\}ScH(PMe_3)$ and $[\{(\eta^5\text{-}C_5H_3CMe_3)_2SiMe_2\}ScH]_2$, only the head-to-tail dimerization products are observed.[18] Primary insertion is indicated by the position of the

double bond formed in the β-hydrogen abstraction step. The regioselectivity of olefin insertion by these systems can be attributed to steric control from the cyclopentadienyl ligands as well as to the electronic preference for locating the partial positive charge on the substituted carbon in the transition state for olefin insertion into the scandium-alkyl.

To examine the regioselectivity of olefin insertion by (Cp*SiNR)ScR systems, the propene trimers formed with $[(Cp^*SiNR)(PMe_3)ScH]_2$ were examined by GC. These trimers were generated by reacting the catalyst with three equivalents of propene, cleaving the scandium alkyls with H_2 and collecting the volatiles. Of the four possible C_9 regioisomers (Figure 2.14), only the head-to-tail product, 2,4-dimethylheptane, was observed. This result translates into >99% head-to-tail regioselectivity in this system. That this regioselectivity results from primary, or "1-2",olefin insertion is indicated by the structure of the single-insertion product $[(Cp^*SiNR)Sc]_2(\mu\text{-propyl})_2$ as well as by the appearance of vinylidene chain ends in the ^1H NMR of the polymer.

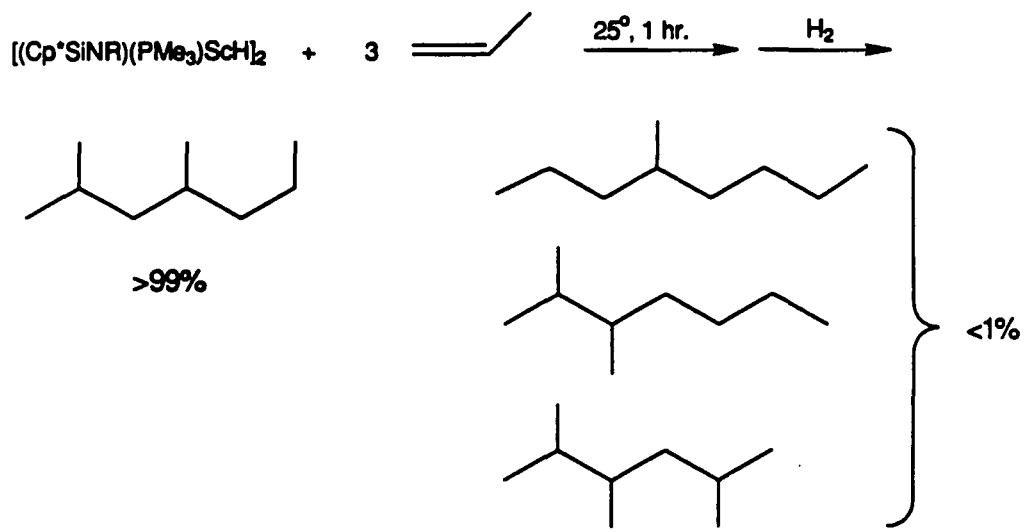

Figure 2.14. Regioselectivity of Propene Insertion by (Cp*SiNR)ScR

The regioselectivity of α-olefin insertion by the (^{tBu}CpSiNR)Sc system has not yet been investigated. While largely head-to-tail material is indicated in the ^{13}C NMR spectrum of polypropene produced with [(^{tBu}CpSiNR)ScMe]$_x$ (*vide infra*), the presence of broad, less intense peaks outside of the designated methyl, methylene and methyne regions suggests the presence of some regioirregular monomer units.[19] Reduction in regioselectivity is consistent with the decreased sterics of the ^{tBu}CpSiNR ligand environment as compared to the Cp*SiNR ligand environment. A GC analysis of propene trimers similar to that described above for the (Cp*SiNR)Sc system is the next step for determining the prevalence and nature of the misinsertions.

Stereospecificity

The stereochemistry of α-olefin insertion can be influenced by the chirality of the last inserted monomer unit in the growing chain (chain-end control), the chirality of the metal center (enantiomorphic site control), as well as by a combination of the two effects.[15a] The relative importance of the two mechanisms of stereocontrol can be determined by examining the effect of the occasional stereochemical defect on the subsequent stereochemistry of the polymer, by examining the stereochemistry of α-olefin insertion following a non-stereoactive ethylene unit and by examining for the stereoselective polymerization of racemic monomers. These methods demonstrated early on that isotactic specific polymerization in heterogeneous systems originates from enantiomorphic site control and regiospecific "1-2" insertion, leading to models concerning the structure of the asymmetric, heterogeneous sites.

Through the development of the chiral ansa-metallocene systems (ethylene-bis-tetrahydroindenyl)MCl_2 (M = Ti, Zr, Hf) by Brintzinger and coworkers (Figure 2.15),[20] the *homogeneous*, isotactic specific polymerization of propene became possible. This was the first example of the deliberate control of polymer microstructure through ligand design. The C_2 symmetry of the complex, which is responsible for this stereospecificity is reminiscent of

the C_2 structures proposed for heterogeneous, isotactic-specific sites of $TiCl_3$-based catalyst systems. Other substituted metallocene systems having C_2 symmetry and varying degrees of isospecificity have since been reported.[21]

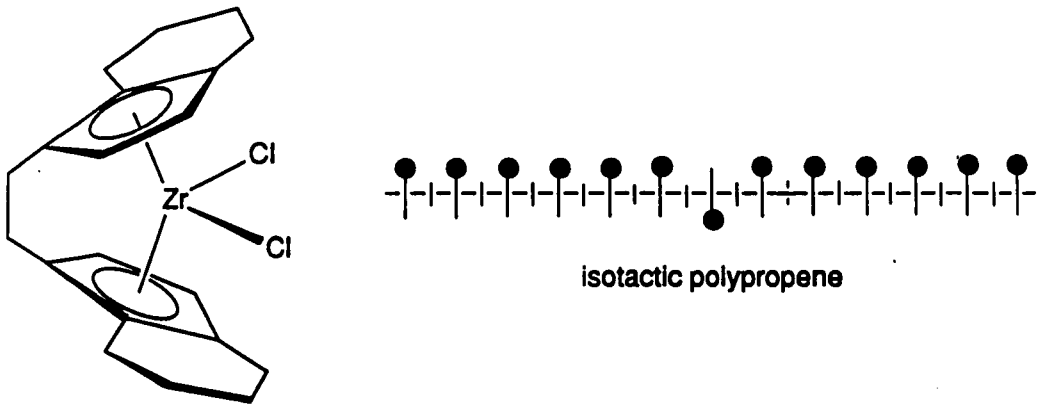

Figure 2.15

Another metallocene system, isopropyl(cyclopentadienyl-1-fluorenyl)hafnium(IV) dichloride (Figure 2.16), reported by Ewen *et al.*,[22] offers the first example of syndiospecific propene polymerization by an enantiomorphic site-control mechanism. The selectivity arises from size disparity between the ring systems on opposite sides of the metal. In contrast to earlier syndiospecific systems,[6] which displayed chain end control through a secondary mode of insertion, this system inserts olefin in a "1-2" fashion. Not surprisingly, the symmetric, normal bis-cyclopentadienyl metal systems do not display site stereocontrol and produce atactic polymer.[23]

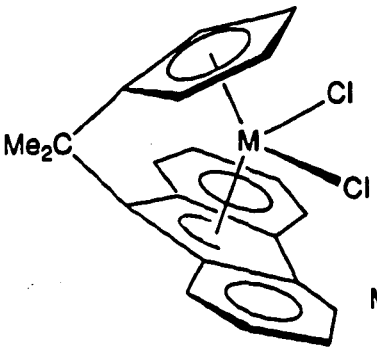

syndiotactic polypropene

Figure 2.16

Our (Cp*SiNR)ScR system is analogous to the mixed-ring complex of Ewen's in that the active species is achiral, and two different ligands of presumably different steric demand (the tetramethylcyclopentadienyl ligand and the tert-butyl amido ligand) define the active site for olefin insertion. Therefore, we anticipated that some syndiospecificity would be observed with this system. To investigate this possibility we examined the ^{13}C NMR spectrum of polypropene prepared with $[(Cp^*SiNR)Sc]_2(\mu\text{-prop})_2$.

^{13}C NMR spectroscopy is a powerful method for the elucidation of polymer microstructure and has found extensive use in the stereochemical analysis of polypropene.[16c-f] Shown in Figure 2.17 is the methyl region (with pentad assignments) of a sample ^{13}C NMR spectrum for somewhat isotactic-rich, head-to-tail polypropylene.[20f] The methyl region of the spectrum is more sensitive to differences in stereochemistry than the methylene and methyne regions of the spectrum, exhibiting a wider range of chemical shifts. From the relative intensities of the pentad bands, one can perform a statistical analysis or "mapping" of the polymer microstructure to evaluate the mechanism of stereocontrol in the catalyst system. These pentad bands, as shown, occur as fine structure to the larger regions corresponding to the mm, the mr and the rr triads.

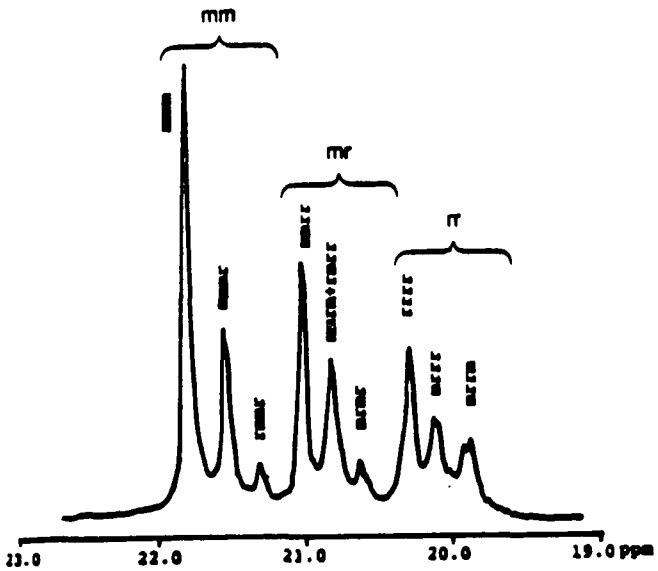

Figure 2.17. Sample ^{13}C NMR spectrum of polypropene showing methyl region with pentad assignments.

Shown in Figure 2.18a is the methyl region of the ^{13}C spectrum of polypropylene prepared at 25°C with $[(Cp^*SiNR)Sc]_2(\mu\text{-prop})_2$. While the spectrum reflects atactic stereochemistry, there is a noticeable preponderance of rr triads over mm triads indicating that the catalyst is, to a small degree, syndiospecific. Although the ^{13}C data are only preliminary and not rigorously quantitative, the band intensities for the methyl carbons should, to a first approximation, represent the relative amounts of the different stereoisomeric sequences. The relative triad and pentad band intensities do not appear to fit neatly into either the Bernoullian or the enantiomorphic-site control models for polymer stereochemistry. Thus, some combination of sterocontrol from the metal complex as well as from the adjacent stereocenter of the growing chain is involved in determining the stereochemistry of the polymer.

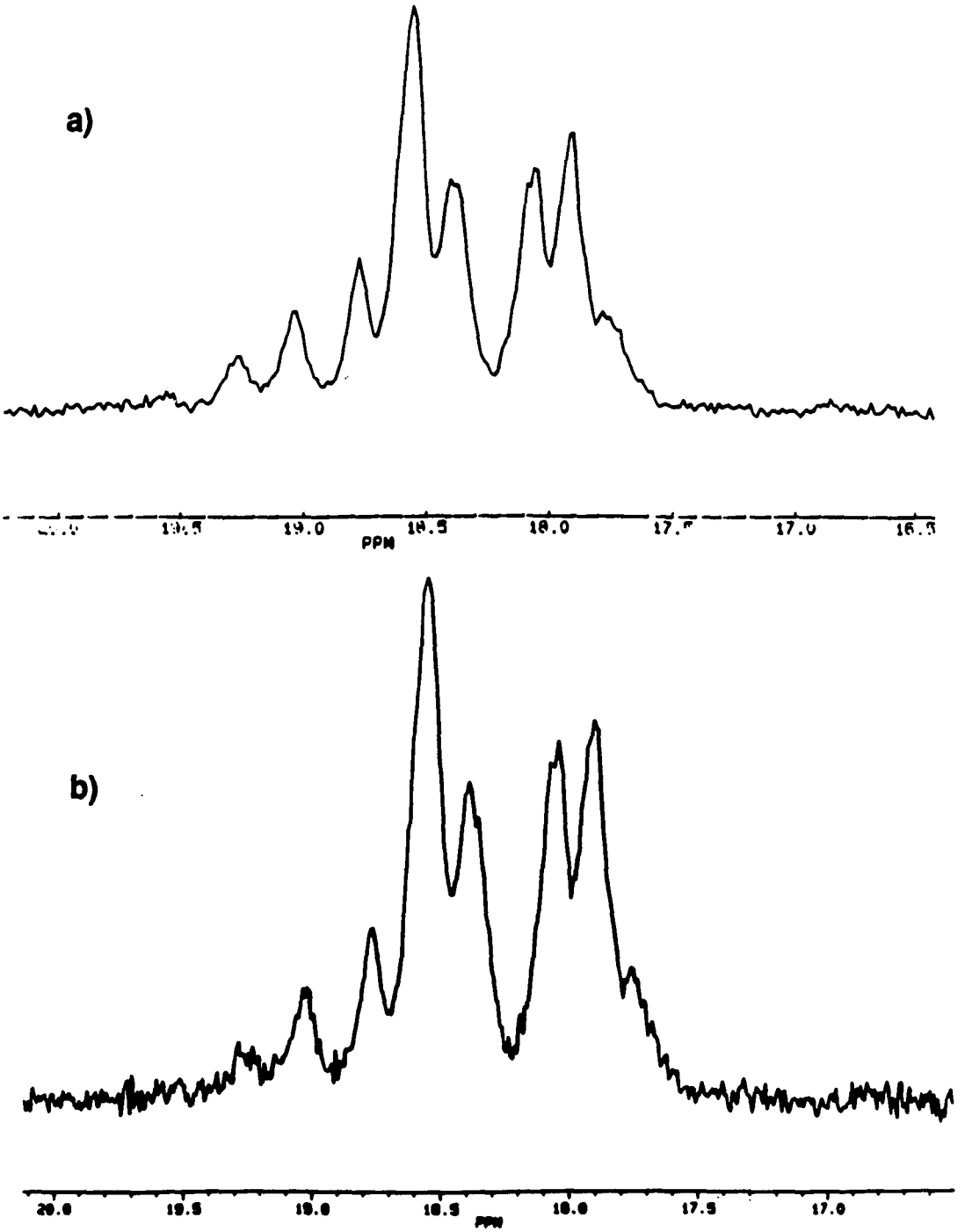

Figure 2.18. a) Methyl region of ^{13}C NMR spectrum of polypropene prepared at 25°C with $[(Cp^*SiNR)Sc(\mu\text{-}CH_2CH_2CH_3)]_2$. b) Methyl region of ^{13}C NMR spectrum of polypropene prepared at -10°C with the same catalyst.

Since the effects of site control and chain end control should be opposite in this system, it was not immediately obvious how lowering the temperature of the polymerization would affect the stereochemistry of the polymer. As can be seen from the ^{13}C NMR spectrum in Figure 2.18b, cooling the polymerization reaction to -10°C does not significantly change the stereochemistry of the polypropene formed.

While our initial goal in preparing the chiral (^{tBu}CpSiNR)ScR system was to promote the isospecific polymerization of α-olefins, it is clear from our results with (Cp*SiNR)ScR that the monocyclopentadienyl-amido ligand-framework does not exert a great deal of steric influence over the stereochemical course of the polymerization. Therefore, it was not surprising that the polypropene produced with [(^{tBu}CpSiNR)ScMe]$_x$ is purely atactic, as can be seen from the essentially 1:2:1 ratio of intensities for the mm, mr and rr triads in the methyl region of the ^{13}C spectrum (Figure 2.19). The absence of stereocontrol from the ^{tBu}CpSiNR ligand system as well as the minimal stereocontrol observed with the Cp*SiNR ligand system can be understood by considering the x-ray crystal structure for (^{tBu}CpSiNR)(PMe_3)$ScCH_2TMS$ discussed in Chapter 1. The tetrahedral position occupied by the PMe_3 marks the position that should be approached by the olefin in the transition state for insertion. This position is fairly removed from the steric influence of the cyclopentadienyl ring system as compared to the "equatorial wedge" of metallocene systems which is greatly affected by the sterics of the Cp rings. Hence, the syndiospecificity of (Cp*SiNR)ScR is not as pronounced as that observed with Ewen's mixed ring system, and the asymmetric environment provided by (^{tBu}CpSiNR)ScR appears to have no influence whatsoever over the steric course of the polymerization.

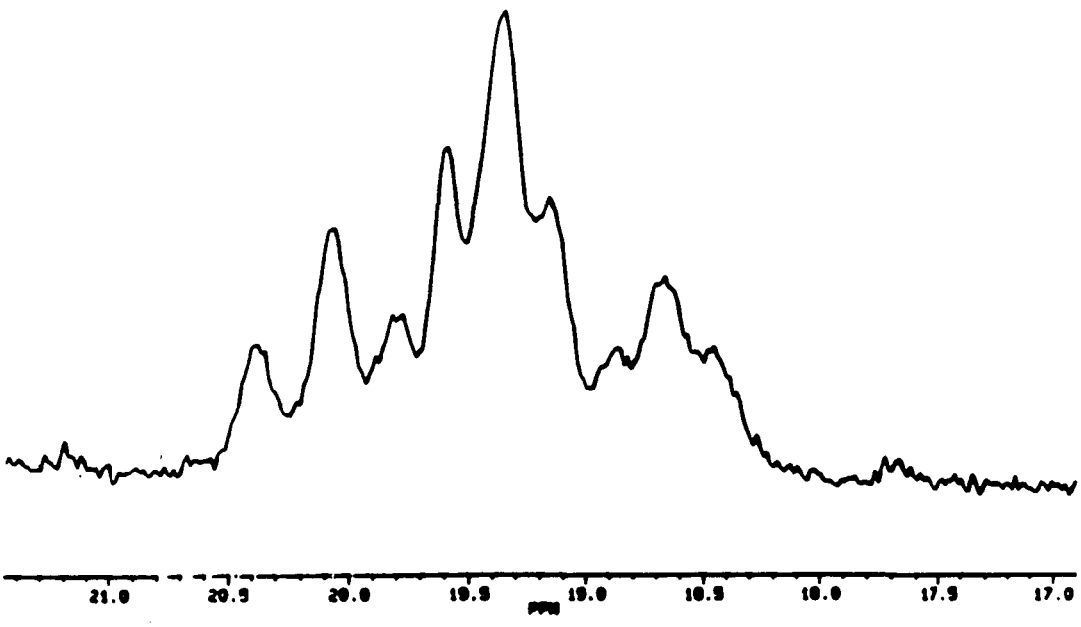

Figure 2.19. Methyl region of ^{13}C NMR spectrum of polypropene prepared under ambient conditions with $[(^{tBu}CpSiNR)ScMe]_x$.

It is clear from existing examples that through the rational design of the supporting ligand environment, one can control the microstructure of the polymer that is formed. Efforts in our group and in others are currently being directed toward understanding the detailed steric interactions responsible for the stereocontrol observed with these systems and perhaps developing formulas for ligand-controlled, stereospecific polymer synthesis. As part of our continuing program of ligand modification, we are seeking to develop a ligand system for scandium that has a greater influence over the steric course of the polymerization than we observe with the (Cp*SiNR)Sc and the (^{tBu}CpSiNR)Sc systems. Work is already in progress in the development of a dimethylsilylene-bridged fluorenyl-amido ligand system, which is expected to have more stereodirecting influence in the formation of syndiotactic polymer.

Summary and Conclusions

Through the experiments described in this chapter we are able to make the following statements about α-olefin polymerization catalysis by our monocyclopentadienyl scandium

amido systems:

1) The catalysis originates from scandium centers formed directly from the scandium hydride or scandium alkyl precatalyst complexes, not from minor impurities in the mixtures. A homogenous mixture of active species is involved in the catalysis. In other words, all of the scandium centers are acting alike. While these conclusions are drawn from an oligomer molecular weight distribution study using $[(Cp^*SiNR)Sc]_2(\mu\text{-}H)_2$, they may be logically extended to the phosphine-free (Cp*SiNR)Sc-R complexes and probably to the analogous $[(^{tBu}CpSiNR)ScMe]_x$ system as well.

2) At least in the case of the [(Cp*SiNR)ScR] catalyst system, the active chain propagating species is the monomeric, 12e-, "naked" scandium alkyl. This was established through analysis of the polymerization rate dependence on PMe_3 concentration, using **4** as the precatalyst and on scandium concentration using **6** as the precatalyst.

3) The [(Cp*SiNR)ScR] system is >99% head-to-tail regioselective for the polymerization of propene. Lower regioselecitivity with $[(^{tBu}CpSiNR)ScMe]_x$ is indicated in the ^{13}C NMR of polypropene made with this system.

4) These dimethylsilylene bridged monocyclopentadienyl-amido ligand-frameworks do not exert much steric influence over the stereochemistry of the polymerization. For the most part, atactic polymer is produced, although a small degree of syndiospecificity is observed with the (Cp*SiNR)ScR. The lack of stereocontrol is attributed to the remoteness of the ring system from the site of the incoming olefin.

There are still a number of unresolved questions concerning the reactivity of these catalyst systems, especially with respect to the mechanisms of chain transfer that are operating and with respect to the cause of decay in the activity of the PMe_3-free $[(Cp^*SiNR)ScR]_2$ complexes. In addition, only preliminary observations concerning catalysis by the $(^{tBu}CpSiNR)ScR$ system have been made.

Nevertheless, we can use the information we have obtained so far to improve our design of future α-olefin-polymerizing catalyst systems. For instance, a considerably bulkier ring system than tetramethylcyclopentadienyl and t-butylcyclopentadienyl would prohibit tight bridging interactions between the scandium centers as well as have a greater influence over the stereochemistry of the polymerization. Our ultimate and rather far-reaching goal is to design single-component organoscandium systems that catalyze the "living" polymerization of α-olefins in a highly stereocontrolled fashion.

Experimental Section

General Considerations. All manipulations were performed by using glovebox and high-vacuum line techniques as described elsewhere.[24] Solvents were dried by standard techniques and further purified by vacuum transfer from titanocene[25] or sodium benzophenone. Toluene-d_8 was dried over activated 4Å molecular sieves and stored over titanocene.

Argon and hydrogen were purified by passage over MnO on vermiculite and activated 4Å molecular sieves. Propene (Matheson) was freeze-pump-thawed at least twice prior to use. PMe_3 (Aldrich) was used without further purification. 1-Pentene (Aldrich) was dried over either titanocene or sodium sand. 1,2,4-Trichlorobenzene (Aldrich) was used as received. Cp_2Fe, used as an internal standard for NMR tube kinetic experiments, was sublimed before use.

NMR spectra were recorded on Varian EM-390 (^1H, 90MHz), JEOL FX90Q(^1H, 89.56), JEOL GX400Q (^1H, 399.78 MHz), and Bruker WM500 (^{13}C, 125.77MHz) spectrometers. GC data were measured on a Perkin-Elmer 8410 gas chromatograph using a 10m x 0.53mm OV-1 macrobore column from Alltech. GCMS data were obtained on a Hewlett Packard 5890A gas chromatograph interfaced with a Hewlett Packard 5970 series mass spectrometer, using a Hewlett Packard 12.5m OV-1 capillary column. GPC analyses were performed on a Waters 150-C ALC/GPC with five styragel columns (10^5-100Å porosity).

Non-linear, least-squares analysis of the kinetic data from the rate dependence of 1-pentene polymerization on added PMe_3 was performed using the program Gauss, System Version 2.0 (Copyright 1988, Aptech Systems Inc., Kent, Washington) on an IBM pc. All other linear and non-linear, least-squares fits were performed with the program Cricketgraph on a Macintosh computer.

Sample Polymer Syntheses

a)Poly-1-butene Synthesis by 4

To a solution of compound 4 (0.03g, 0.04mmol) in 5mL toluene in a thick-walled glass vessel were added *ca* 1600 equivalents of 1-butene (790 Torr, 1.5L) at -196°C. After stirring for 7 days at room temperature, the reaction was quenched by the addition of 0.3mL methanol against an argon counterflow. The scandium was removed from the polymer product by extraction of the toluene solution with dilute HCl. The toluene phase was dried over $MgSO_4$, and the toluene was then removed under reduced pressure to afford 2.5g of polymer with a number average molecular weight of 4000 and a PDI of 1.7 (GPC vs. polystyrene).

b)Poly-1-pentene Synthesis by 4

Compound 4 (0.031g, 0.042mmol) was dissolved in 10.8mL 1-pentene and the reaction was stirred at room temperature for 19hrs. The reaction was quenched with 2mL methanol, and the excess pentene was removed under vacuum. The residue was dissolved in ethyl ether, extracted with 6M HCl followed by concentrated $NaHCO_3$ and then water. The ether phase was dried over $MgSO_4$, and the ether was removed under reduced pressure to afford 5g polymer with a number-average molecular weight of 2900 and a PDI of 2.08 (GPC vs. polystyrene). The reaction was carried out in a similar fashion at 0° in a constant temperature bath (37mg 4, 10.2mL pentene) to afford after *ca* 25hrs. 0.044g polypentene (M_n = 7,000, PDI = 1.7).

c)Polypropene Synthesis by 6

Approximately 0.016 mole propene (760 Torr, 0.4L) was was stirred over titanocene at -80°C and then condensed onto a solution of 6 (21.5mg, 0.032mmol) in 2.5mL toluene at -196°C. The reaction was stirred for approximately 8 hrs while submerged in a constant

temperature bath set at 24°C. The reaction was quenched at this temperature by the addition of *ca* 1mL MeOH against an argon counterflow. The resulting toluene solution was extracted with dilute HCl, dried over $MgSO_4$, and the toluene was removed under reduced pressure to afford 0.5g polymer. M_n = 5,206, PDI = 2.75 (GPC vs. polystyrene). The reaction was carried out in a similar fashion at a constant temperature of -9°C to afford 0.6g polymer (M_n = 16,500, PDI = 1.7).

c)Polypropene Synthesis by [(^{tBu}CpSiNR)ScMe]$_x$ (17)

Approximately 0.016 mole propene (760 Torr, 0.4L) was stirred over titanocene at -80°C and then condensed onto a solution of 17 (19.8mg, 0.064mmol) in 2.5mL toluene at -196°C. The reaction was stirred for approximately 2 days at room temperature. The reaction was quenched by the addition of *ca* 1mL EtOH against an argon counterflow. A work-up of the polymer similar to that described for the polypropene syntheses above afforded 0.2g polymer. M_n = 3060, PDI = 2.15 (GPC vs. polystyrene).

Oligomer Molecular Weight Distributions. In a standard oligomerization run, propene (3-8 equiv.) was measured into a calibrated gas volume and condensed at -196°C into a small reaction vessel containing a 0.5 mL solution of 3 (*ca* 0.1M) in toluene-d_8. The reaction mixture was stirred at room temperature for 1-2 hrs. The volatiles were then vacuum-transferred into an NMR tube at -196°C along with a measured amount of hexamethyldisiloxane. The amount of unreacted propene was determined by integrating it relative to the hexamethyldisiloxane standard at -80°C by ^{1}H NMR spectroscopy. The reaction residue containing the propene insertion products was redissolved in *ca* 1 mL benzene and stirred under 4atm H_2 at room temperature overnight. The resulting mixture was exposed to air and immediately passed through a plug of silica-gel to remove all scandium byproducts, and the solution of saturated oligomers was analyzed by gc and gc/ms. Because of the unavailability of authentic hydrocarbon standards, gc/ms was used to verify the identity of the oligomers. The response factors of the oligomers, using flame

ionization detection, were assumed to be linearly related to their carbon number and were scaled accordingly.

Kinetic Analysis of 1-Pentene Polymerization by 4; Rate Dependence on Scandium Concentration

In a nitrogen-filled glovebox, a stock solution was prepared by dissolving 100.3mg of 4 and 126.8mg of Cp_2Fe in 3mL toluene-d_8. Serial dilutions of the stock solution were prepared in five different NMR tubes by adding the appropriate amount of toluene-d_8 to a 0.2mL, 0.3mL, 0.4mL, 0.5mL and a 0.6mL aliquot of the stock solution to bring the final volume of each sample to 0.6mL. Each NMR tube had a 14/20 ground-glass joint, which could be attached to a needle valve. To add 1-pentene to each sample, the NMR tube/needle valve assembly was attached to a 104.3mL gas volume on the vacuum line. The sample was frozen at -196°C, the NMR tube was evacuated and 240 Torr of 1-pentene were admitted to the gas bulb and then condensed into the NMR tube. The pentene was estimated to contribute an additional 0.15mL to the volume of the sample in calculating concentrations of catalyst and olefin. The tube was then sealed with a torch and stored at -196°C prior to the experiment.

Each NMR tube sample was fully submerged in a 32°C oil bath and removed at regular intervals to monitor the change in 1-pentene concentration relative to the internal ferrocene standard on an EM390 ^{1}H NMR spectrometer, probe temperature 32°C. Spectra were generally recorded over the duration of 3-4 half lives for each sample.

Kinetic Analysis of 1-Pentene Polymerization by 4; Rate Dependence on Added Phosphine

In a nitrogen-filled glove box, a stock solution was prepared by dissolving 133.9mg of 4 and 164.4mg of Cp_2Fe in 4mL toluene-d_8. Five NMR tube samples were prepared by adding a 0.6mL aliquot of the stock solution to each tube. Each tube had a 14/20 ground-

glass joint, which could be attached to a needle valve. PMe_3 was added to each sample by attaching the NMR tube/needle assembly to a 2.8(±0.4)mL gas volume on the vacuum line. The sample was frozen at -196°C, the NMR tube was evacuated and a diffent amount of PMe_3 (30 Torr, 120 Torr, 210 Torr, 300 Torr and 390 Torr) was admitted to the gas volume for each sample and then condensed into the NMR tube. 1-Pentene was then added to each sample by replacing the 2.8mL gas volume with the large 104.3mL gas volume, admitting 240 Torr of 1-pentene into the gas volume and condensing it into the NMR tube. Again, the contribution of added 1-pentene to the total volume of the sample was estimated to be 0.15mL. The tube was then sealed with a torch and stored at -196°C until use.

Each NMR tube sample was fully submerged in a 32°C oil bath and the kinetics were monitored over 3-4 half lives for each sample by ^1H NMR on an EM390 instrument.

Kinetic Analysis of 1-Pentene Polymerization by 6; Rate Dependence on Scandium Concentration

In a nitrogen-filled glovebox, a stock solution was prepared by dissolving 12.3mg of 6 and 45.5mg of Cp_2Fe in 0.9mL toluene-d_8. Three NMR tube samples containing different concentrations of catalyst were prepared by serial dilution of the stock solution. The first tube contained 0.3mL of the stock solution, the second tube contained 0.15mL of the stock solution diluted with 0.15mL toluene-d_8 and the third tube contained 0.075mL of the stock solution diluted with 0.225mL toluene-d_8. Each tube was attached to a needle valve via a ground-glass joint and frozen immediately in liquid nitrogen to minimize catalyst decomposition. Each NMR tube/needle valve assembly was connected to a 104.3mL gas volume on the vacuum line. The NMR tube, while still frozen, was evacuated, and 240 Torr of 1-pentene were admitted to the gas bulb and and then condensed into the sample. The tube was then sealed with a torch and stored at -196°C prior to the experiment.

The NMR probe of a JEOL FX90Q spectrometer was cooled to -6°C, as calibrated by

a CH_3OH standard. Prior to being loaded into the precooled probe, each sample was thawed in a -78° dry ice/acetone slush bath and shaken to redissolve solids that had precipitated from the solution. The concentration of 1-pentene in each sample was monitored relative to the ferrocene standard over two half-lives. The temperature of the probe was checked with a CH_3OH standard before each sample as well as at the end of the experiment. Before and after the experiment the temperature of the probe was found to be -6°C. Before the second sample (containing 0.0075M scandium dimer) the temperature was measured as -2°C, and before the last sample (containing 0.0038M scandium dimer), the temperature was measured as -4°C. These apparent temperature fluctuations correspond to at most ± 3Hz change in the 166Hz chemical shift difference between the methanol peaks and are most likely due to errors in the chemical shift method of temperature measurement.

Generation of Propene Trimers by 4 for GC Analysis

Three equivalents of propene (23Torr, 132.6) were condensed from a gas bulb into a solution containing 20.0mg (0.054mmol) of 4 in 1-2mL benzene in a thick-walled vessel cooled to -196°C. The reaction was warmed to room temperature and stirred for one hour. H_2 (4 atm.) was admitted to the reaction mixture, which was then stirred overnight at room temperature. The H_2 was removed by freeze-pump-thawing the reaction, and the volatiles were vacuum transferred to a separate vessel and analyzed by GC.

^{13}C NMR Analysis of Polypropene Samples

Polypropene samples (0.2-0.5g) produced by $[(Cp^*SiNR)Sc]_2(\mu\text{-propyl})_2$ and by $[(^{tBu}CpSiNR)ScMe]_x$ were dissolved in 2-3mL 1,2,4-trichlorobenzene and the solutions were placed in 10mm NMR tubes. A coaxial tube containing DMSO-d_6 was used as an external NMR standard. The samples were heated to *ca* 80°C in the NMR probe to obtain adequate resolution of the methyl pentad signals. Proton-decoupled ^{13}C spectra were obtained with a pulse delay of 1 sec. Normally, 2000 scans gave sufficient signal to noise.

References

1. a) Sheldon, R. A. *Chemicals from Synthesis Gas*; D. Reidel: Dodrecht, 1983; Chapter 3. b) Ertl, G. *Catal. Rev.* **1980**, *21*, 201. c) Gates, B. C.; Katzer, J. R.; Schuit, G. C. A. *Chemistry of Catalytic Processes*; McGraw-Hill: New York, 1979; Chapter 4.

2. a) Henrici-Olivé G.; Olivé, S. *Angew. Chem., Int. Ed. Engl.* **1967**, *6*(9), 790. b) Breslow, D. S.; Newberg, N. R. *J. Am. Chem. Soc.* **1957**, *79*, 5072. c) Breslow, D. S.; Newberg, N. R. *J. Am. Chem. Soc.*, **1959**, *81*, 81.

3. a) Sinn, H.; Haminsky, W. *Adv. Organomet. Chem.* **1980**, *18*, 99. b) Kaminsky, W.; Steiger, R. *Polyhedron*, **1988**, *7*(22/23), 2375. c) Gianetti, E.; Nicoletti, G. M.; Mazzocchi; R. *J. Polym. Sci., Polym. Chem. Ed.*, **1985**, 23, 2117.

4. Lauher, J. W.; Hoffmann, R. *J. Am. Chem. Soc.* **1976**, 98, 1729.

5. Cotter, W. D. unpublished results.

6. Doi, Y.; Keii, T. *Synthesis of "Living" Polyolefins with Soluble Ziegler-Natta Catalysts and Applications to Block Copolymerization*; Advances in Polymer Science; Springer-Verlag: West Berlin, 1986; Vol. 73/74; p.201.

7. For a discussion of living polymerizations, see: Swarc, M. *Living Polymers and Mechanisms of Anionic Polymerization*; Advances in Polymer Science; Springer-Verlag: West Berlin, 1983; Vol. 49.

8. The Poisson function, $N_n/N = [1/(n-1)!]\nu^{n-1}e^{-\nu}$, is a statistical model that applies to an ideal "living: polymerization in which there is no chain transfer or chain termination, and all active centers are growing at the same rate. For a discussion of the Poisson model for polymer size distribution, see: Flory, P. J. *J. Am. Chem. Soc.* **1940**, 62, 1561.

9. a) Watson, P. L.; Herskovitz, T. *ACS Symp. Ser.* **1983**, *No. 212*, 459. b) Watson, P. L. *J. Am. Chem. Soc.* B1982, 104, 337.

10. Jordan, R. F. *J. Chem. Ed.* **1988**, 65(4), 285.

11. This value for K_1 corresponds to 30% phosphine dissociation (i.e, *ca* 0.02M free PMe_3) in a 0.07M solution of the complex $(Cp^*SiNR)(PMe_3)ScR$ (the experimental concentration) in the absence of externally added PMe_3.

12. The numbers in parentheses beside the values for the parameters k_1 and K_1 are the standard deviations determined in the non-linear, least-squares analysis.

13. This assumes an activation energy for olefin insertion of approximately 10 kcal mol^{-1} (Keii, T. In *Transition Metals and Organometallics as Catalysts for Olefin Polymerization;* Kaminsky, W.; Sinn, H., Eds.; Springer-Verlag: Berlin, 1988; p. 3.

14. Dividing the concentrations of added phosphine (L) in half in the non-linear, least-squares analysis of the six data points increases the value for k_1 to 0.050(23)$M^{-1}sec^{-1}$ and decreases the value for K_1 to 0.00011(5) M^{-1}. Halving the scandium concentration has a less significant effect, resulting in values for k_1 and K_1 of

0.030(13)$M^{-1}sec^{-1}$ and 0.00075(33)M respectively. Likewise, reducing K_2 by a factor of 2 has only a minor effect, resulting in a k_1 of 0.034(14)$M^{-1}sec^{-1}$ and a K_1 of 0.00033(15)M.

15. Pino, P.; Mülhaupt, R. *Angew.Chem. Int. E. Eng.* **1980**, *19*, 857 and references therein.

16. a) Corradini, P.; Busico, V.; Guerra, G. In *Comprehensive Polymer Science*; Allen, G., Bevington, J. C., Eds.; Pergamon Press: Oxford, 1989; Chapter 1. b) Corradini, P.; Busico, V. Guerra, G. In *Transition Metals and Organometallics as Catalysts for Olefin Polymerization;* Kaminsky, W.; Sinn, H., Eds.; Springer-Verlag: Berlin, 1988; p. 337.

17. a)Bovey, F. A.; Jelinski, L. W. *Chain Structure and Conformation of Macromolecules*; Academic Press: New York, 1982; Chapter 3. b) Bovey, F. A. In *Comprehensive Polymer Science*; Allen, G., Bevington, J. C., Eds.; Pergamon Press: Oxford, 1989; Chapter 17. c) Zambelli, A.; Dorman, D. E.; Brewster, A. I.; Bovey, F.A. *Macromolecules* **1973**, *6*(6), 925. d) Zambelli, A.; Locatelli, P.; Bajo, G.; Bovey, F. A. *Macromolecules*, **1975**, *8*(5), 687. e) Ferro, D. R.; Zambelli, A.; Provasoli, P.; Locatelli, P.; Rigamonti, E. *Macromolecules*, **1980**, *13*, 179. f) Tonelli, A. E.; Schilling, F. C. *Macromolecules* **1980**, *13*, 270.

18. Bunel, E. Ph.D. Thesis, California Institute of Technology, **1988**.

19. a) Zambelli, A.; Gatti, G. *Macromolecules*, **1978**, *11*(3), 485. b) Zambelli, A.; Grassi, A.; Resconi, L.; Albizzati, E.; Mazzocchi, R. *Macromolecules*, **1988**, *21*, 617.

20. Kaminsky, W.; Kulper, K.; Brintzinger, H. H.; Wild, F. W. P. *Angew. Chem. Int. Ed. Engl.* **1985**, *24*, 507.

21. a) Röll, W.; Brintzinger, H. H.; Rieger, B.; Zolk, R. *Angew. Chem., Int. Ed. Engl.*, **1990**, *29*(3), 279. b) Erker, G. *Pure & Appl. Chem.*, **1989**, *61*(10), 1715.

22. Ewen, J. A.; Jones, R. L.; Razavi, A. *J. Am. Chem. Soc.*, **1988**, *110*, 6255.

23. a) Ref. 18 b) Ref. 5a c) An exception to this is the low-temperature polymerization of propene by $Cp_2Ti(Ph)_2$, which yields isotactic polymer as a consequence of chain-end control. Ewen, J. A. *J. Am. Chem. Soc.* **1984**, *106*, 6355.

24. Burger, B. J.; Bercaw, J. E. In *New Developments in the Synthesis, Manipulation and Characterization of Organometallic Compounds*; Wayda, A. L., Darensbourg, M. Y. Eds.; ACS Symposium Series 357; American Chemical Society: Washinton, D. C., **1987**; pp. 17-98.

25. Marvich, R. H.; Brintzinger, H. H. *J. Am. Chem. Soc.* **1971**, *93*, 2046.

Part II

Hydrazido(1-) and 2,2-Dimethylhydrazido(1-) Derivatives of Permethylscandocene. Preparation and Structural Characterization of Their Products from Reactions with Acetonitrile

INRODUCTION

In the first part of this thesis we discussed the olefin-insertion activity of monocyclopentadienyl scandium amido complexes. This second part describes some work that was actually initiated prior to the olefin polymerization project and involves insertion chemistry with the permethylscandocene system. Besides olefins, there are a number of unsaturated substrates such as CO,[1] CO_2,[2] nitriles,[3] alkynes[4] and organic carbonyls,[2] which undergo insertion chemistry with scandium hydride and alkyl derivatives. Because of the heteroatom affinity of the Lewis acidic, electronically unsaturated scandium center, oxygen and nitrogen containing substrates are especially reactive. The reaction chemistry between these small molecules and scandium has been explored primarily with the permethylscandocene system.

A particularly interesting reaction of permethylscandocene hydride is its reduction of nitriles in the presence of H_2 (Figure 1).[3]

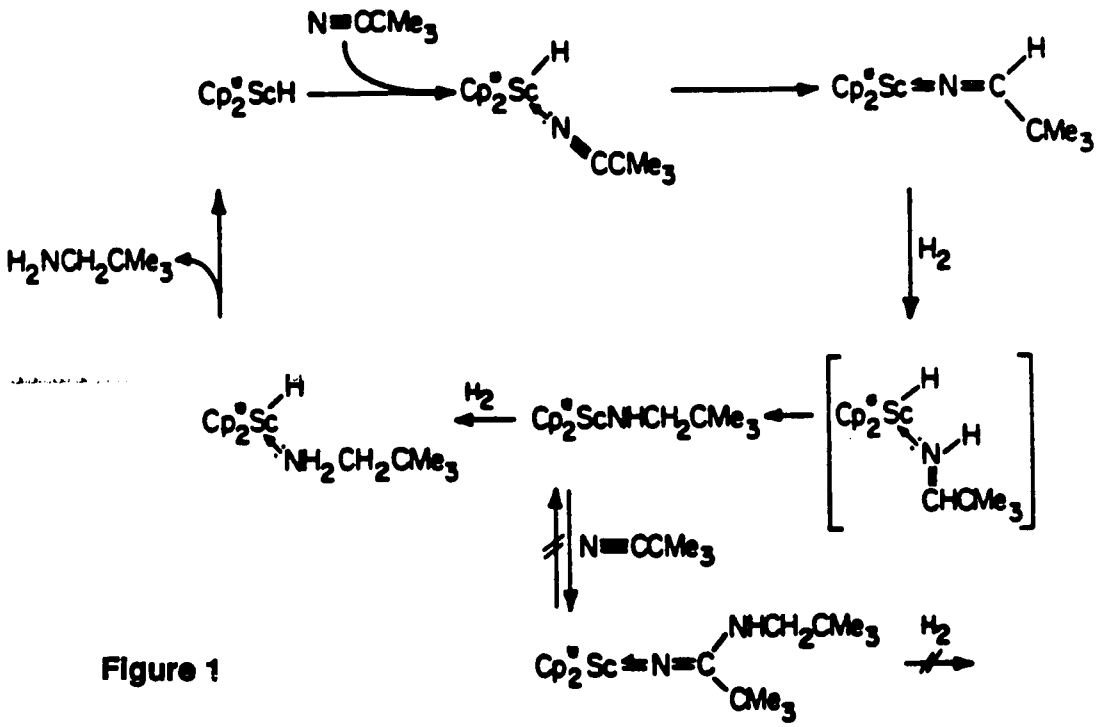

Figure 1

The facility with which the scandium amide bonds are hydrogenated (leading to moderate catalysis for the hydrogenation of t-butylnitrile to neopentylamine) was surprising, since it had been assumed that early transition metal-nitrogen bonds were too inert to be involved in such a catalytic cycle. The recent discovery by Gagne and Marks[5] of a catalytic cycle involving the hydroamination/cyclization of amino olefins with organolanthides has further served to dispel this misconception.

We were interested in exploring the possibility of extending the chemistry between permethylscandocene hydride and nitriles to the reduction of N_2 (Equation 1).

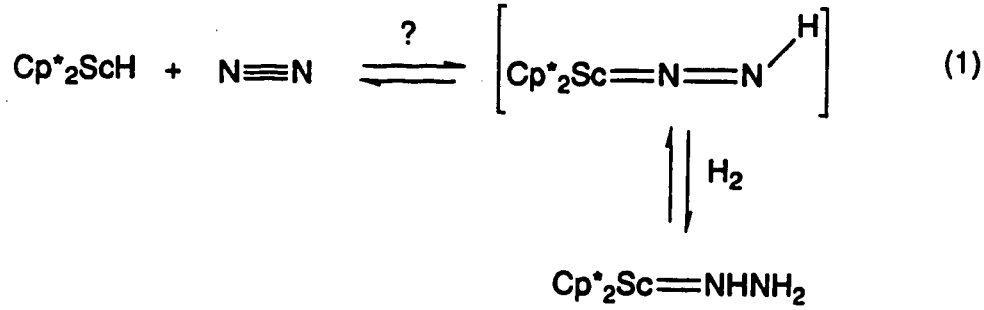

(1)

The homogeneous, transition-metal promoted reduction of N_2 with H_2 has been a long-standing goal of inorganic chemists that would have important commercial applications.[6]

The unfavorable thermodynamics for the partial reduction of N_2 to either N_2H_2 or N_2H_4[7] posed a potential difficulty, since the hypothetical reactions shown in Equation 1 are also likely to be endothermic.

$$N_{2(g)} + H_{2(g)} \rightleftharpoons N_2H_{2(g)} \qquad \Delta H^\circ = +43.5 \text{ kcal mol}^{-1}$$

$$N_{2(g)} + 2\,H_{2(g)} \rightleftharpoons N_2H_{4(g)} \qquad \Delta H^\circ = +20.3 \text{ kcal mol}^{-1}$$

$$N_{2(g)} + 3\,H_{2(g)} \rightleftharpoons 2\,NH_{3(g)} \qquad \Delta H^\circ = -24.9 \text{ kcal mol}^{-1}$$

In order for the reaction to be productive, further reduction or disproportion of the $Cp^*_2Sc{=}NHNH_2$ species would be required (Equations 2 and 3).

$$Cp^*_2ScNHNH_2 + Cp^*_2ScH \xrightarrow{?} 2\,Cp^*_2ScNH_2 \qquad (2)$$

$$? \; H_2 \;\rightleftharpoons$$

$$2\,Cp^*_2ScH + 2\,NH_3$$

$$2\,Cp^*_2ScNHNH_2 \xrightarrow{?} Cp^*_2ScNH_2 + Cp^*_2ScH + NH_3 \qquad (3)$$

$$N_2$$

Therefore, we directed our efforts toward the synthesis of the permethylscandocene hydrazido(1-) complex to determine the possibility of promoting H_2 reduction of this species to ammonia or disproportion to N_2 and NH_3.

While the parent hydrazido(1-) derivative, $Cp^*_2ScNHNH_2$, was straightforwardly prepared, the acidic nature of the N-H moieties makes this complex an unlikely intermediates in a catalytic process for N_2 reduction. In addition, no productive hydrogenation of this species was observed.

At the time of this work, unsubstituted hydrazido(1-) metal complexes were quite rare, presumably because of the instability of the highly reducing N_2H_3- ion.[8] There are still relatively few reported examples of complexes having the unsubstituted hydrazido(1-) ligand,[9] two of which have been recently confirmed by x-ray structures.[9c] By contrast, there are several examples of fully characterized, alkyl and aryl substituted hydrazido(1-) species.[10,11,12]

During our efforts (albeit unsuccessful) to obtain crystals of $Cp^*_2ScNHNH_2$, we discovered an interesting reaction between this species and acetonitrile to form the five-membered heterometallacycle, $Cp^*ScNHC(CH_3)NNH_2$. An X-ray structure determination confirmed the identitiy of this species. Our investigation of the mechanism by which this

heterometallacycle is formed is the focus of this chapter. As will be discussed, a 1,3-dipolar insertion of the acetonitrile into the Sc-N bond of the hydrazide derivative is the most likely mechanism for this reaction. The closely related compounds $Cp^*_2ScNHNMe_2$ and $Cp^*_2Sc\overline{N(H)C(CH_3)NNMe_2}$ also have been prepared and the crystal structure determination of the latter complex is reported as well.

Results and Discussion

Preparation $Cp^*_2ScNHNH_2$. The synthesis of permethylscandocene amide complexes according to Eq. 4 has been previously reported.[3]

$$Cp^*_2ScCH_3 + HNRR' \longrightarrow Cp^*_2ScNRR' + CH_4 \qquad (4)$$

We find this method useful for the synthesis of scandium hydrazido(1-) derivatives as well (Eq. 5).

$$Cp^*_2ScCH_3 + H_2NNRR' \longrightarrow Cp^*_2ScNHNRR' + CH_4 \qquad (5)$$
$$\mathbf{1}: R = R' = H$$
$$\mathbf{2}: R = R' = CH_3$$

Although the reaction between $Cp^*_2ScCH_3$ and one equivalent of NH_2NH_2 proceeds cleanly (^1H NMR), excess hydrazine protiolytically cleaves the [Cp*-Sc] bonds, resulting in decomposition accompanied by loss of Cp*H (^1H NMR). $Cp^*_2ScNHNH_2$ (1) appears to be indefinitely stable in the solid state at 25°C, but it decomposes in benzene solution over several days, again with the appearance of free Cp*H (^1H NMR), likely the result of (sterically hindered, thus slower) intermolecular protiolytic cleavage of [Sc-Cp*] bonds by [Sc-$NHNH_2$]. The room temperature, 400 MHz ^1H NMR spectrum for an unpurified sample of 1 displays an average signal for all three [$NHNH_2$] protons, which separates into two (still rather broad) signals of 2:1 relative intensity upon cooling to -96°C. A recrystallized sample, however, displays the two separate hydrazide proton resonances at room temperature. Presumably, trace amounts of residual hydrazine catalyze proton exchange between the two types of

hydrazide sites, analogous to the base-catalyzed hydrazide(1-) proton exchange noted earlier for $Cp^*W(CH_3)_3(\eta^2\text{-}NHNH_2)$.[9c] Infrared, ^1H NMR, mass spectral and analytical data for 1 are given in the Experimental Section. The spectral data do not, however, distinguish between $Cp^*_2Sc(\eta^1\text{-}NHNH_2)$ and $Cp^*_2Sc(\eta^2\text{-}NHNH_2)$ structures (or some other fluxional alternative with an N-H agostic interaction[13]) for 1. Because of the novelty of its formulation (particularly so at the time of its first isolation), many attempts were made to obtain crystals of $Cp^*_2ScNHNH_2$ suitable for an x-ray structural determination; unfortunately all such attempts have been unsuccessful. In view of the *dihapto* coordination found by Schrock and coworkers for $[Cp^*W(CH_3)_3(\eta^2\text{-}NHNH_2)]^+$ and $Cp^*W(CH_3)_4(\eta^2\text{-}NHNH_2)$[9c] and the β C-H agostic structure we have observed for $Cp^*_2ScCH_2CH_3$,[14] we favor the *dihapto* structure for 1.

Reaction of $Cp^*_2ScNHNH_2$ with Acetonitrile. Upon addition of excess acetonitrile to 1 in benzene at 25°C, clear crystals are deposited from solution within minutes. Incorporation of one molecule of acetonitrile in this new compound (Eq. 6) is indicated by ^1H and ^{13}C NMR data; however, an IR stretch in the region 2100-2300 cm^{-1} diagnostic of a C=N group (attributable, for example, to a simple acetonitrile adduct, $Cp^*_2Sc(N{=}CCH_3)(\eta^1\text{-}NHNH_2)$) is absent.

$$\underset{\mathbf{1}}{Cp^*_2ScNHNH_2} + CH_3C{\equiv}N \longrightarrow \underset{\mathbf{3}}{Cp^*_2Sc\overline{N(H)C(CH_3)NNH_2}} \qquad (6)$$

Lower frequency vibrations at 1591 cm^{-1} and 1607 cm^{-1}, not present for 1, are observed, however. A single-crystal x-ray structure analysis was then undertaken, and the ORTEP drawing of the molecular structure is shown in Figure 1. As is apparent, the acetonitrile and hydrazido(1-) moieties have combined, forming a five-membered heterometallacycle, $Cp^*_2Sc\overline{NH\text{-}C(CH_3)\text{-}N\text{-}NH_2}$ (3). The planarity of the ring (to within ±0.12Å) and nearly equivalent C1-N2 and C1-N3 bond lengths suggest resonance stabilization in the ring, with the two canonical forms shown in Scheme 1 (*vide infra*) being the principal contributors. The

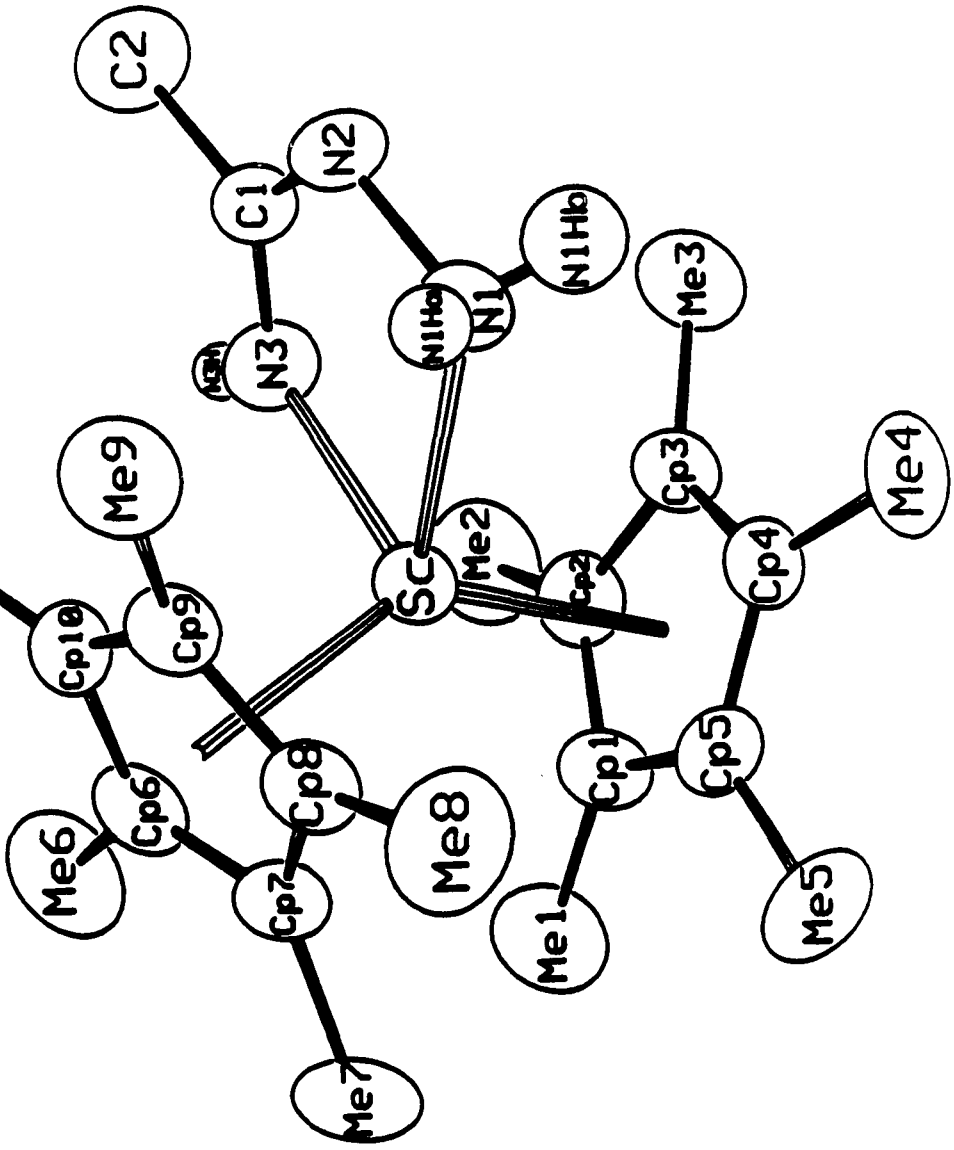

Figure 1. ORTEP drawing of $Cp^*_2ScN(H)C(CH_3)NNH_2$ (3). Thermal ellipsoids are shown at the 50% probability level.

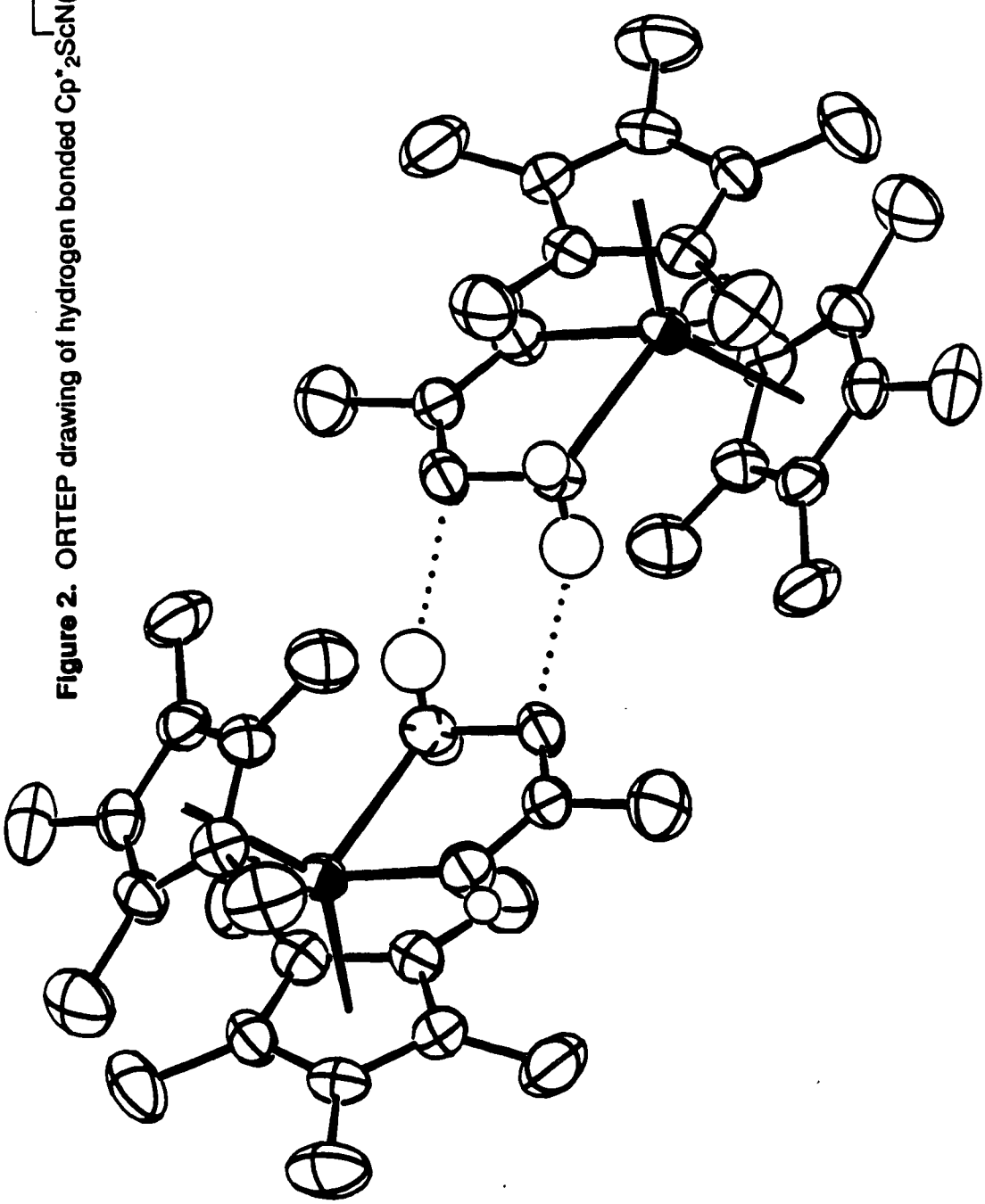

Figure 2. ORTEP drawing of hydrogen bonded $Cp^*_2ScN(H)C(CH_3)NNH_2$ pair.

N1-N2 bond length of 1.483(5)Å is rather long in comparison to that found for other hydrazido(1-) complexes[10,11,12] but comparable to that found for N_2H_4.[15]

An interesting feature of the crystal structure is the N1-N1Hb····N2 hydrogen bonding between two centrosymmetrically related molecules, as evidenced by the short *inter*molecular N1-N2 distance of 3.08(5)Å. An ORTEP drawing showing the hydrogen-bonded pair of molecules is given in Figure 2. Involvement of hydrazide protons in hydrogen bonding has been observed in a variety of metal hydrazide complexes[9c,10a,10c,12a,12b].

The mechanism for the formation of **3** from **1** and CH_3CN is of some interest. Since the acetonitrile unit could be oriented in either the C2C1-N2 or C2C1-N3 position, a number of possible mechanisms for the formation of **3** present themselves (Schemes 1 and 2). The most direct pathway is mechanism **A** (Scheme 1), involving cycloaddition of acetonitrile with $NH\text{-}NH_2$ bond cleavage. The alternative direction of cycloaddition (mechanism **B**) would initially yield a tautomer of **3**, which would need to undergo a subsequent hydrogen shift from one α N atom to the other to generate **3**. While the two cycloaddition mechanisms shown in Scheme 1 place the acetonitrile in positions C2C1-N2,[16] two (more plausible) mechanisms that place the acetonitrile in the C2C1-N3 position must also be considered (Scheme 2). Mechanism **C** involves 1,3 migration of the hydrazide (1-) group to the carbon atom of coordinated acetonitrile, analogous to the reactivity of permethylscandocene alkyl, aryl and hydride derivatives with nitriles (Eq. 7)[3], followed by tautomerization to **3**.

$$Cp^*_2Sc\text{-}R + R'C{\equiv}N \longrightarrow Cp^*_2Sc{=}N{=}CRR' \qquad (7)$$

$(R = H, CH_3, C_6H_5;\ R' = C_6H_5, CMe_3)$

Finally, the distinguishing feature of mechanism **D** is intramolecular nucleophilic attack by the terminal nitrogen of the hydrazide group at the carbon atom of the coordinated nitrile, a proposal of some merit in light of the generally observed activation of unsaturated ligands

Scheme 1

mechanism A

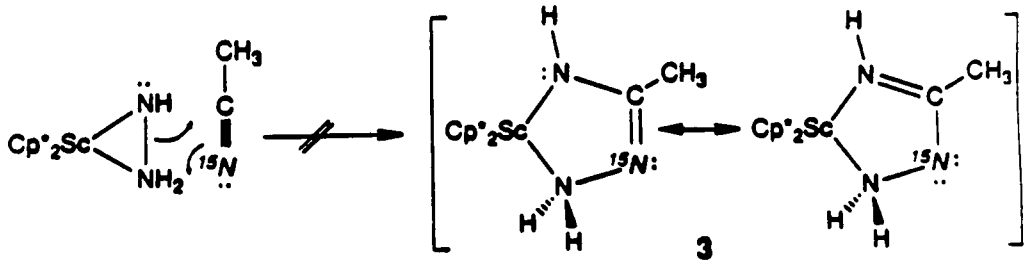

mechanism B

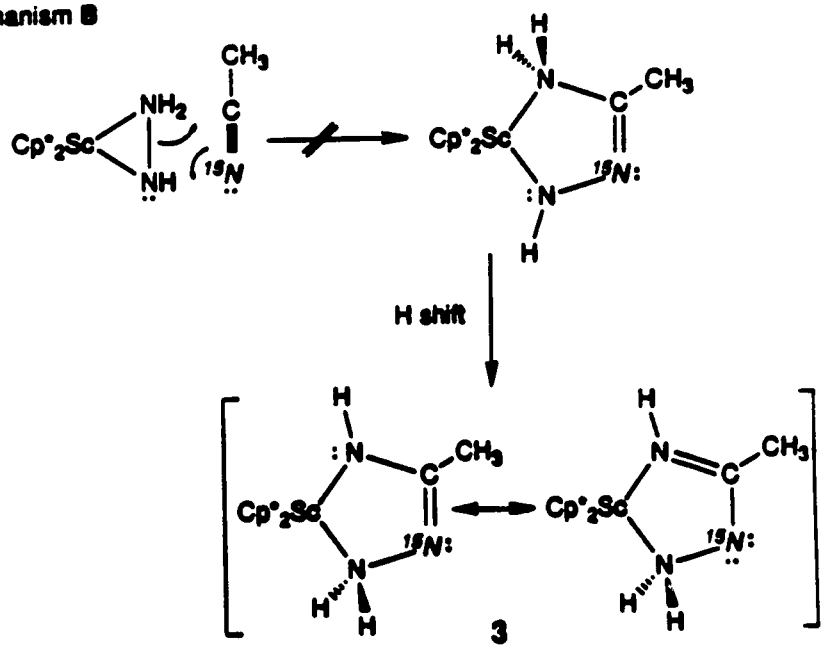

Scheme 2

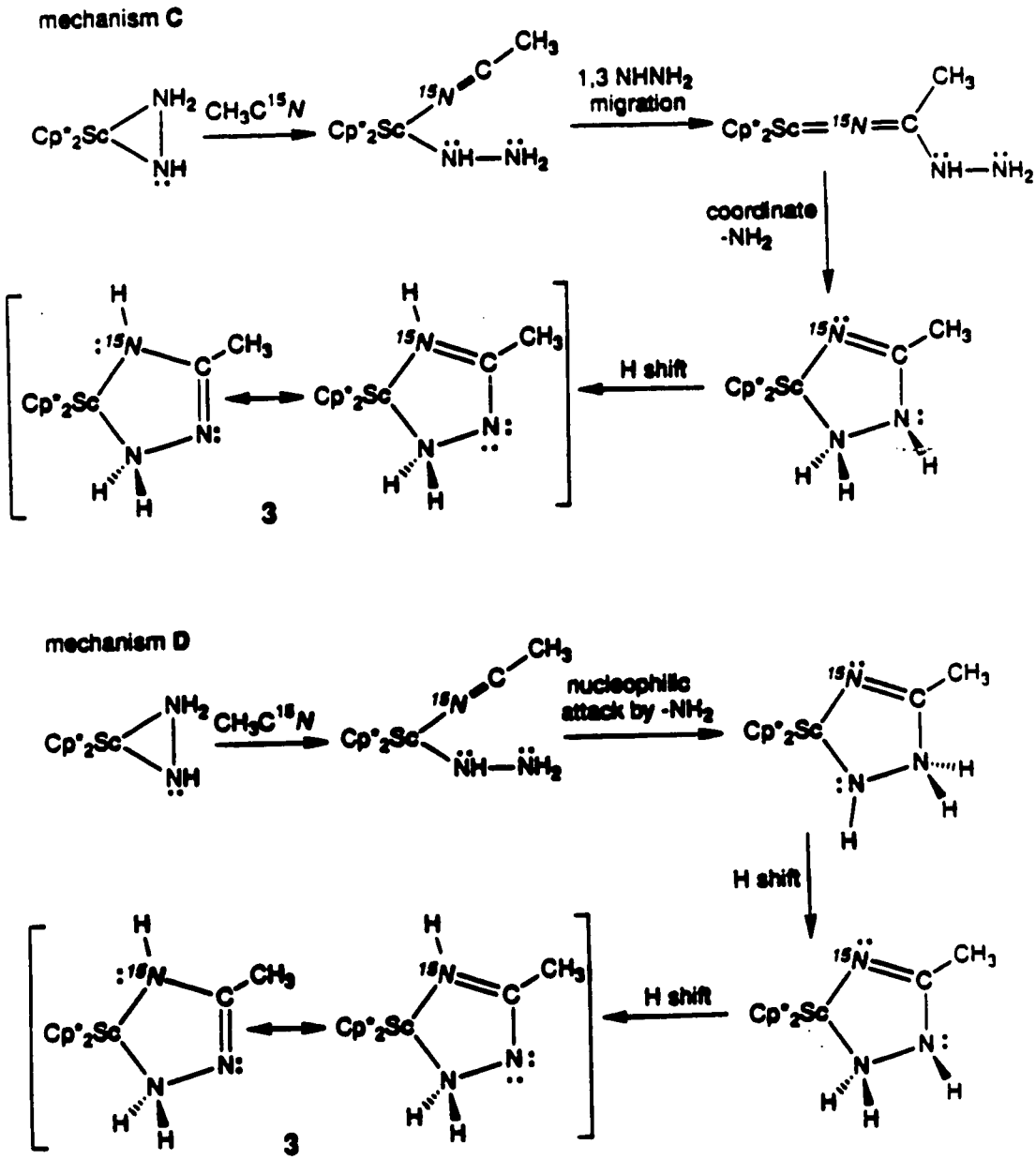
mechanism C
1,3 NHNH2 migration
coordinate -NH2
H shift
3
mechanism D
nucleophilic attack by -NH2
H shift
H shift
3

toward nucleophilic attack by coordination to an electron-deficient metal.[17] The requirement to move both hydrogens from N2, one to N1 and one to N3, to generate **3** is an unattractive feature of this alternative, however.

A labeling experiment carried out with $^{15}N{\equiv}CCH_3$ revealed that the acetonitrile nitrogen finally resides at N3, apparent from the sharper proton resonance at δ 3.05, with $^1J_{15N\text{-}H}$ = 70 Hz attributable to $Cp^*_2Sc\overline{^{15}N(H)C(CH_3)NNH_2}$. Hence, mechanisms **A** and **B**, and for that matter any mechanism that positions the acetonitrile nitrogen other than at N3, may be discarded.

Reaction of $Cp^*_2ScNHNMe_2$ with Acetonitrile. To decide between the remaining two mechanisms, we examined the reaction of acetonitrile with $Cp^*_2ScNHNMe_2$ (**2**). We reasoned that by replacing the two hydrogens on the terminal nitrogen of the hydrazide with two methyl groups, formation of a complex analogous to **3** could not occur by mechanism **D**, since the necessary hydrogen shift would no longer be possible. Reaction of **2** with ^{15}N labeled acetonitrile resulted in a new species that displayed ^{15}N-^1H coupling in the ^1H NMR (δ 3.9 with $^1J_{15N\text{-}H}$ = 73 Hz), indicating that a product analogous to **3** had formed. Moreover, infrared data also indicated that the acetonitrile once again had reacted beyond simple adduct formation (Eq. 8).

$$\underset{\mathbf{2}}{Cp^*_2ScNHNMe_2} + CH_3C{\equiv}N \longrightarrow \underset{\mathbf{4}}{Cp^*_2Sc\overline{N(H)C(CH_3)NNMe_2}} \quad (8)$$

Ultimately, positive structural verification was provided by a single-crystal x-ray analysis for **4** (Figure 3). A four-membered metallacycle is formed in this case. The smaller ring size adopted by **4** relative to **3** is undoubtedly due to the steric bulk of the dimethylamino group, which prevents coordination to the [Cp^*_2Sc] moiety. Resonance stabilization attributable to the two canonical forms shown for **4** in Scheme 3 is apparent from the similarity of the two C-N bond lengths (C1-N3 1.306(7)Å; C1-N2 1.316(7)Å). Hydrogen bonding between monomers, analogous to that observed in the solid state for **3**, is not expected and is not

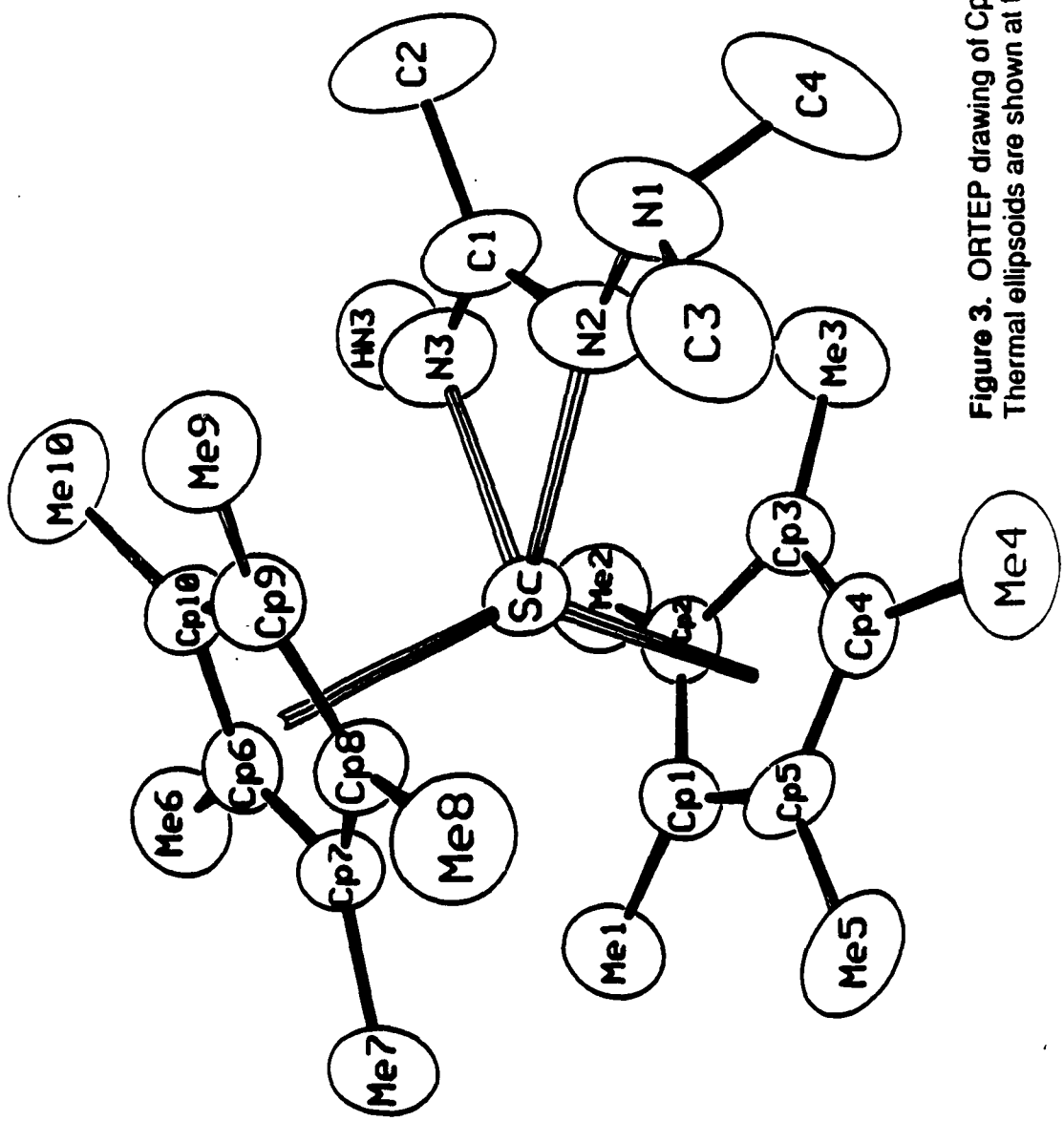

Figure 3. ORTEP drawing of $Cp^*_2ScN(H)C(CH_3)NNMe_2$ (**4**). Thermal ellipsoids are shown at the 50% probability level.

Scheme 3

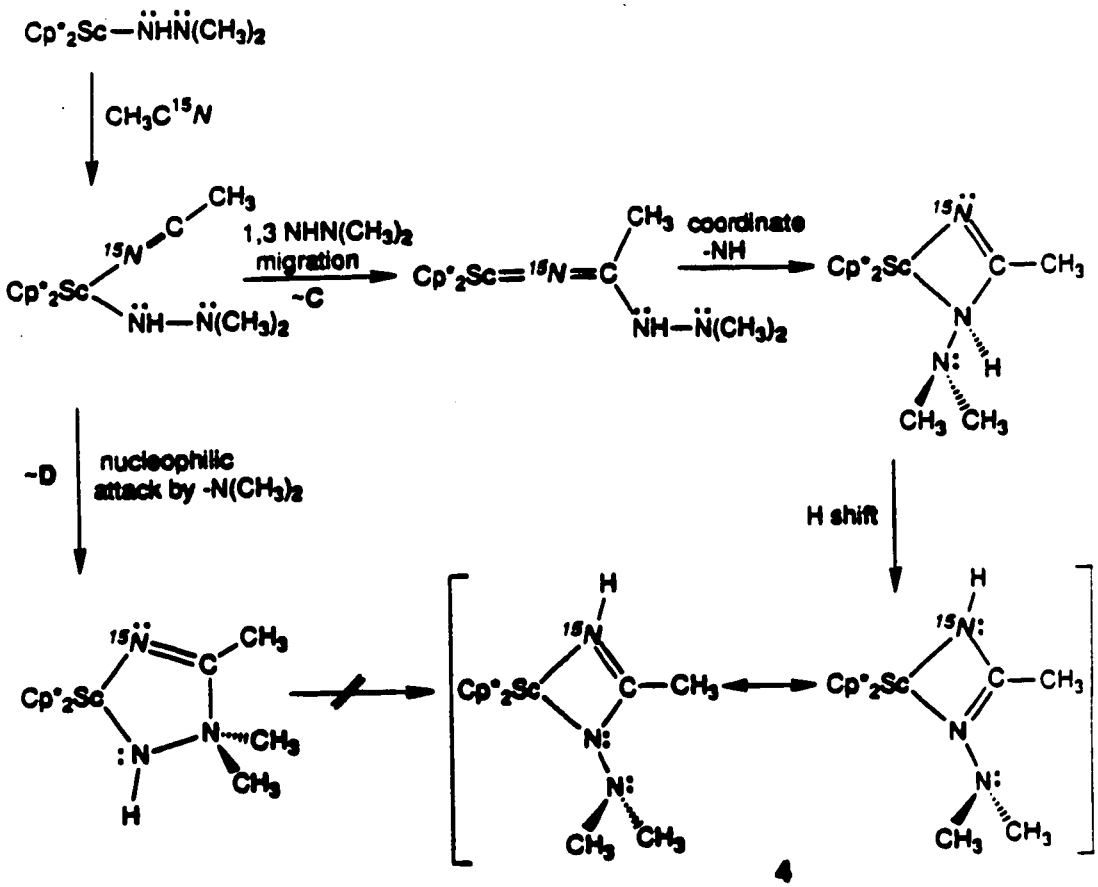
Cp*2Sc—NHN(CH3)2
CH3C15N
1,3 NHN(CH3)2 migration
-C
coordinate -NH
-D
nucleophilic attack by -N(CH3)2
H shift
4

observed for **4**.

The implications from the reaction of **2** with acetonitrile (Scheme 3) concerning the mechanism for the formation of **3** (mechanism **C** *vs.* **D**, Scheme 2) are not, however, definitive. Although one may safely infer that mechanism **C** is plausible, mechanism **D** is not ruled out conclusively. When the β nitrogen of the hydrazido(1-) ligand does bear two hydrogens, the reaction with acetonitrile may choose to follow pathway **D** rather than **C**.

The balance of evidence does argue for mechanism **C**, nonetheless. Insertion of a C=N bond into a scandium-nitrogen bond has been observed before as a competing reaction in the catalytic hydrogenation of *tert*-butylnitrile to *tert*-butylamine by permethylscandocene hydride.[3] In some related chemistry of amide derivatives of aluminum, nitrile insertion has been observed to occur at the Al-N bond in preference to the Al-C bond.[18] Moreover, the insertion of a nonpolar unsaturated group into a transition metal-nitrogen bond is a key step in the catalytic hydroamination/cyclization of α,ω-amino olefins,[5] as mentioned earlier, as well as in the recently reported formation of 2,3-diazametallacyclopentenes from the reaction of $Cp_2Zr(N_2Ph_2)$ with internal alkynes.[19] The tautomerization of the initial product of the nitrile insertion, *via* a formal 1,3 hydrogen shift (mechanism **D**, Scheme 2), bears some resemblance to the analogous process observed for the insertion product of $Cp^*_2Ti(\eta^2\text{-}C_2H_4)$ with acetonitrile, which yields $Cp^*_2\overline{TiCH_2CH{=}C(CH_3)NH}$.[20]

Summary and Conclusions

The modest stability of these hydrazido(1-) derivatives of permethylscandocene, $Cp^*_2ScNHNH_2$ and $Cp^*_2ScNHN(CH_3)_2$, may be traced, in part, to the very high reduction potential of these formally Sc(III) complexes, although in view of the moderate stability of the formally W(VI) complexes $[Cp^*W(CH_3)_3(NHNH_2)]^+$ and $Cp^*W(CH_3)_4(NHNH_2)$,[9b,c] one may question the premise that the high reduction potential for $[N_2H_3]^-$ is a principal reason for the

paucity of examples of stable transition metal derivatives with the hydrazido(1-) ligand. The susceptibility of the [Sc-Cp*] bonds to protiolytic cleavage limits the stability, especially for $Cp^*_2ScNHNH_2$, and restricts the types of chemistry that may be explored. For example, a clean reaction with acetone to yield $[Cp^*_2ScNHN{=}C(CH_3)_2]$ is unlikely, since water (the co-product) reacts rapidly with all permethylscandocene compounds we have prepared to date. On the other hand, the insertion chemistry observed with acetonitrile is particularly clean, and may provide an efficient means to trap less stable adducts in other systems.

Table I. ^{1}H and ^{13}C data for $Cp^{*}_{2}Sc$ Complexes.[a]

Compound	Assignment	δ ^{1}H (ppm)	δ ^{13}C (ppm)	Coupling (Hz)
$Cp^{*}_{2}ScNHNH_2$ (1) (toluene-d_8)	$C_5(CH_3)_5$	1.87 s		
	$NHNH_2$	2.68 s br		
	$NHNH_2$	2.86 s br		
$Cp^{*}_{2}ScNHN(CH_3)_2$ (2) (C_6D_6)	$C_5(CH_3)_5$	1.98 s		
	$NHN(CH_3)_2$	2.3 s		
	$NHN(CH_3)_2$		54.03	
	$C_5(CH_3)_5$		11.16	
	$C_5(CH_3)_5$		119.26	
$Cp^{*}_{2}ScN(H)C(CH_3)NNH_2$ (3) (C_6D_6)	$C_5(CH_3)_5$	1.86 s		
	$NHC(CH_3)NHNH_2$	1.80 s		
	$NHC(CH_3)NHNH_2$	3.05 s		
	$NHC(CH_3)NHNH_2$	4.04 s br		
	$C_5(CH_3)_5$		11.22	
	$C_5(CH_3)_5$		117.63	
	$NHC(CH_3)NHNH_2$		22.64	

Table I. ^{1}H and ^{13}C data for $Cp^{*}_{2}Sc$ Complexes (continued).

Compound	Assignment	δ ^{1}H (ppm)	δ ^{13}C (ppm)	Coupling (Hz)
$Cp^{*}_{2}ScN(H)C(CH_3)NNMe_2$ (4) (C_6D_6)	$C_5(CH_3)_5$	1.92 s		
	$NHC(CH_3)NHN(CH_3)_2$	?1.92 s		
	$NHC(CH_3)NHN(CH_3)_2$	2.4 s		
	$NHC(CH_3)NHN(CH_3)_2$	3.8 s		
	$C_5(CH_3)_5$		12.1	
	$C_5(CH_3)_5$		118.0	
	$NHC(CH_3)NHN(CH_3)_2$		48.5	
	$NHC(CH_3)NHN(CH_3)_2$		18.5	

[a] ^{1}H and ^{13}C NMR spectra were obtained at ambient temperature at an observation frequency of 399.78 MHz and 100.38MHz, respectively. Chemical shifts for both nuclei are reported in ppm relative to tetramethylsilane and were referenced to signals from the solvent.

Table II. Crystal and Intensity Collection Data for

$Cp_2^*\overline{ScN(H)C(CH_3)NNH_2}$

Formula: $ScN_3C_{22}H_{38}$ Formula weight: 387.53

Crystal size: (estimated.) 0.7 × 0.3× < 0.5 mm

Crystal color: Colorless

Space group: $P2_1/n$ #14 Absences: $0k0, k$ odd; $h0l, h+l$ odd

$a = 9.506(3)$Å

$b = 14.742(2)$Å $\beta = 101.30(1)°$

$c = 15.608(2)$Å

$V = 2177.0(6)$Å^3 $Z = 4$

$\mu = 3.09$ cm^{-1} $\rho_{calc} = 1.139$ g cm^{-3}

CAD-4 diffractometer ω scan

$\lambda = 0.71073$ Å Graphite monochromator

2θ range: 2°–20° Octants collected: $-h, \pm k, \pm l$

2θ range: 20°–25° Octants collected: $-h, -k, \pm l$

T = 294°K

Number of reflections measured: 6734

Number of independent reflections: 3855

Number with $F_o^2 > 0$: 3276

Number with $F_o^2 > 3\sigma(F_o^2)$: 2604

Goodness of fit for merging data: 0.945

R for merging duplicate reflections: 0.040

Number of reflections used in refinement: 2267

Final R-index: 0.117 (0.051 for $F_o^2 > 3\sigma(F_o^2)$)

Final goodness of fit: 1.34 for 380 parameters

Table III. Non-Hydrogen Atom Coordinates and Displacement Parameters for $Cp_2^*Sc\overline{N(H)C(CH_3)NNH_2}$

x, y, z and U_{eq}[a] $\times 10^4$

Atom	x	y	z	U_{eq}
Sc	3113(.8)	2326(.4)	359(.5)	337(2)
N1	4588(4)	1152(3)	65(2)	421(11)
N2	4191(4)	662(2)	−739(2)	471(10)
N3	2168(4)	1543(3)	−660(2)	462(11)
C1	2925(5)	914(3)	−1019(3)	427(12)
C2	2421(10)	438(6)	−1830(5)	692(20)
Cp1	2796(4)	2455(3)	1952(2)	402(11)
Cp2	1472(4)	2677(3)	1552(2)	425(11)
Cp3	972(4)	1890(3)	1136(2)	434(12)
Cp4	1935(4)	1180(3)	1284(2)	407(11)
Cp5	3068(4)	1543(3)	1785(2)	390(11)
Cp6	3731(5)	4001(2)	383(3)	438(12)
Cp7	5007(4)	3517(2)	293(3)	395(11)
Cp8	4947(4)	3109(2)	−519(3)	394(11)
Cp9	3641(5)	3308(3)	−926(3)	430(12)
Cp10	2886(4)	3845(2)	−365(3)	421(11)
Me1	3658(8)	3006(5)	2591(4)	673(19)
Me2	644(7)	3527(4)	1665(5)	691(18)
Me3	−434(6)	1798(5)	651(5)	710(20)
Me4	1749(9)	227(4)	989(5)	672(19)

Table III. (Cont.)

Atom	x	y	z	U_{eq}
Me5	4299(7)	1002(5)	2162(4)	647(17)
Me6	3497(10)	4716(4)	1045(5)	726(20)
Me7	6279(7)	3554(6)	904(5)	746(19)
Me8	6150(6)	2660(4)	−951(4)	661(16)
Me9	3249(10)	3083(5)	−1833(4)	743(21)
Me10	1431(7)	4241(5)	−583(5)	761(20)

• $U_{eq} = \frac{1}{3} \sum_i \sum_j [U_{ij}(a_i^* a_j^*)(\vec{a}_i \cdot \vec{a}_j)]$

Table IV. Hydrogen Atom Coordinates and Displacement Parameters for $Cp_2^*Sc[N(H)C(CH_3)NNH_2]$

x, y and $z \times 10^4$

Atom	x	y	z	B
N1HB	4719(39)	662(23)	384(22)	4.5(12)*
N1HA	5343(36)	1390(22)	−31(22)	2.6(11)*
N3H	1501(32)	1608(23)	−882(20)	1.5(10)*
C2HA	2678(66)	−99(39)	−1939(34)	11.2(23)*
C2HB	1779(50)	199(37)	−1711(34)	6.3(22)*
C2HC	2144(47)	910(29)	−2224(28)	7.7(16)*
H1A	3332(49)	3532(31)	2746(28)	6.4(16)*
H1B	3748(36)	2714(22)	3130(23)	4.4(10)*
H1C	4281(56)	3305(38)	2388(33)	9.4(21)*
H2A	885(50)	3826(29)	2169(29)	7.7(17)*
H2B	573(53)	3911(31)	1150(32)	9.8(18)*
H2C	−156(47)	3395(30)	1816(30)	7.0(17)*
H3A	−493(56)	1235(33)	283(32)	11.4(21)*
H3B	−1182(52)	1749(31)	1014(29)	8.9(17)*
H3C	−650(46)	2312(26)	328(25)	7.0(15)*
H4A	2483(50)	−69(32)	961(29)	6.8(19)*
H4B	1374(45)	−66(29)	1391(25)	5.8(15)*
H4C	1540(50)	119(30)	394(27)	8.4(17)*
H5A	4980(47)	1369(29)	2095(28)	6.2(16)*
H5B	4178(42)	853(26)	2744(25)	6.2(13)*
H5C	4452(50)	376(30)	1890(27)	9.0(17)*
H6A	4047(45)	5190(30)	1033(26)	6.2(14)*
H6B	2742(70)	5031(47)	920(41)	15.2(33)*
H6C	3639(53)	4500(31)	1602(29)	8.7(18)*
H7A	6138(56)	3992(34)	1337(33)	10.5(21)*
H7B	6380(56)	3021(34)	1183(33)	10.7(22)*
H7C	6995(59)	3758(37)	658(34)	10.8(23)*
H8A	6760(42)	2440(26)	−530(24)	5.4(13)*
H8B	5864(46)	2062(28)	−1276(26)	7.9(15)*
H8C	6485(55)	3049(33)	−1348(32)	10.5(20)*
H9A	3281(54)	2474(32)	−1958(29)	8.5(18)*
H9B	2355(57)	3074(39)	−1985(37)	10.5(25)*
H9C	3434(46)	3464(27)	−2196(27)	5.6(14)*
H10A	1512(43)	4653(26)	−1038(24)	5.9(13)*
H10B	749(64)	3736(38)	−685(35)	13.1(25)*
H10C	1308(49)	4643(27)	−154(27)	6.7(17)*

Table V. Anisotropic Thermal Displacement Parameters for $Cp_2^*ScN(H)C(CH_3)NNH_2$

Atom	U_{11}	U_{22}	U_{33}	U_{12}	U_{13}	U_{23}
Sc	298(4)	328(4)	385(4)	24(4)	20(3)	−1(4)
Cp1	413(26)	460(31)	340(23)	−84(23)	97(20)	−30(21)
Cp7	351(27)	357(25)	481(28)	−74(22)	58(23)	13(21)
Cp8	367(28)	354(24)	469(28)	−3(21)	119(24)	25(21)
N2	551(26)	451(22)	407(22)	141(20)	−36(19)	−120(18)
N3	395(28)	514(25)	465(26)	94(22)	−120(22)	−66(19)
Cp2	421(28)	356(24)	509(26)	36(25)	156(22)	−13(23)
N1	416(28)	358(25)	486(26)	15(22)	−28(21)	12(21)
Me9	1026(63)	683(47)	508(38)	−51(40)	−124(37)	166(35)
Cp3	305(27)	512(28)	490(27)	−31(23)	89(23)	44(23)
Cp9	495(30)	418(27)	377(27)	9(23)	14(24)	54(21)
Me8	635(39)	640(37)	731(41)	129(35)	294(34)	65(37)
Cp4	432(28)	324(26)	467(27)	−79(23)	32(22)	16(21)
Cp6	557(31)	313(25)	459(27)	−22(22)	188(25)	−29(21)
Me6	1048(56)	372(34)	785(47)	−143(38)	366(43)	−137(32)
Cp5	409(28)	404(26)	361(25)	19(23)	51(22)	64(21)
Me2	622(43)	635(40)	843(50)	127(34)	362(40)	46(38)
Me7	622(44)	925(52)	681(44)	−216(41)	−76(35)	30(42)
Me10	597(43)	710(46)	977(54)	240(38)	54(39)	226(44)
C2	787(54)	677(48)	592(42)	13(45)	−191(39)	−153(36)
Me1	850(48)	767(50)	409(35)	−288(40)	120(33)	−115(33)
Cp10	369(27)	341(25)	553(29)	52(22)	27(24)	79(23)
C1	559(33)	343(26)	375(27)	−6(24)	−39(24)	−35(21)
Me4	795(51)	481(38)	743(51)	−91(38)	82(40)	61(35)
Me5	722(45)	741(47)	470(34)	155(39)	−78(32)	183(33)
Me3	347(34)	866(47)	914(47)	−20(33)	−18(33)	126(43)

$U_{i,j}$ values have been multiplied by 10^4

The form of the displacement factor is:

$$\exp -2\pi^2(U_{11}h^2a^{*2} + U_{22}k^2b^{*2} + U_{33}l^2c^{*2} + 2U_{12}hka^*b^* + 2U_{13}hla^*c^* + 2U_{23}klb^*c^*)$$

Table VI. Complete Distances and Angles for $Cp_2^*ScN(H)C(CH_3)NNH_2$

		Distance(Å)				Angle(°)
Sc	-N3	2.132(4)	Cen1	-Sc	-Cen2	138.5
Sc	-N1	2.287(4)	Cp5	-Cp1	-Cp2	108.0(3)
Sc	-Cen1	2.210	Me1	-Cp1	-Cp2	127.9(4)
Sc	-Cen2	2.236	Me1	-Cp1	-Cp5	123.0(4)
Cp1	-Cp2	1.419(5)	Cp6	-Cp7	-Cp8	107.6(3)
Cp1	-Cp5	1.395(5)	Me7	-Cp7	-Cp8	126.1(4)
Cp1	-Me1	1.503(8)	Me7	-Cp7	-Cp6	125.7(4)
Cp7	-Cp8	1.403(5)	Cp9	-Cp8	-Cp7	108.7(3)
Cp7	-Cp6	1.419(5)	Me8	-Cp8	-Cp7	126.2(4)
Cp7	-Me7	1.508(8)	Me8	-Cp8	-Cp9	124.4(4)
Cp7	-Cen2	1.205	C1	-N2	-N1	109.9(3)
Cp8	-Cp9	1.401(5)	N3H	-N3	-C1	112.2(26)
Cp8	-Me8	1.505(7)	Cp3	-Cp2	-Cp1	106.8(3)
N2	-N1	1.483(5)	Me2	-Cp2	-Cp1	127.1(4)
N2	-C1	1.316(5)	Me2	-Cp2	-Cp3	125.4(4)
N3	-C1	1.315(6)	N1HB	-N1	-N2	95.9(23)
N3	-N3H	0.72(3)	N1HA	-N1	-N2	104.4(24)
Cp2	-Cp3	1.403(6)	N1HA	-N1	-N1HB	110.3(33)
Cp2	-Me2	1.494(8)	Cp4	-Cp3	-Cp2	109.6(3)
N1	-N1HB	0.88(4)	Me3	-Cp3	-Cp2	125.4(4)
N1	-N1HA	0.82(3)	Me3	-Cp3	-Cp4	124.9(4)
Me9	-Cp9	1.486(9)	Me9	-Cp9	-Cp8	124.5(4)
Cp3	-Cp4	1.402(6)	Cp10	-Cp9	-Cp8	107.6(3)
Cp3	-Me3	1.513(8)	Cp10	-Cp9	-Me9	127.4(4)
Cp9	-Cp10	1.401(6)	Cp5	-Cp4	-Cp3	106.7(3)
Cp4	-Cp5	1.410(5)	Me4	-Cp4	-Cp3	125.9(4)
Cp4	-Me4	1.487(8)	Me4	-Cp4	-Cp5	127.4(4)
Cp6	-Me6	1.499(8)	Me6	-Cp6	-Cp7	125.0(4)
Cp6	-Cp10	1.407(6)	Cp10	-Cp6	-Cp7	107.2(3)
Cp5	-Me5	1.515(7)	Cp10	-Cp6	-Me6	126.2(4)
Me10	-Cp10	1.527(8)	Cp4	-Cp5	-Cp1	109.0(3)
C2	-C1	1.507(9)	Me5	-Cp5	-Cp1	125.6(4)
N1HB	-N1HA	1.39(5)	Me5	-Cp5	-Cp4	125.2(4)
			Cp6	-Cp10	-Cp9	108.8(3)
			Me10	-Cp10	-Cp9	124.1(4)
			Me10	-Cp10	-Cp6	127.0(4)
			N3	-C1	-N2	124.5(4)
			C2	-C1	-N2	113.3(4)
			C2	-C1	-N3	121.8(5)

Table VII. Crystal and Intensity Collection Data for

$Cp_2^*\overline{ScN(H)C(CH_3)NN(CH_3)_2}$

Formula: $ScN_3C_{24}H_{40}$ — Formula weight: 415.56

Crystal color: Colorless — Habit: Prismatic

Crystal size: 0.11 × 0.37 × 0.64 mm

Space group: $P2_1/n$ #14 — Absences: $0k0, k$ odd; $h0l, h + l$ odd

$a = 10.953(2)$Å

$b = 19.733(1)$Å — $\beta = 101.30(1)°$

$c = 11.441(1)$Å

$V = 2424.9(5)$Å^3 — $Z = 4$

$\mu = 3.24$ cm^{-1} ($\mu r_{max} = 0.12$) — $\rho_{calc} = 1.138$ g cm^{-3}

CAD-4 diffractometer — ω scan

$\lambda = 0.71073$ Å — Graphite monochromator

2θ range: 2°–40° — Octants collected: $\pm h, k, \pm l$

T = 294°K

Number of reflections measured: 4873

Number of independent reflections: 2267

Number with $F_o^2 > 0$: 2089

Number with $F_o^2 > 3\sigma(F_o^2)$: 1540

Goodness of fit for merging data: 1.08

R for merging duplicate reflections: 0.0368

Number of reflections used in refinement: 2267

Final R-index: 0.0640 (0.0416 for $F_o^2 > 3\sigma(F_o^2)$)

Final goodness of fit: 1.78 for 253 parameters

Table VIII. Non-Hydrogen Atom Coordinates and Displacement Parameters for $Cp_2^*Sc\overline{N(H)C(CH_3)NN(CH_3)_2}$

x, y, z and $U_{eq}^a \times 10^4$

Atom	x	y	z	U_{eq}
Sc	8390(.7)	1456(.4)	7213(.7)	390(2)
Cp1	10255(4)	2235(2)	7708(4)	432(13)
Cp2	9191(4)	2629(2)	7718(4)	412(13)
Cp3	8672(4)	2427(2)	8689(4)	427(13)
Cp3	9391(5)	1898(2)	9270(4)	463(14)
Cp5	10372(4)	1778(2)	8665(4)	486(15)
Me1	11218(4)	2396(3)	6972(4)	716(16)
Me2	8757(5)	3208(3)	6898(4)	703(16)
Me3	7556(5)	2759(2)	9045(4)	712(16)
Me4	9265(5)	1579(3)	10434(4)	830(19)
Me5	11444(5)	1304(3)	9107(4)	841(18)
Cp6	8881(4)	1176(2)	5204(4)	438(13)
Cp7	9713(4)	788(2)	6021(4)	465(14)
Cp8	9013(4)	318(2)	6543(4)	446(14)
Cp9	7750(4)	394(2)	5994(4)	448(14)
Cp10	7675(4)	925(2)	5171(4)	438(14)
Me6	9189(4)	1714(3)	4357(4)	707(16)
Me7	11110(4)	744(3)	6111(4)	727(17)
Me8	9544(5)	−243(3)	7387(5)	748(17)
Me9	6687(5)	−72(3)	6089(4)	673(16)
N1	6166(4)	702(2)	8743(4)	775(15)
N2	6758(4)	1164(2)	8055(4)	583(13)
N3	6592(4)	1925(2)	6619(4)	632(14)

Table VIII.

C1	6017(4)	1516(3)	7230(6)	664(20)
C2	4611(5)	1451(3)	6998(6)	1175(27)
C3	7028(6)	162(3)	9191(5)	890(20)
C4	5807(6)	1050(3)	9755(6)	1227(23)

[a] $U_{eq} = \frac{1}{3} \sum_i \sum_j [U_{ij}(a_i^* a_j^*)(\vec{a}_i \cdot \vec{a}_j)]$

Table IX. Assigned Hydrogen Atom Coordinates and Displacement Parameters for $Cp_2^*Sc\overline{N(H)C(CH_3)NN(CH_3)_2}$

x, y and $z \times 10^4$

Atom	x	y	z	B
H1a	11681	2774	7320	7.2
H1b	10803	2490	6188	7.2
H1c	11740	2010	6993	7.2
H2a	9374	3548	7020	7.1
H2b	7996	3369	7062	7.1
H2c	8635	3042	6097	7.1
H3a	7316	2488	9653	6.8
H3b	6906	2776	8367	6.8
H3c	7786	3197	9335	6.8
H4a	9374	1105	10369	8.0
H4b	8466	1682	10578	8.0
H4c	9895	1763	11042	8.0
H5a	12094	1407	8700	7.9
H5b	11157	852	8934	7.9
H5c	11699	1368	9935	7.9
H6a	10067	1739	4456	6.7
H6b	8851	2128	4546	6.7
H6c	8830	1577	3568	6.7
H7a	11345	1071	5592	6.8
H7b	11299	300	5877	6.8
H7c	11501	828	6910	6.8
H8a	9572	−644	6937	7.3
H8b	9024	−302	7949	7.3
H8c	10358	−113	7773	7.3
H9a	6300	−212	5313	6.6
H9b	6108	172	6453	6.6
H9c	7001	−449	6565	6.6
H10a	6538	1599	4181	7.1
H10b	5816	993	4600	7.1
H10c	6533	895	3561	7.1
HN3	6313	2295	6101	5.9
HC2a	4294	1563	6187	10.4
HC2b	4299	1761	7507	10.4
HC2c	4402	1002	7162	10.4
HC3a	7258	−59	8534	8.2
HC3b	6619	−144	9629	8.2
HC3c	7731	356	9694	8.2
HC4a	5397	732	10164	10.5
HC4b	5249	1406	9439	10.5
HC4c	6526	1222	10244	10.5

*Isotropic displacement parameter, B

Table X. Anisotropic Thermal Displacement Parameters $\times 10^4$ for $Cp_2^*Sc\overline{N(H)C(CH_3)NN(CH_3)_2}$

Atom	U_{11}	U_{22}	U_{33}	U_{12}	U_{13}	U_{23}
Sc	339(5)	352(5)	468(6)	24(5)	49(4)	−26(5)
Cp1	410(32)	444(34)	455(34)	−68(27)	120(26)	−109(27)
Cp2	471(32)	326(31)	423(33)	−52(26)	52(26)	6(25)
Cp3	441(31)	368(32)	487(32)	−30(26)	131(27)	−78(26)
Cp3	590(35)	406(33)	362(32)	−61(28)	17(27)	23(26)
Cp5	351(31)	451(34)	577(36)	50(26)	−105(27)	−85(29)
Me1	571(34)	814(42)	806(40)	−199(31)	243(30)	−278(32)
Me2	824(41)	535(36)	738(40)	4(31)	126(31)	59(31)
Me3	752(38)	606(39)	852(42)	−51(32)	336(32)	−225(32)
Me4	1156(47)	754(44)	543(36)	−228(37)	79(32)	60(32)
Me5	785(40)	848(47)	733(39)	222(36)	−234(32)	−205(33)
Cp6	474(33)	458(33)	384(31)	−30(28)	90(26)	−43(26)
Cp7	355(32)	486(35)	544(34)	25(29)	62(27)	−163(28)
Cp8	447(33)	342(31)	505(33)	138(27)	−17(27)	−32(26)
Cp9	469(35)	337(33)	528(33)	−22(27)	76(27)	−78(27)
Cp10	395(34)	453(35)	431(32)	4(26)	−3(25)	−49(26)
Me6	765(39)	768(42)	609(36)	−89(32)	187(30)	−61(31)
Me7	466(36)	864(43)	852(41)	78(31)	131(30)	−336(34)
Me8	813(41)	543(38)	828(41)	216(32)	10(33)	−66(31)
Me9	673(37)	565(38)	770(40)	−135(30)	111(30)	−93(29)
N1	726(34)	597(35)	1134(42)	−128(29)	504(32)	−148(31)
N2	495(29)	482(28)	822(35)	−57(25)	249(26)	−67(25)
N3	534(29)	477(30)	846(35)	152(24)	38(25)	12(25)
C1	356(35)	587(42)	1025(49)	57(33)	74(34)	−259(39)
C2	397(35)	1169(55)	1907(64)	100(38)	100(38)	−308(51)
C3	1074(52)	722(47)	980(49)	−244(40)	463(41)	−53(38)
C4	1372(59)	1086(54)	1552(66)	−270(46)	1092(54)	−267(50)

The form of the displacement factor is:

$$\exp -2\pi^2(U_{11}h^2a^{*2} + U_{22}k^2b^{*2} + U_{33}\ell^2c^{*2} + 2U_{12}hka^*b^* + 2U_{13}h\ell a^*c^* + 2U_{23}k\ell b^*c^*)$$

Table XI. Complete Distances and Angles for $Cp_2^*Sc\overline{N(H)C(CH_3)NN(CH_3)_2}$

Distance(Å)			Angle(°)			
Sc	-N2	2.264(4)	CpA	-Sc	-CpB	137.8
Sc	-N3	2.161(4)	CpA	-Sc	-N2	108.5
Sc	-CpA	2.233	CpA	-Sc	-N3	107.4
Sc	-CpB	2.231	CpB	-Sc	-N2	110.6
Sc	-Cp1	2.531(5)	CpB	-Sc	-N3	105.6
Sc	-Cp2	2.502(4)	N3	-Sc	-N2	59.8(2)
Sc	-Cp3	2.533(5)	Sc	-N3	-C1	94.2(3)
Sc	-Cp4	2.547(5)	Sc	-N2	-C1	89.3(3)
Sc	-Cp5	2.542(5)	C3	-N1	-N2	109.2(4)
Sc	-Cp6	2.523(5)	C4	-N1	-N2	110.8(4)
Sc	-Cp7	2.545(5)	C4	-N1	-C3	108.8(5)
Sc	-Cp8	2.512(5)	C1	-N2	-N1	116.5(4)
Sc	-Cp9	2.539(5)	N3	-C1	-N2	114.6(5)
Sc	-Cp10	2.542(4)	C2	-C1	-N2	122.8(5)
N1	-N2	1.439(6)	C2	-C1	-N3	122.6(5)
N1	-C3	1.450(8)	Cp5	-Cp1	-Cp2	107.3(4)
N1	-C4	1.465(8)	Me1	-Cp1	-Cp2	124.2(4)
N2	-C1	1.316(7)	Me1	-Cp1	-Cp5	127.2(4)
N3	-C1	1.306(7)	Cp3	-Cp2	-Cp1	108.4(4)
C1	-C2	1.516(8)	Me2	-Cp2	-Cp1	125.4(4)
Cp1	-Cp2	1.403(6)	Me2	-Cp2	-Cp3	125.9(4)
Cp1	-Cp5	1.405(7)	Cp4	-Cp3	-Cp2	108.2(4)
Cp1	-Me1	1.507(7)	Me3	-Cp3	-Cp2	124.5(4)
Cp2	-Cp3	1.401(6)	Me3	-Cp3	-Cp4	127.3(4)
Cp2	-Me2	1.496(7)	Cp5	-Cp4	-Cp3	107.8(4)
Cp3	-Cp4	1.395(6)	Me4	-Cp4	-Cp3	126.5(4)
Cp3	-Me3	1.511(7)	Me4	-Cp4	-Cp5	125.1(4)
Cp4	-Cp5	1.407(7)	Cp4	-Cp5	-Cp1	108.3(4)
Cp4	-Me4	1.504(7)	Me5	-Cp5	-Cp1	127.2(4)
Cp5	-Me5	1.510(7)	Me5	-Cp5	-Cp4	124.0(4)
Cp6	-Cp7	1.398(6)	Cp10	-Cp6	-Cp7	108.1(4)
Cp6	-Cp10	1.405(6)	Me6	-Cp6	-Cp7	127.8(4)
Cp6	-Me6	1.519(7)	Me6	-Cp6	-Cp10	123.6(4)
Cp7	-Cp8	1.408(6)	Cp8	-Cp7	-Cp6	107.9(4)
Cp7	-Me7	1.516(7)	Me7	-Cp7	-Cp6	126.4(4)
Cp8	-Cp9	1.411(6)	Me7	-Cp7	-Cp8	124.0(4)
Cp8	-Me8	1.509(7)	Cp9	-Cp8	-Cp7	108.0(4)
Cp9	-Cp10	1.400(6)	Me8	-Cp8	-Cp7	125.5(4)
Cp9	-Me9	1.504(7)	Me8	-Cp8	-Cp9	125.7(4)
Cp10	-Me10	1.505(7)	Cp10	-Cp9	-Cp8	107.6(4)
			Me9	-Cp9	-Cp8	127.5(4)
			Me9	-Cp9	-Cp10	124.1(4)
			Cp9	-Cp10	-Cp6	108.3(4)
			Me10	-Cp10	-Cp6	125.8(4)
			Me10	-Cp10	-Cp9	125.4(4)

EXPERIMENTAL SECTION

General Considerations. All manipulations were performed using glovebox and high-vacuum techniques as described elsewhere.[21] Argon, hydrogen and nitrogen were purified by passage over MnO on vermiculite and activated 4Å molecular sieves. Solvents were dried and purified by prolonged reflux over a suitable drying agent, followed by distillation under an atmosphere of dinitrogen. Ether solvents were stored over sodium benzophenone ketyl; hydrocarbon solvents were stored over titanocene;[22] and methylene chloride and acetonitrile were stored over CaH_2. Anhydrous hydrazine (Aldrich) was transferred to a Kontes microflex vial with rotary-type valve and used without prior purification. 1,1-Dimethylhydrazine (Aldrich) was stored over 4Å molecular sieves in a flask under vacuum and used as received.

NMR spectra were recorded on Varian EM-390 (^{1}H, 90MHz), JEOL FX90Q (^{1}H, 89.56 MHz; ^{13}C, 22.50MHz) and JEOL GX400Q (^{1}H, 399.78 MHz) instruments. Infrared spectra were measured as Nujol mulls on KBr plates and recorded on a Beckman IR-4240 spectrometer. Elemental analyses were performed by L. Henling and F. Harvey at the Caltech Analytical Laboratory. Mass spectra were obtained from the UC Riverside facility.

Cp^*_2ScCl and $Cp^*_2ScCH_3$ were prepared as described previously.[14]

$Cp^*_2ScNHNH_2$ (1). Method a: Cp^*_2ScCl (2.54 g, 7.26 mmol) was dissolved in 40 mL of toluene. 5.3 mL of a 1.5M $LiCH_3$ solution in diethyl ether (7.95 mmol) were added slowly by syringe to the solution, which was stirring under argon. After 2 hr at room temperature, the volatiles were removed from the reaction mixture under reduced pressure. The residue was washed with 30 mL of petroleum ether and the resulting solution was filtered. Anhydrous hydrazine (22.5μl, 7.1 mmol) was syringed into the solution with stirring under argon. The reaction mixture immediately turned from light-orange to maroon. After approximately twenty minutes the color dissipated and a white precipitate of 1 formed. The

precipitate was filtered and dried to yield 1.29g (51%) of product. IR: 3330, 1565, 1012, 712 cm^{-1}. Anal. Calcd for $C_{20}H_{33}N_2Sc$: C, 69.4; H, 9.62; N, 8.09. Found: C, 67.83; H, 9.35, N, 8.08. MW Calcd: 345.9. MS largest peak: m/e = 346.

Method b: An isolated sample of $Cp^*_2ScCH_3$ was used. The reaction with hydrazine was performed under the same conditions as in method a. 0.837g of $Cp^*_2ScCH_3$ (2.54 mmol) afforded 0.518g of 1 (59%).

$Cp^*_2ScNHN(CH_3)_2$ (2): $Cp^*_2ScCH_3$ (1.0g, 3.0 mmol) was dissolved in 30 mL of petroleum ether. 1,1-Dimethylhydrazine, 3.0 mmol, were measured into a gas volume and condensed into the solution at -78°C. The reaction mixture turned from light-orange to bright-yellow as it warmed to room temperature. After being stirred for one hour, the solution was concentrated and cooled to -78°C to afford yellow crystals of 2. Yield 0.45g (40%). IR: 3175, 2782, 2740, 1208, 1196, 1142, 1080, 1050, 1016, 995, 850, 710, 650, 595, 550, 409 cm^{-1}. Anal. Calcd for $C_{22}H_{37}N_2Sc$: C, 70.56; H, 9.96; N, 7.48. Found: C, 70.77; H, 9.57; N, 7.25.

$Cp^*_2\overline{ScN(H)C(CH_3)NNH_2}$ (3). Compound 1 (0.79g, 2.3mmol) was dissolved in 25 mL of methylene chloride. Acetonitrile, 0.5 mL, was vacuum transferred to the solution. The reaction was stirred for 30 min at room temperature. The volatiles were removed under vacuum and the white residue was taken up in 20 mL of petroleum ether as a slurry, which was cooled to -78°C. The resulting white solid was filtered and dried. Yield 0.54g (61%). IR: 3370, 3290, 1607, 1591, 1540, 1417, 1355, 1250, 1230, 1156, 720, 550 cm^{-1}. Anal. Calcd for $C_{22}H_{36}N_3Sc$: C, 68.19; H, 9.36; N, 10.84. Found: C, 67.84; H, 9.10; N, 10.81.

$Cp^*_2\overline{ScN(H)C(CH_3)NNMe_2}$ (4). Compound 2 (0.145g, 0.388mmol) was dissolved in 15 mL of petroleum ether. Acetonitrile, 0.16 mL, was transferred to the solution. The reaction was stirred for 30 min at room temperature. Volatiles were removed under vacuum and the residue was dissolved in 3 mL of pentane and cooled at -78°C overnight to

precipitate a tan powder, which was filtered cold and dried. Yield 0.059g (39%). IR: 3389, 1650, 1508, 1235, 1033, 1192, 1033. Anal. Calcd for $C_{24}H_{39}N_4Sc$: C, 69.4; H, 9.7; N, 10.1. Found: C, 69.3; H, 9.5; N, 9.75.

Structure Determination for $Cp^*_2\overline{ScN(H)C(CH_3)NNH_2}$. A colorless crystal obtained from an NMR tube reaction of $Cp^*_2ScNHNH_2$ with CH_3CN in deuterobenzene was mounted in a thin-walled glass capillary under N_2. The crystal was centered on a CAD-4 diffractometer. Unit cell parameters and an orientation matrix were obtained by a least-squares calculation from the setting angles of 24 reflections. Two quadrants of intensity data out to a 2θ of 40° and one quadrant of data in the 2θ range 40°-50° were collected. No absorption or decay corrections were applied, and the data were reduced to F_o^2 values and merged to yield the final data set. Systematic absences led to the choice of space group $P2_1/n$. The coordinates of the scandium atom were obtained from a Patterson map; locations of the other non-hydrogen atoms were determined from successive structure factor-Fourier calculations. Hydrogen atom positions for the methyl groups and for the heterometallacyclic ring were determined from difference maps and were refined along with their isotropic B values. The full least-squares matrix, consisting of coordinates, anisotropic U_{ij}'s and isotropic B values for all of the atoms and a scale factor, contained 380 parameters. A final difference Fourier map showed deviations ranging from -0.61eÅ^{-3} to 0.63eÅ^{-3}. The refinement converged with an R factor of 0.117 (0.051 for $F_o^2>3\sigma$) and a goodness of fit of 1.34 for all 3855 reflections.

A summary of the data collection information is given in Table II, coordinates and U_{eqs} for non-hydrogen atoms are listed in Table III, parameters for the hydrogen atoms are listed in TAble IV, anisotropic displacement parameters are in Table V, and complete distances and angles are given in Table VI.

Structure Determination for $Cp^*_2\overline{ScN(H)C(CH_3)NNMe_2}$. A colorless crystal grown from a petroleum ether solution of the complex cooled at -60°C was mounted in a

thin-walled glass capillary under N_2. The crystal was centered on a CAD-4 diffractometer. Unit-cell parameters and an orientation matrix were obtained by a least-squares calculation from the setting angles of 24 reflections with $35° < 2\theta < 39°$. Two equivalent intensity data sets out to a 2θ of 40° were collected, corrected for absorption (transmission coefficient: 0.889-0.956) and a slight decay, reduced to F_o^2 values and merged to yield the final data set. Systematic absences led to the choice of space group $P2_1/n$. Coordinates of the scandium atom were obtained from a Patterson map; locations of the other non-hydrogen atoms were determined from successive structure factor-Fourier calculations. Hydrogen atom positions were determined from difference maps for the methyl groups and by calculation for the other one. All hydrogen atoms were given isotropic B values 20% greater than that of the attached atom; no hydrogen parameters were refined. The full least squares matrix, consisting of coordinates and anisotropic U_{ij}'s for the non-hydrogen atoms and a scale factor, contained 253 parameters. A final difference Fourier map showed deviations ranging from -0.30 $eÅ^{-3}$ to 0.38 $eÅ^{-3}$. The refinement converged with an R factor of 0.0640 (0.0416 for $F_o^2 > 3\sigma(F_o^2)$) and a goodness of fit of 1.78 for all 2267 reflections.

A summary of the data collection information is given in Table VII, coordinates and U_{eqs} for non-hydrogen atoms are listed in Table VIII, parameters for the hydrogen atoms are listed in TAble IX, anisotropic displacement parameters are in Table X, and complete distances and angles are given in Table XI.

All calculations were carried out on a VAX 11/750 computer using the CRYM system of programs and ORTEP. Scattering factors and corrections for anomalous scattering were taken from a standard reference (International Tables for X-ray Crystallography, Vol. IV, p. 71, p. 149; Birmingham, Kynoch Press, 1974).

References

1. St. Clair, M. A.; Santarsiero, B. D.; Bercaw, J. E. *Organometallics* 1989, *8*, 17.

2. St. Clair, M. A. Ph.D. Thesis, California Institute of Technology, 1989.

3. Bercaw, J. E.; Davies, D. L.; Wolczanski, P. T. *Organometallics* 1986, *5*, 443.

4. Thompson, M. E. Ph.D. Thesis, California Institute of Technology, 1985.

5. Gagne, M. R.; Marks, T. J. *J. Am. Chem. Soc.* 1989, 111, 4108.

6. a) Leigh, G. J. In *Recent Developments in Nitrogen Fixation* Newton, W., Postgate, J. R., Rodriguez-Barruco, C., Eds.; Academic Press: New York, 1977; p. 1. b) Chatt, J; Dilworth, J.R.; Richards, R.L. *Chem. Rev.*, 1978, *78*(6), 589. c)Henderson, R.A.; Leigh, G.S.; Pickett, C.J. *Adv. in Inorg. Chem. and Radiochem.*, 1983, *27*, 197. c)

7. Stiefel, E. I. In *Recent Developments in Nitrogen Fixation* Newton, W., Postgate, J. R., Rodriguez-Barruco, C., Eds.; Academic Press: New York, 1977; p. 69.

8. a) Latham, I.A.; Leigh G.J. *J. Chem. Soc. Dalton Trans.*, 1986, 399. b) Clark, C.C.; *Hydrazine*; Mathieson Chemical Corporation: Maryland, 1953; Chapter 1.

9. a). McCleverty, J. A.; Rae, A. E.; Wolochowicz, I.; Bailey, N.A.; Smith, J. M. A. *J. Chem. Soc., Dalton. Trans.*, 1983, 71. b) Murray, R. C.; Schrock, R. R. *J. Am. Chem. Soc.*, 1985, *107*, 4557. c) Schrock, R. R.; Liu, A. H.; O'Regan, M. B.; Finch, W. C.; Payack, J. F. *Inorg. Chem.*, 1988, *27*, 3574.

10. a) Carroll, J. A.; Sutton, D; Cowie, M.; Gauthier, M. D. *J. Chem. Soc., Chem. Commun.*, 1979, 1058. Carroll, J. A.; Sutton, D. *Inorg. Chem.*, 1980, *19*, 3137. b) Cowie, Martin; Gautier, M. D. *Inorg. Chem.*, 1980, *19*, 3142. c) Chatt., J.; Dilworth, J. R. ; Dahlstrom, J. R.; Zubieta, P. L. *J. Chem. Soc., Chem. Commun.*, 1980, 786. d) Dilworth, J. R.; Latham, I. A., Leigh, G. J.; Huttner, G.; Jibril, I. *J. Chem. Soc., Chem. Commun.*, 1983, 1368. e) Latham, I. A.; Leigh, G. J.; Huttner, G.; Jibril, I. *J. Chem. Soc., Dalton Trans.*, 1986, 385.

11. a) Barrientos-Penna, C. K.; Campana, C. F.; Einstein, F. W. B.; Jones, T.; Sutton, D.; Tracey, A. S. *Inorg. Chem.*, 1984, *23*, 363. b) Nicholson, T.; Zubieta, J. A. *J. Chem. Soc., Chem. Commun*, 1985. c) Nicholson, T.; Zubieta, J. *Polyhedron*, 1988, *7*, 171.

12. (a) Fitzroy, M. d.; Frederiksen, J. M.; Murray, K. S.; Snow, M. R. *Inorg. Chem.*, 1985, *24*, 3265. (b) Butcher, A. V.; Chatt, J.; Dilworth, J. R.; Leigh, G. J.; Hursthouse, M. B.; Jayaweera, S. A. A.; Quick, A. *J. Chem. Soc., Dalton Trans.*, 1979, 921.
(c) Mattes, R.; Scholand, H. *Angew. Chem. Int. Ed. Engl.*, 1983, 22(3), 245.

13. a) Cotton, F. A.; Luck, R. L. *Inorg. Chem.* 1989, *28*, 3210-3213. b) Brookhart, M.; Green, M. L. H. *J. Organomet. Chem.* 1983, *250*, 395.

14. Thompson, M. E.; Baxter, S. M.; Bulls, A. R.; Burger, B. J.; Nolan, M. C.; Santarsiero, B. D.; Schaefer, W. P.; Bercaw, J. E. *J. Am. Chem. Soc.* 1987, *109*, 203.

15. Pauling, L. *The Nature of the Chemical Bond*; Cornell University Press: Ithaca, 1960; p. 228.

16. Other mechanisms may also be envisioned that would result the acetonitrile's being ultimately positioned C2C1-N2. For example, a mechanism analogous to that proposed for the epoxidation of olefins by d^0 metal alkylperoxides (see *Comprehensive Coordination Chemistry*, Wilkinson, G.; Gillard, R. D.; McCleverty, J. A. Eds. Pergamon, Oxford, 1987; Volume 6, Chapter 61.3, p 345), in which the nucleophilic olefin is replaced by nitrogen of incoming acetonitrile and the η^2-alkyl peroxide ligand with an η^2-$NHNH_2$. Following heterolytic cleavage of the N-N bond, nucleophilic attack by the Sc-NH_2 at the carbon center would generate the first product in mechanism B (Scheme 1).

17. Collman, J. P.; Hegedus, L. S.; Norton, J. R.; Finke, R. G. *Principles and Applications of Organotransition Metal Chemistry*. University Science Books: Mill Valley, CA, 1987; Chapter 7.

18. Hirabayashi T.; Itoh, K.; Sakai, S.; Ishii, Y. J. *Organometal. Chem.* **1970**, *21*, 273.

19. Walsh, P. J.; Hollander, F. J.;Bergman, R. G. *J. Am. Chem. Soc.* **1990**, *112*, 894.

20. Cohen, S. A.; Bercaw, J. E. *Organometallics*, **1985**, *4*, 1006

21. Burger, B. J.; Bercaw, J. E. In *New Developments in the Synthesis, Manipulation and Characterization of Organometallic Compounds*; Wayda, A. L., Darensbourg, M. Y. Eds.; ACS Symposium Series 357; American Chemical Society: Washington, D. C., 1987; pp. 17-98.

22. Marvich, R. H.; Brintzinger, H. H. *J. Am. Chem. Soc.* **1971**, *93*, 2046.